and altered mode of fracture [6]. The existence of discrete Al_2O_3 grains in sintered PZT–Al_2O_3 nanocomposites has been reported, based on TEM evidence [9].

In the case of antiferroelectric materials such as lead zirconate, PZ, to our knowledge the nanocomposite approach for improving mechanical properties has not been reported. In the present work, we report results showing the effect of Al_2O_3 nanoparticle additions on: ceramic densification, microstructure, fracture behaviour, Vickers hardness and dielectric properties. We also show evidence that the matrix reacts with the Al_2O_3 component during sintering to form lead aluminium oxides; these second phases may play an important role in the properties of Pb-based perovskite nanocomposites.

2. Experimental

$PbZrO_3$ powders were prepared by the mixed-oxide method using reagent grade PbO (>99.9%, Aldrich) and ZrO_2 (99%, Aldrich). The starting powders were ball-milled in isopropanol for 24 h using zirconia grinding media. After mixing, the slurry was dried, ground using a mortar and pestle and sieved before calcining for 3 h at 800 °C, with a heating/cooling rate of 5 °C/min.

To form the nanocomposites, Al_2O_3 powder (Aldrich), with an average primary particle size of 40 nm, was blended with the calcined $PbZrO_3$ powder. Before blending, the Al_2O_3 powder was treated in a vibratory mill for 20 min using zirconia grinding media and isopropanol, to reduce agglomeration. This was then mixed with the PZ powder in ratios of between 0.5 and 5 vol% (approximately 0.25–2.5 wt%), together with 1 wt% PVA binder. The PZ–Al_2O_3 mixture, with added organic binder, was ball-milled in isopropanol for 24 h using zirconia grinding media. Then, the slurry was dried and sieved to form a fine powder which was pressed at 100 MPa into cylindrical pellets 15 mm in diameter and 1.5 mm in thickness. Pellets were then sintered at 1200 or 1300 °C for 2 h using a heating rate of 5 °C/min. The sintering profile included a binder burn-out step at 550 °C, using a heating rate of 1 °C/min.

The density of the sintered samples was measured by the Archimedes method using distilled water as the fluid medium. In order to study phase formation, X-ray diffraction analysis (XRD) was performed using a Philips AP 1700 diffractometer with CuKα radiation. To help identify the products of reactions occurring during sintering, a PZ–10 vol% Al_2O_3 pellet was prepared specifically for XRD analysis. Microstructural evolution was examined using scanning electron microscopy (SEM LEO-1530 and LEO-1455VP). The average grain size of the sintered samples was measured by the linear intercept method. Vickers hardness was performed on polished surface using a microhardness testers (Struers duramin 0.01). Dielectric measurements were carried out using an impedance analyzer (HP 4192A LF) in conjunction with a non-inductively wound tube furnace. Fired-on silver electrodes (Gwent Electronics Materials, UK) were applied to pellets which had been ground to a thickness of 1.0 mm. An electrical contact was made to the pellets using a sprung silver wire. The permittivity was measured at a frequency of 1 kHz over a range of temperatures.

3. Results and discussion

X-ray diffraction results for sintered ceramics containing up to 5 vol% Al_2O_3 (~2.5 wt%) are shown in Fig. 1. All patterns were similar, and showed only PZ diffraction peaks [10], with no measurable change in *d*-spacing for different

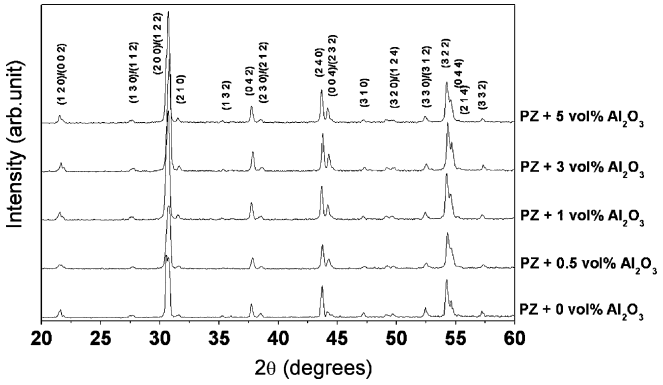

Fig. 1. X-ray diffraction patterns of the surface of PZ and PZ–Al_2O_3 pellets sintered at 1300 °C; peaks are indexed against PZ [10].

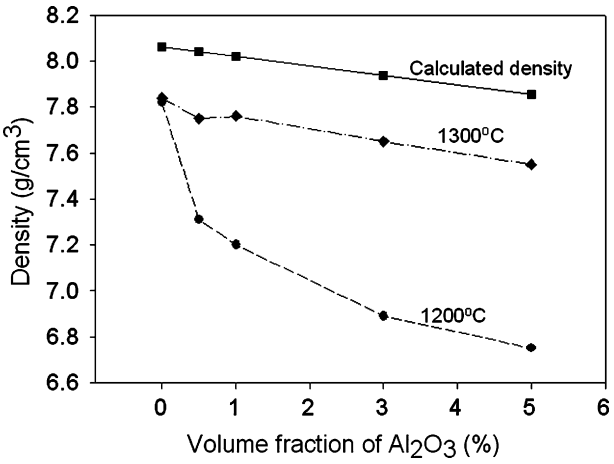

Fig. 2. Values of sintered pellet density vs. Al_2O_3 content for samples sintered at 1200 and 1300 °C.

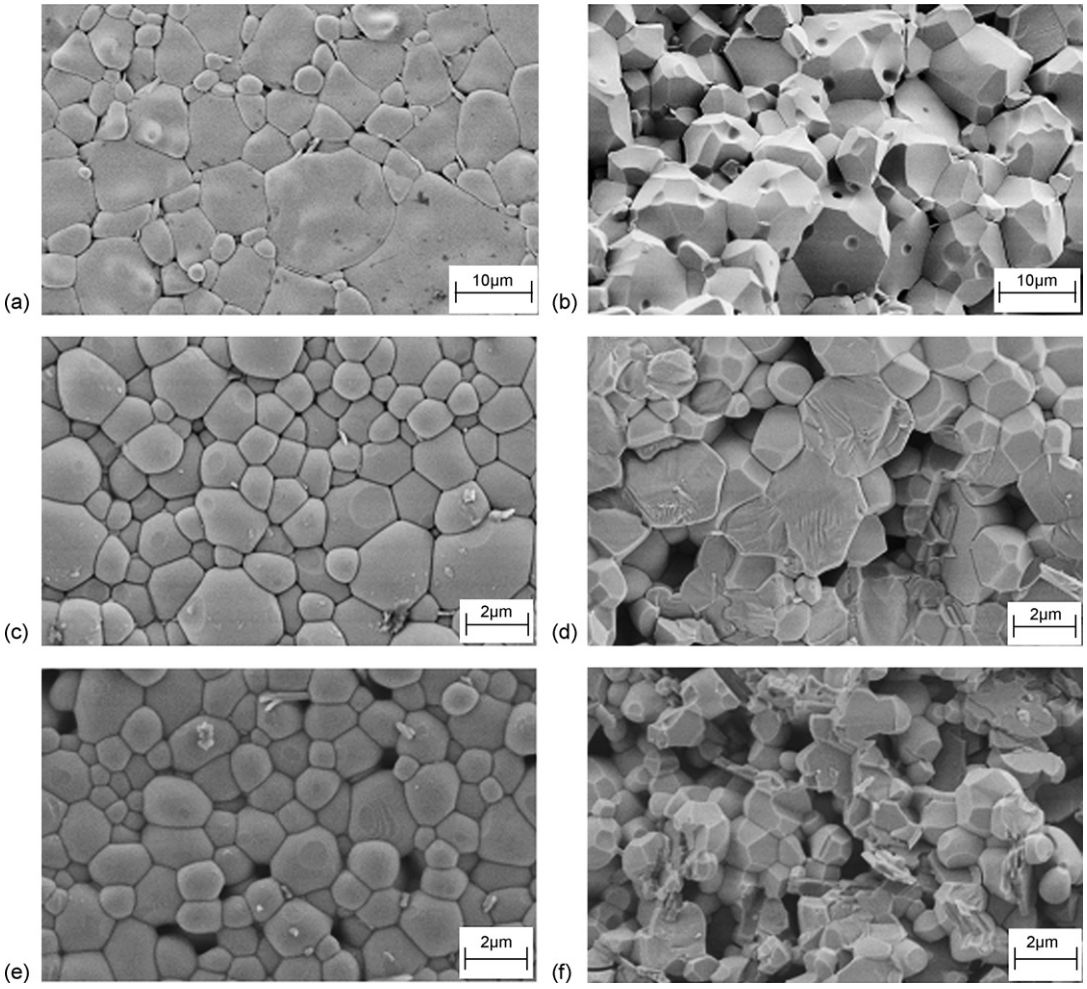

Fig. 3. SEM micrographs of as-sintered and fracture surfaces of samples sintered at 1200 °C (a and b) PZ, (c and d) PZ–1 vol% Al_2O_3, (e and f) PZ–5 vol% Al_2O_3.

Al_2O_3 contents. The densities of the PZ–Al_2O_3 ceramics, sintered at 1200 °C, were lower than for unmodified PZ. The density decreased from 7.82 g cm^{-3} for PZ to 7.31 g cm^{-3} for the PZ–0.5 vol% Al_2O_3 sample, and to 6.75 g cm^{-3} for the PZ–5 vol% Al_2O_3 sample (Fig. 2). Raising the sintering temperature to 1300 °C brought about a significant increase in the measured density of the PZ–Al_2O_3 samples, with densities of 7.75 g cm^{-3} for PZ–0.5 vol% Al_2O_3 and 7.55 g cm^{-3} for the PZ–5 vol% Al_2O_3 samples. Hence, samples sintered at 1300 °C showed only a slight fall in density with increasing Al_2O_3 content. The porosity levels evident in SEM micrographs of the pellet surfaces were consistent with trends in measured density values (Figs. 3 and 4). A full kinetic study would be required to resolve the reasons for the inhibiting effect of the added nanoparticles on densification (which was most evident at the lower sintering temperature). It is possible that second-phase particles impede diffusion along grain boundaries, and/or that the process of removing material from grain boundaries for subsequent diffusion to pores is energetically more difficult, as has been suggested for other types of ceramic composites [9,11]. Differential shrinkage of second-phase material may also have an inhibiting effect.

Microstructural analysis revealed that Al_2O_3 additions produced a notable decrease in grain size (Figs. 3 and 4). Average values of grain size, as measured by the linear intercept method, decreased from ~13 μm for unmodified PZ to ~1 μm for all PZ–Al_2O_3 compositions sintered at 1300 °C (Fig. 5). For the lower sintering temperature of 1200 °C, the grain size was ~6 μm for PZ and ~1 μm for the PZ–Al_2O_3 samples. Hence, Al_2O_3 inhibited grain growth to the

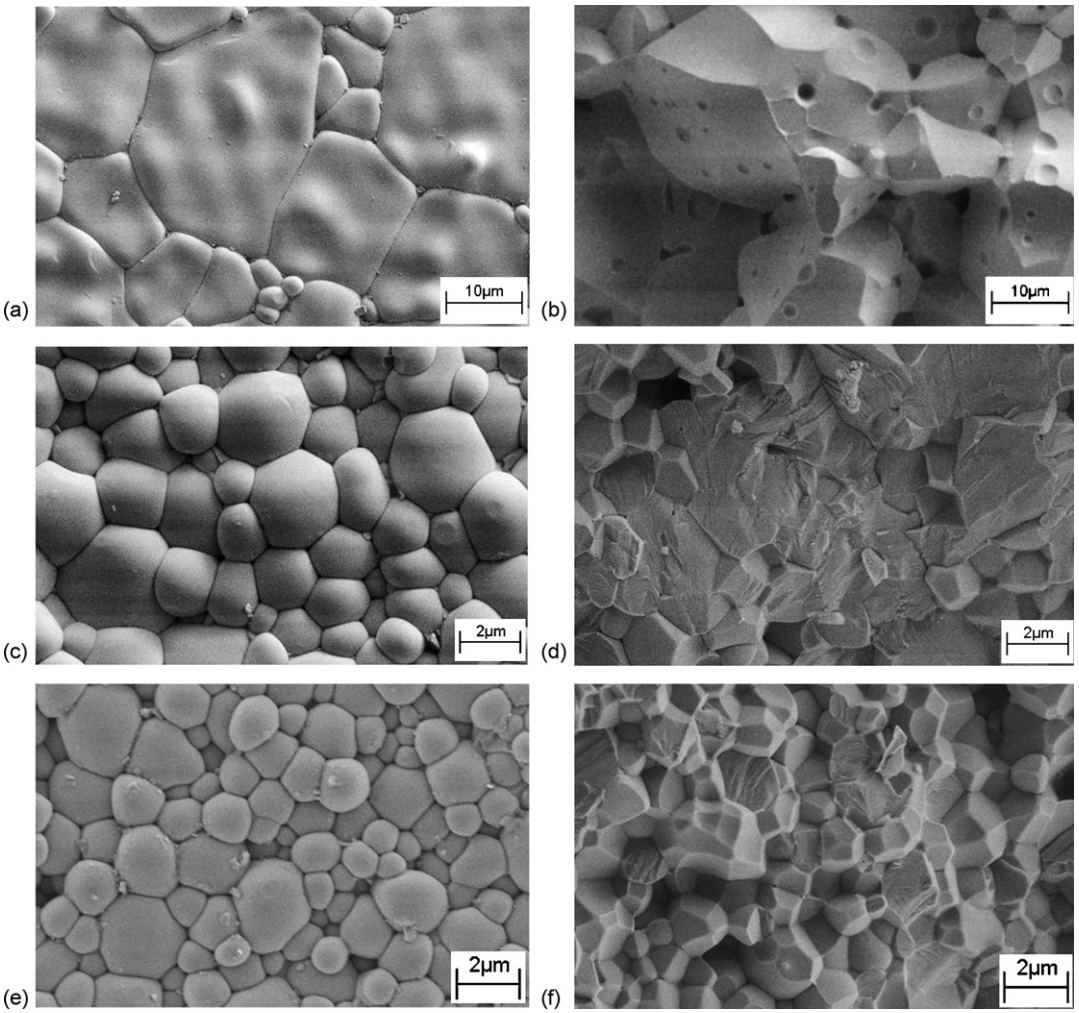

Fig. 4. SEM micrographs of as-sintered and fracture surfaces of samples sintered at 1300 °C (a and b) PZ, (c and d) PZ–1 vol% Al_2O_3, (e and f) PZ–5 vol% Al_2O_3.

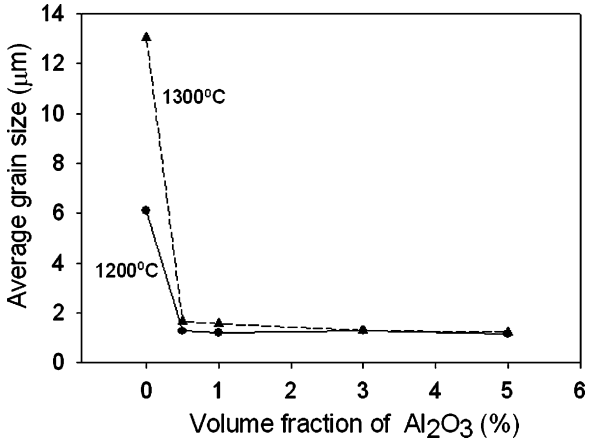

Fig. 5. Average grain size vs. Al_2O_3 content for samples sintered at 1200 and 1300 °C.

extent that there was little or no increase in grain size on increasing the sintering temperature from 1200 to 1300 °C. There was a high uniformity in grain size across each sample, implying that the processing method produced a reasonably uniform distribution of the additive. The suppression of grain growth may imply that changes in surface and/or grain boundary energies take place as a consequence of chemical interactions between the PZ matrix grains and the original Al_2O_3 particles.

A detailed examination of the SEM micrographs from the present PZ–Al_2O_3 compositions revealed evidence of ~100 nm grains at some triple points, and other grain boundary regions. These are highlighted by arrows in Fig. 6, for a PZ–1 vol% sample. This type of feature was also present in other PZT–Al_2O_3 samples. Back-scattered SEM imaging did not reveal any atomic number contrast difference which would have indicated the nanosized grains to differ in composition from the larger grained matrix. However, this finding is inconclusive, as the ~100 nm grains in question are much smaller than the penetration volume of the electron beam in the sample. The effects of beam overlap with the matrix would obscure any difference in chemical composition of the nanograins and matrix.

Fracture surfaces of dense samples of PZ and PZ–Al_2O_3 sintered at 1300 °C indicated a change from predominantly inter-granular fracture in unmodified PZ, Fig. 4(b), to mostly intra-granular (transgranular) cleavage for the PZ–Al_2O_3 samples (Fig. 4(d and f)). It is estimated that the fractional area showing intra-granular fracture increased to ~80% coverage for both 0.5 and 1 vol% Al_2O_3 samples, but fell to ~40% for the 3 and 5 vol% Al_2O_3 compositions. An intra-granular mode of fracture is consistent with a strengthening of the grain boundaries, which encourages the crack to pass through the grain rather than along the grain boundary [12]. Grain size is also known to affect the mode of fracture, although there are conflicting reports as to the precise relationship between grain size and fracture mode [13,14]. Here, we find intra-granular fracture in the smaller grained PZ–Al_2O_3 samples, and mainly inter-granular fracture in the coarse grained PZ samples. The increasing proportion of inter-granular fracture in the 3 and 5 vol%

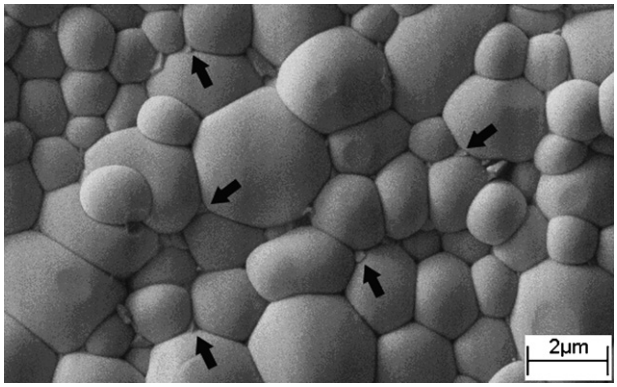

Fig. 6. SEM micrograph of a PZ–1 vol% Al_2O_3 sample sintered at 1300 °C: arrows indicate possible Al_2O_3 grains.

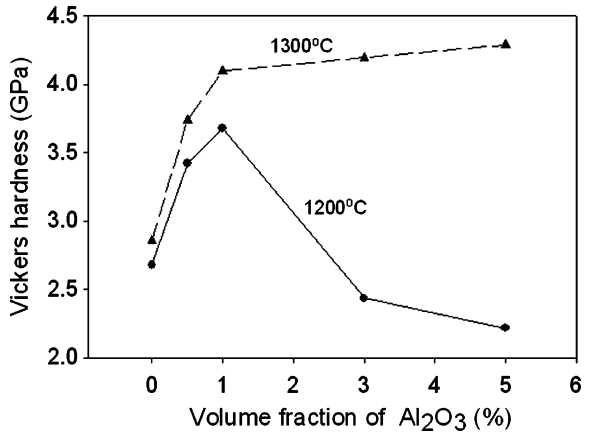

Fig. 7. Values of Vickers hardness vs. Al_2O_3 content for samples sintered at 1200 and 1300 °C.

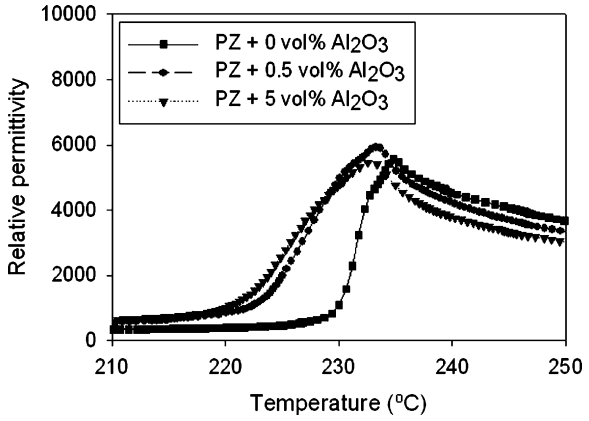

Fig. 8. Relative permittivity, ε_r (at 1 kHz) vs. temperature for samples of differing Al_2O_3 content sintered at 1300 °C.

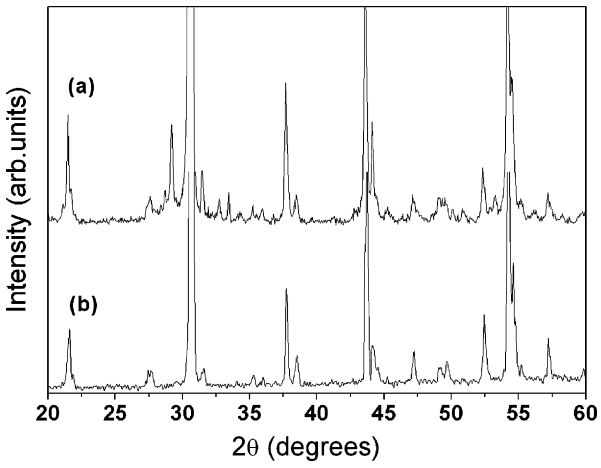

Fig. 9. X-ray diffraction patterns: (a) PZ–10 vol% Al_2O_3 (PZ–5 wt% Al_2O_3) sintered pellet showing extra peaks compared to those of PZ and (b) pattern of PZ–0 wt% Al_2O_3 reproduced at a similar intensity scale for comparison. The *d*-spacing and intensity data from (a) are listed in Table 1.

samples, relative to the 0.5 and 1 vol% samples of comparable grain size, is probably associated with the slightly more porous microstructures of the former (Fig. 4(e)). However, any segregation of second-phase material in the microstructures may also affect fracture mode [15]. The PZ–Al_2O_3 samples obtained by sintering at 1200 °C, showed extensive regions of inter-granular fracture, as anticipated from their significantly lower densities (Fig. 2).

Vickers hardness data indicated that Al_2O_3 additions increased the hardness of all high-density samples (Fig. 7). In samples sintered at 1300 °C there was a sharp increase from 2.9 GPa for PZ to 4.1 GPa for PZ–1 vol% Al_2O_3, but subsequently there was a more gradual increase reaching 4.4 GPa for the 5 vol% sample. The increased hardness, which loosely can be expected to relate to an increased fracture strength in the nanocomposites [6] is in agreement with the change in the observed mode of fracture, from inter- to intra-granular [9,15]. For the lower sintering temperature, 1200 °C, initially the trend was similar to the 1300 °C sample, but hardness values decreased to below those of unmodified PZ for the two highest Al_2O_3 contents. This fall-off is again consistent with the much lower density of the 3 and 5 vol% Al_2O_3 samples at the lower sintering temperature.

Table 1
X-ray diffraction data for a PZ–10 vol% Al_2O_3 (5 wt% Al_2O_3) sample together with JCPDS data for $PbZrO_3$ [10], $Pb_2Al_2O_5$ [18] and $PbAl_2O_4$ [19]; only *d*-spacings of peaks with $I/I^* \geq 20$ are listed for the lead aluminium oxides

PZ–5 wt% Al_2O_3		$PbZrO_3$ [10]		$Pb_2Al_2O_5$ [18]		$PbAl_2O_4$ [19]	
d-spacing	I/I^*	*d*-spacing	I/I^*	*d*-spacing	I/I^*	*d*-spacing	I/I^*
7.590	1			7.660	20		
6.621	1			6.630	20		
5.873	2	5.892	1	5.920	70		
5.417	2			5.420	20		
5.295	2	5.268	5				
5.233	2						
4.701	1			4.680	20	4.620	60
4.438	1						
4.376	1			4.420	40	4.450	90
4.211	2					4.240	50
4.142	8	4.165	11				
4.097	2	4.113	7			4.060	70
4.047	1			3.990	50		
3.860	1			3.820	20		
				3.540	50		
3.260	2	3.268	2	3.310	70		
3.237	3	3.242	3	3.210	100		
3.144	2			3.120	60		
3.113	3					3.120	80
3.061	11					3.070	100
2.930	80	2.946	46	2.957	100		
2.917	100	2.926	100				
2.846	6	2.856	4				
2.737	2			2.704	90		
2.681	3						
2.619	1					2.631	70
2.550	2	2.558	1			2.541	60
2.500	2					2.514	50
2.390	15	2.395	11	2.419	30		
2.350	2	2.356	2			2.381	20
2.340	3	2.346	2	2.308	70	2.308	20
				2.339	40		
2.228	2					2.236	60
						2.223	50
2.188	2			2.177	40	2.176	40
						2.152	20
2.114	2					2.116	40
2.078	36	2.080	19				
2.054	11	2.056	11				

Measurements of relative permittivity (ε_r) as a function of temperature revealed subtle differences between unmodified PZ and PZ–Al_2O_3 samples (Fig. 8). PZ is antiferroelectric (AFE) with an orthorhombic structure at room temperature. The orthorhombic phase transforms to a ferroelectric (FE) rhombohedral phase a few degrees below the Curie temperature (T_c), which occurs at ~235 °C signifying the transition of the ferroelectric phase to the paraelectric (PE) cubic phase [16]. In the present PZ samples, the measured T_c value for the ferroelectric to paraelectric transition was ~236 °C, consistent with literature values [16]. For all of the PZ–Al_2O_3 samples, the T_c values were 2–3 °C lower than for PZ. Although the variation is in the error range often associated with this type of measurement, the small difference in T_c values was reproducible in all repeat experiments. Further evidence that a real effect was being observed was found in the change in the shape of the ε_r–T plots below T_c. Generally, transitions between AFE and FE phases give rise to changes in slope of ε_r–T plots. Therefore, chemical reactions may have occurred in the nanocomposites during sintering which affect both the AFE–FE and FE–PE transitions, leading to slight changes in the ε_r–T plots.

We found no evidence of reaction products in the XRD patterns of PZ–Al_2O_3 for 0.5–5 vol% samples, but as the XRD detection limit is a few wt%, it would be unlikely that any second-phase reaction products would show up, even in the limiting composition (2.5 wt% Al_2O_3). Similarly, if the original nanoparticles remained as discrete Al_2O_3 grains they would be difficult to detect. In order to increase the probability that Al_2O_3, or secondary reaction products, if present, were detectable by XRD, a sample with a higher Al_2O_3 content, 5 wt% (10 vol%), was prepared. In the pre-sintered sample, second-phase γ-Al_2O_3 [17] arising from the starting nanopowder was evident. After sintering at 1300 °C, no second-phase Al_2O_3 peaks were present, but other faint peaks appeared (Fig. 9(a)). The high additive did allow the identification of second-phase reaction products, but the porosity of the sample was too high for meaningful physical property evaluation. Searches of JCPDS data revealed that the extra peaks corresponded to the published XRD patterns of $Pb_2Al_2O_5$ [18] and $PbAl_2O_4$ [19]. The experimental and standard XRD data are presented in Table 1. Similar standard XRD patterns are also reported for $PbAl_{12}O_{19}$, $Pb_9Al_8O_{21}$ and $Pb_{11}Al_{12}O_{19}$ phases, therefore, the possibility of their co-existence with $Pb_2Al_2O_5$ and $PbAl_2O_4$ cannot be discounted.

Based on these findings it is possible that the ~100 nm grains observed in the microstructures of nanocomposites with lower Al_2O_3 contents (Fig. 6) may be lead aluminium oxides, formed by diffusion reactions during high temperature sintering. It would be difficult to unambiguously identify lead aluminium oxide grains by SEM or TEM chemical analysis techniques, due to matrix interference effects.

With reference to the changes in dielectric response (Fig. 8), the formation of lead aluminium oxides would denude the PZ matrix of PbO, leading to the formation of Pb and O ion vacancies. The resulting change in defect chemistry may be the reason for the slight changes in transition temperatures. Limited substitution of Al^{3+} on the PZ lattice to form a PZ–Al_2O_3 solid solution (PZ_{ss}) could also occur and affect the properties.

At this stage the compositional limit (i.e. starting PZ/Al_2O_3 ratio) between a microstructure composed of single phase PZ_{ss}, and one containing PZ_{ss} and lead aluminium oxides, is uncertain. It is possible that lead aluminium oxide phases form, and contribute to property changes, in at least some of the PZ 0.5–5 vol% Al_2O_3 samples studied here. Hence, Al_2O_3 nanoparticles may not be directly responsible for the properties of the sintered ceramic, and care has to be exercised when using the term ''PZ–Al_2O_3 nanocomposite''.

4. Conclusions

Additions of Al_2O_3 nanoparticles in the range 0.5–5 vol% to lead zirconate were found to inhibit densification, and suppress grain growth, resulting in an approximately 10-fold decrease in average grain size. The additive promoted intra-granular fracture and Vickers hardness values increased by up to ~50%. X-ray diffraction results for a $PbZrO_3$–10 vol% Al_2O_3 ceramic indicated that a reaction between the matrix and additive occurred during sintering. The products were lead aluminium oxides, but no Al_2O_3 was detected. The reactions may play an important role in determining the microstructure and properties of such materials.

Acknowledgements

This work was supported by The Thailand Research Fund, Ministry of Education (Thailand) and Graduate School, Chiang Mai University. The authors would like to thank Prof. Dr. Tawee Tunkasiri for his help in many facilities. Thanks are also expressed to colleagues at the University of Leeds for practical advice and to A. Chowdhury for assistance with XRD data processing.

References

[1] K. Niihara, J. Ceram. Soc. Jpn. 99 (10) (1991) 974–982.
[2] A. Nakahira, K. Niihara, J. Ceram. Soc. Jpn. 100 (4) (1991) 448–453.
[3] C.E. Borsa, S. Jiao, R.I. Todd, R.J. Brook, J. Microscopy 177 (3) (1995) 305–312.
[4] H.J. Hwang, K. Niihara, J. Mater. Sci. 33 (2) (1998) 549–558.
[5] H.J. Hwang, K. Watari, M. Sando, M. Toriyama, K. Nihara, J. Am. Ceram. Soc. 80 (3) (1997) 791–793.
[6] K. Tajima, H.J. Hwang, M. Sando, K. Niiihara, J. Eur. Ceram. Soc. 19 (6–7) (1999) 1179–1182.
[7] H.J. Hwang, K. Tajima, M. Sando, M. Toriyama, K. Niihara, J. Ceram. Soc. Jpn. 108 (4) (2000) 339–344.
[8] K. Tajima, H. Hwang, M. Sando, K. Niihara, J. Am. Ceram. Soc. 83 (3) (2000) 651–653.
[9] K. Tajima, H.J. Hwang, M. Sando, K. Niihara, Key Eng. Mater. 175–176 (2000) 229–234.
[10] Powder Diffraction File No. 81-2042, International Centre for Diffraction Data, Newton Square, PA, 2000.
[11] L.C. Stearns, J. Zhao, M.P. Harmer, J. Eur. Ceram. Soc. 10 (6) (1992) 473–477.
[12] K. Niihara, A. Nakahira, in: P. Vincenzini (Ed.), Advanced Structural Inorganic Composites, Elsevier Science Publisher Ltd., 1990, pp. 637–664.
[13] P.L. Gutsall, G.E. Cross, Eng. Fract. Mech. 1 (1969) 463–471.
[14] R.M. Spriggs, J.B. Mitchell, T. Vasilos, J. Am. Ceram. Soc. 47 (7) (1964) 323–327.
[15] R.W. Rice, J. Am. Ceram. Soc. 77 (10) (1994) 2539–2553.
[16] B.A. Scott, G. Burns, J. Am. Ceram. Soc. 55 (7) (1972) 331–333.
[17] Powder Diffraction File No. 79-1558, International Centre for Diffraction Data, Newton Square, PA, 2000.
[18] Powder Diffraction File No. 19-0672, International Centre for Diffraction Data, Newton Square, PA, 2000.
[19] Powder Diffraction File No.19-0673, International Centre for Diffraction Data, Newton Square, PA, 2000.

Available online at www.sciencedirect.com
ScienceDirect
Current Applied Physics 8 (2008) 253–257
Current Applied Physics
An official journal of the KPS
www.elsevier.com/locate/cap
www.kps.or.kr

Development of electrical properties in lead-free bismuth sodium lanthanum titanate–barium titanate ceramic near the morphotropic phase boundary

P. Jarupoom, K. Pengpat *, N. Pisitpipathsin, S. Eitssayeam, U. Intatha, G. Rujijanagul, T. Tunkasiri

Department of Physics, Faculty of Science, Chiang Mai University, Chiang Mai 50200, Thailand

Available online 25 October 2007

Abstract

The near morphotropic phase boundary (MPB) of lead-free piezoelectric ceramics based on bismuth sodium lanthanum titanate ($Bi_{0.487}Na_{0.487}La_{0.017}TiO_3$:BNLT) and barium titanate ($BaTiO_3$:BT) was carefully investigated by a modified two step mixed-oxide method. In this case the BNLT and BT powders were produced separately using calcination temperatures of 900 °C and 1200 °C, respectively. After that they were mixed with the desired compositions of $(1-x)$BNLT–xBT, where $x = 0.00$, 0.02, 0.04, 0.06, 0.08, and 0.10. Then the powders were pressed and subsequently sintered at various temperatures to obtain the maximum density under each condition. It was found that the BT addition has a significant effect on grain growth inhibition of the BNLT–BT ceramics and this in turn gave rise to an enhancement in dielectric constant (ε_r) of the corresponding ceramics. The piezoelectric coefficient (d_{33}) was also improved greatly to about 130 pC/N in the 0.96BNLT–0.04BT ceramic sample sintered at 1125 °C. This offered an opportunity to obtain a good candidate for replacing the lead-based piezoelectrics.

PACS: 77.65.Bn; 71.45.Gm; 61.05.cp; 68.37.Hk

Keywords: BNLT; BT; Lead-free piezoelectric ceramic; Two step mixed-oxide method

1. Introduction

In the past few decades, extensive studies have been carried out in order to find replacements for lead-based piezoelectric materials, such as (Pb, Zr)TiO_3 (PZT), $PbTiO_3$ (PT) and $Pb(Mg_{1/3}Nb_{2/3})O_3$ (PMN), because of environmental concern. One of the most studied compounds is ferroelectric bismuth sodium titanate ($Bi_{0.5}Na_{0.5})TiO_3$ (BNT), discovered by Smolenskii et al. [1]. It has interesting electrical properties (good dielectric constant (ε_r) and acceptable piezoelectric coefficient (d_{33})). Its crystal structure is rhombohedral with strongly ferroelectric behavior. The Curie temperature T_c is about 320 °C, remanent polarization $P_r = 38\ \mu C/cm^2$ and coercive field $E_c = 73$ kV/cm. Another phase transition occurs at about 200 °C (T_p) which is believed to be the transition from ferroelectric rhombohedral to antiferroelectric tetragonal, which is further changed to the paraelectric cubic phase at T_c [2,3]. It is normally found that the ε_r–T curve at the T_c of this material has a high degree of broadness, indicating relaxor-type ferroelectric behavior.

However, the Bi ion is highly volatile at high temperature above 1130 °C during sintering, making this material difficult to pole due to its high conductivity [4]. The solution to this problem has been found by many researchers who were able to modify the BNT crystal by the substitution of other A- and B-site cations, such as in $(Bi_{0.5}Na_{0.5})_{(1-1.5x)}La_xTiO_3$: BNLT [5], BNT–$BaTiO_3$ [6], BNT–$KNbO_3$ (KN) [7], and BNT–Ba(Ti, Zr)O_3 [8]

* Corresponding author.
E-mail address: kpengpat@gmail.com (K. Pengpat).

1567-1739/$ - see front matter © 2007 Elsevier B.V. All rights reserved.
doi:10.1016/j.cap.2007.10.010

solid-solution ceramic systems. The piezoelectric properties of these ceramics were significantly improved. Recently, another interesting system was reported by Pengpat et al. [9] who combined two ideas, (1) the rare earth additive of La^{3+} suggested by Herabut and Safari [5], and (2) a solid solution of BNT–BT suggested by Takenaka et al. [6], in order to produce a new system of $(1-y)(Bi_{0.5}Na_{0.5})_{(1-1.5x)}La_xTiO_3$ (BNLT)–$yBaTiO_3$ (BT), where $x = 0.017$ and $y = 0$, 0.06, 0.1, 0.15, 0.2. They found that a maximum d_{33} of about 112 pC/N could be achieved with the composition of $y = 0.15$ which is not the morphotropic phase boundary (MPB) composition ($y = 0.1$) reported in this work. Moreover, this MPB composition is different from that of the $(1-x)$BNT–xBT system of Takenaka et al. whose MPB was observed at about $x = 0.06$. This may be due to different homogeneity of the samples prepared using different preparation methods. Moreover, the series of compositions of varying BT content (y) from $(1-y)$BNLT–yBT is not complete enough to determine the exact MPB of this system, making it difficult to compare the results to those of the previous works.

In this work, the $(1-x)$BNLT–xBT system has been further investigated by conventional methods, where the range of x values was chosen near the MPB of BNT–BT system (about 6 mol% BT) and 1.7 mol% La^{3+} doped BNT which is the optimum composition of the BNLT system. The physical, dielectric and piezoelectric properties of the BNLT–BT ceramics were investigated. The microstructures of the ceramics in this system were also examined. The results were compared to those of the previous works.

2. Experimental procedure

High purity (purity > 99.0%) powders of bismuth oxide (Bi_2O_3), sodium carbonate (Na_2CO_3), lanthanum oxide (La_2O_3), titanium oxide (TiO_2) and barium carbonate ($BaCO_3$) were used as starting materials for producing $(1-x)(Bi_{0.487}Na_{0.487}La_{0.017}TiO_3)$–$x(BaTiO_3)$, where $x =$ 0.0, 0.02, 0.04, 0.06, 0.08 and 1.0. The batch compositions of BNLT and BT were weighed and mixed by ball-milling for 24 h. Then both mixtures of BNLT and BT compositions were dried and calcined at 900 °C and 1200 °C, respectively, which are the optimum calcination temperatures for producing highly pure powders of both phases. Both powders were then mixed corresponding to the above formula by ball-milling for 24 h with acetone as the dispersion media. After drying and sieving the mixtures, the obtained powder was made into pellets of 15 mm in diameter by uniaxial pressing in a stainless steel die. The pellets were sintered between 1050 °C and 1150 °C in an electric furnace in an air atmosphere under controlled heating and cooling rates of 5 °C/min with 2 h dwell time. The phase identification and density of the sintered ceramic samples was investigated using X-ray diffraction (XRD: Siemen D-500) and Archimedes' method, respectively. Scanning electron microscopy (SEM: JSM-6335F) was used to observe the microstructures of the ceramics. The grain sizes of each sample were measured by the mean linear intercept. The two parallel surfaces of the sintered ceramics were polished and coated with silver paste as electrodes for electrical contact. To measure the relevant electrical properties, the prepared ceramic samples were poled in a silicone oil bath at 50 °C at 3.0 KV/mm for 15 min. The samples were then left at room temperature for 24 h after poling, and the piezoelectric measurements were measured using a piezoelectric-d_{33}-meter (Model 8000, Pennebaker). The dielectric constant (ε_r) of all ceramic samples was measured at various frequencies from 1 kHz, 10 kHz and 100 kHz and their temperature vs ε_r curves were also measured using an LCZ-meter (Model 4276A, Hewlett Packard).

3. Results and discussion

The XRD patterns of the dense ceramics from BNLT–BT system are shown in Fig. 1. It can be seen that all the peaks in the XRD pattern of the BNLBT0 ceramic correspond to the BNT phase of the JCPDS file No. 34-0360 with rhombohedral structure. The addition of BT phase of $x \geqslant 0.04$ resulted in a splitting of the 200 peak into two peaks of (002) and (200) reflections. This splitting is obvious at $x = 0.06$ and can be clearly seen in the extended XRD patterns of the corresponding ceramics at 2θ between 44° and 48° (Fig. 2). This indicates the change in crystal structure from rhombohedral to tetragonal symmetry of these ceramics and the MPB of this system is found to lie between $x = 0.04$ and $x = 0.06$, where the rhombohedral and tetragonal symmetries coexist, with more BT added, more of the tetragonal phase could be detected in the XRD patterns of the BNLBT ceramics. From the previous work, it was reported that the MPB of the $(1-x)$BNT–xBT system was at $x = 0.06$ [6]. In this work, La^{3+} doping of the BNT–BT has, however, shown no significant effect on the MPB as we found our MPB in the similar region of x between 0.4 and 0.6. This may be attributed to the difference between the ionic radius of La^{3+} ion (130 pm) and

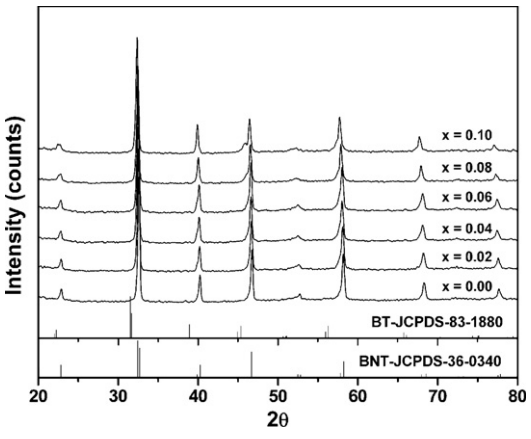

Fig. 1. X-ray diffraction patterns of $(1-x)$BNLT–xBT ceramics, where $x = 0.0$–0.10.

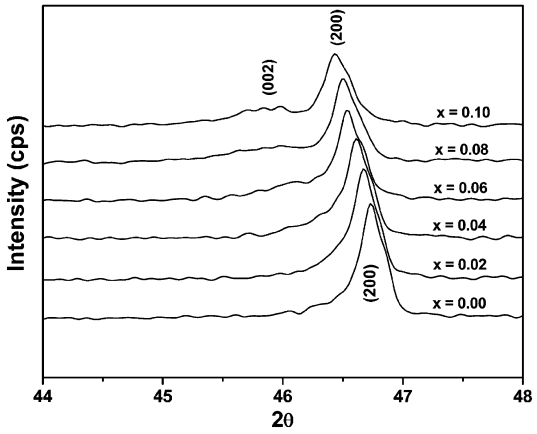

Fig. 2. X-ray diffraction patterns of $(1-x)$BNLT–xBT ceramics at 2θ between 44° and 48°.

Bi^{3+} ion (131 pm) being so small (about 0.8%) and both ions also having the same valency.

The microstructural analysis of all ceramics has been carried out and the SEM micrographs of the as-formed surfaces are illustrated in Fig. 3. All have a dense structure with low porosity. The small addition of BT, however, inhibited grain growth dramatically, as can be seen from the average grain size (Table 1) which was reduced from 4.10 ± 0.46 μm for pure BNLT (Fig. 3(a)) to about 1.86 ± 0.19 μm for the 2 mol% BT added sample (Fig. 3b). This may be attributed to the large difference between ionic radius of Ba^{2+} (156 pm) and Bi^{3+} (131 pm) and the possibility that Ba^{2+} aggregates and forms secondary phases on a very small scale at the grain boundaries. This may prevent grain boundary movement during the sintering process [10]. However, increasing the amount of BT from 0.04 to 0.10 had no significant effect on the grain size and shape of the ceramics as can be seen in Fig. 3c–f.

The experimental on dielectric measurements at room temperature for various BT contents are graphically presented in Fig. 4. It can be clearly seen that ε_r increases with

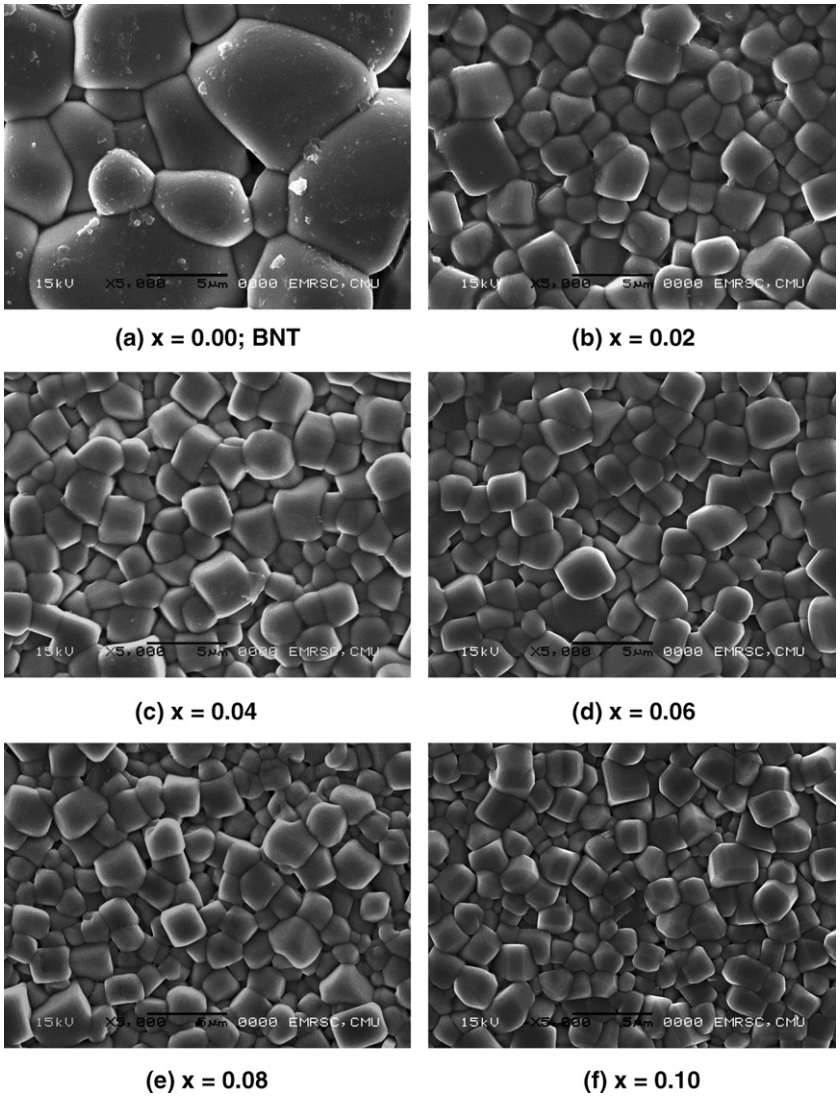

Fig. 3. SEM micrographs of (a) BNT and $(1-x)$BNLT–xBT ceramics, where (b) $x = 0.02$ to (f) $x = 0.10$.

Table 1
The values of density, grain size, dielectric constant (ε_r) and piezoelectric coefficient (d_{33}) at room temperature of $(1-x)$BNLT–xBT samples

Samples	Density (g/cm^3)	Grain size (μm)	ε_r ($T_{room/1\,kHz}$)	d_{33} (pC/N)
BNLT	5.85 ± 0.02	4.10 ± 0.46	780	72
0.98BNLT–0.02BT	5.86 ± 0.03	1.86 ± 0.19	863	118
0.96BNLT–0.04BT	5.86 ± 0.01	1.69 ± 0.16	1060	125
0.94BNLT–0.06BT	5.85 ± 0.01	1.57 ± 0.19	1547	52
0.92BNLT–0.08BT	5.84 ± 0.01	1.55 ± 0.23	1598	24
0.90BNLT–0.10BT	5.84 ± 0.01	1.47 ± 0.15	1615	25

increasing BT (x) and reaches a maximum at $x = 0.06$. Further addition of BT gradually increases ε_r up to $x = 0.10$. Initially, the considerable increase in ε_r values from $x = 0.02$ (rhombohedral structure) to $x = 0.06$ (rhombohedral + tetragonal structures) may be mainly due to the presence of tetragonal phase coexisting in the MPB compositions, but above this point the grain size and density may play a more important role in controlling the ε_r values of these ceramics, since the density values and grain size of the BNLT–BT samples changes slightly with increasing BT as shown in Table 1. This trend was observed at all frequencies. The dielectric loss ($\tan\delta$) was found to increase slightly up to $x = 0.04$, above which it increases monotonically with increasing BT content. This can be related to the density, which was found to decrease, indicating greater porosity, when the BT content is greater than $x = 0.04$.

The temperature dependence of the dielectric constant for all the BNLT–BT ceramics is shown in Fig. 5. A reduction of T_c was observed for the BT-containing samples, which is expected because the BT ceramic has a lower value of T_c (~130 °C compared with that of BNLT, ~340 °C). This result is consistent with the previous work [6]. The $\tan\delta$ value of all BT-containing samples is found to be lower than that of the pure BNLT sample, leading to the lower conductivity of these BNLT–BT ceramics at higher temperature (>90 °C). The important mechanism of ionic

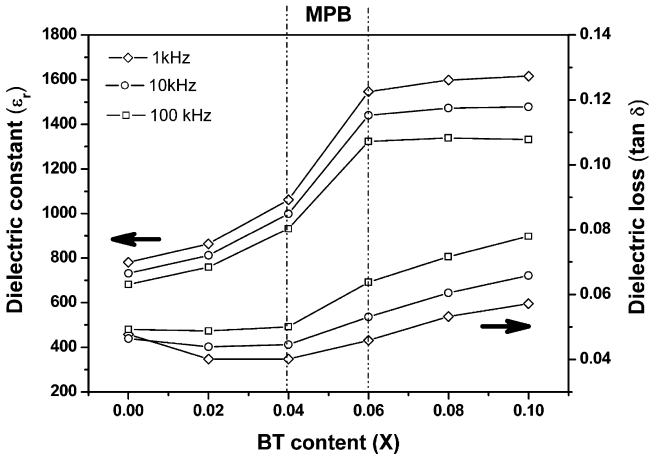

Fig. 4. The dielectric constant (ε_r) and loss tangent ($\tan\delta$) at room temperature vs BT content (x) in the $(1-x)$BNLT–xBT system.

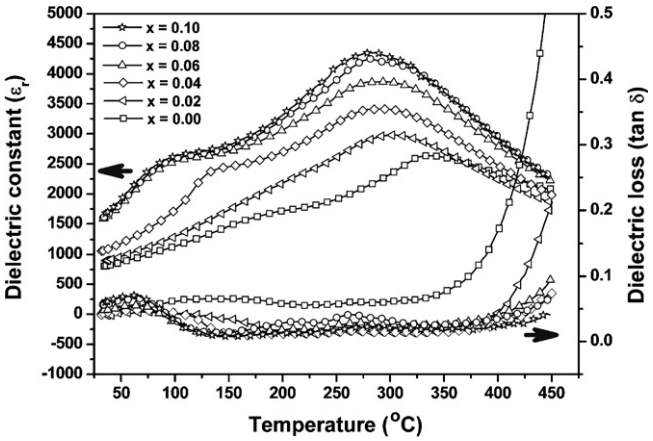

Fig. 5. Variation of dielectric constant (ε_r) and loss tangent ($\tan\delta$) with temperature for $(1-x)$BNLT–xBT ceramics at 1 kHz.

conductivity in these ceramics is the movement of ions which are the current carriers. It has been long known that the alkali ion is a good current carrier in ceramics; therefore, this ion plays an important role in the conductivity of the BNLT ceramics, since the Na^+ ions in BNLT move easily upon heating, resulting in the increase in conductivity with increasing temperature. In BT doping ceramics, the large Ba^{2+} (156 pm) ions are substituted into the A-sites of the BNLT, which possibly blocks the passage of the Na^+ current carriers, causing a reduction of conductivity in the BNLT–BT ceramics which gradually increases upon heating. When the temperature is further increased above T_c, the conductivity or ($\tan\delta$) is found to increase dramatically, as a result of the structural change from tetragonal to cubic at the Curie temperature.

The piezoelectric coefficient (d_{33}) values were measured by a d_{33} meter. Table 2 shows that BT content reaches a limit in enhancing the d_{33} value at $x = 0.04$ at which the maximum d_{33} value is about 130 pC/N. After that, the increase in tetragonal phase lowers the d_{33} value of the ceramics, reducing it to as low as 32 pC/N in the $x = 0.10$ sample. This may be attributed to the decrease in density of the high BT content samples.

Table 2 shows the important properties of the BNLT, and BNLT–BT samples prepared in this work, compared to previous results. It is clearly seen that the BT phase has a significant effect in enhancing the d_{33} of BNLT ceramics. In this work, the maximum d_{33} value was about

Table 2
The values of dielectric constant (ε_r), loss tangent ($\tan\delta$) and piezoelectric coefficient (d_{33}) at room temperature of selected samples compared to the literature values

Samples	ε_r (T_{room})	$\tan\delta$ (T_{room})	d_{33} (pC/N)
BNLT (this work)	730 (1 kHz)	0.05 (1 kHz)	72
0.96BNLT–0.04BT (this work)	1000 (10 kHz)	0.04 (10 kHz)	130
BNLT [5]	550 (1 kHz)	0.04 (1 kHz)	91
0.94BNT–0.06BT [3]	950 (10 kHz)	0.01 (10 kHz)	125

130 pC/N at the MPB composition of $x = 0.04$ (0.96BNLT–0.04BT), which is slightly higher than for the BNT–BT system (about 125 pC/N) [3].

4. Conclusions

The dielectric and piezoelectric properties of $(1 - x)$BNLT–xBT ceramics were determined. The piezoelectric coefficient (d_{33}) can be improved to a value of about 130 pC/N in the 0.96BNLT–0.04BT ceramic sample. The dielectric constant (ε_r) of the BNLT–BT ceramics was enhanced by the addition of BT content, while at the same time, their T_c was lowered. Moreover, BT doping helped to reduce the dielectric loss ($\tan\delta$) of the ceramics at high temperature.

Acknowledgements

The authors would like to thank the Thailand Research Fund and Faculty of Science, Chiang Mai University for financial support. The sincere thanks also go to the Research Laboratory for Excellent Electronic Materials, Department of Physics, and Graduate School, Chiang Mai University.

References

[1] G.A. Smolenskii, V.A. Isupov, A.I. Agranovskaya, N.N. Kraink, Sov. Phys. Solid State 2 (1961) 2651.
[2] K. Sakata, Y. Masuda, Ferroelectrics 5 (1994) 347.
[3] T. Takenaka, K. Maruyama, K. Sakata, Jpn. J. Appl. Phys. 30 (9B) (1991) 2246.
[4] T. Takenaka, H. Nagata, J. Eur. Ceram. Soc. 25 (2005) 2693.
[5] A. Herabut, A. Safari, J. Am. Ceram. Soc. 80 (11) (1997) 2954.
[6] T. Takenaka, K. Sakata, K. Toda, Jpn. J. Appl. Phys. 28 (1989) 59.
[7] H. Ishii, H. Nagata, T. Takenaka, Jpn. J. Appl. Phys. 40 (9B) (2001) 5660.
[8] C. Peng, J.F. Li, W. Gong, Mater. Lett. 59 (2005) 1576.
[9] K. Pengpat, S. Hanphimol, S. Eitssayeam, U. Intatha, G. Rujijanagul, T. Tunkasiri, J. Electroceram. 16 (2006) 301.
[10] S.H. Lee, C.B. Yoon, S.B. Seo, H.E. Kim, J. Mater. Res. 18 (2003) 1765.

Available online at www.sciencedirect.com
ScienceDirect
Current Applied Physics 8 (2008) 328–331
Current Applied Physics
An official journal of the KPS
www.elsevier.com/locate/cap
www.kps.or.kr

Electrical properties and phase transition behaviors of Sr-doped 0.8PZT–0.2PNN ceramics

Sukum Eitssayeam, Gobwute Rujijanagul *

Department of Physics, Faculty of Science, Chiang Mai University, Chiang Mai 50200, Thailand

Available online 25 October 2007

Abstract

Dielectric properties and phase transition behaviors of Sr-doped $0.8PbZr_{1/2}Ti_{1/2}O_3$–$0.2PbNi_{1/3}Nb_{2/3}O_3$ ceramics have been investigated. The ceramics were prepared by a normal solid-state method. For undoped sample, very high relative permittivity >30,000 (at 1 kHz) was observed at the transition temperature of 278 °C. With increasing Sr concentration, the degree of diffuse phase transition was enhanced and a linear reduction in the transition temperature was produced.

PACS: 77.84.Dy; 77.80.−e; 77.80.Bh

Keywords: Dielectric properties; Phase transition; Lead zirconate

1. Introduction

Lead zirconate titanate ($Pb(Zr_{1-x}Ti_x)O_3$ or PZT) is a normal ferroelectric material which has been extensively investigated in the literatures because of their high dielectric properties and high piezoelectric coefficient. The high piezoelectric properties of PZT have been observed for compositions near the morphotropic phase boundary (MPB), i.e. at $PbZrO_3$:$PbTiO_3 \sim 0.52$:0.48 [1,2]. The properties of PZT can also improved by doping some ions of alkaline-earth metals such as Ca^{2+}, Sr^{2+} or Ba^{2+}. For example, Sr-modified PZT showed higher dielectric and piezoelectric properties than pure PZT [3]. Commercial PZT ceramics are thus designed in the vicinity of the MPB with various doping elements and these materials have been widely used in electronic applications such as actuators, transducers, and motors [2].

Lead nickel niobate ($Pb(Ni_{1/3}Nb_{2/3})O_3$ or PNN) is a relaxor ferroelectric material originally reported by Smolenskii and Agranovskaya [4]. It shows a diffuse phase transition around −120 °C with a peak permittivity of about 4000. PNN and other normal ferroelectric materials were used to from the binary or the ternary ferroelectric material systems to obtain better electrical properties [5,6]. However, it is interesting to vary the transition temperature of the binary or the ternary ferroelectric material systems for capacitor applications. The aim of the present work is to investigate effect of Sr addition in 0.8PZT–0.2PNN ceramics (MPB composition) on the phase transition behavior. Dielectric properties of the ceramics were also studied.

2. Experimental

The Sr-doped $0.8PbZr_{1/2}Ti_{1/2}O_3$–$0.2PbNi_{1/3}Nb_{2/3}O_3$ (0.8PZT–0.2PNN) ceramics in this study were synthesis by the conventional mixed oxide method. The Sr-doped 0.8PZT–0.2PNN powders were firstly prepared by mixing the starting materials of PbO (>99%), ZrO_2 (>99%), TiO_2 (>99%), NiO (99%), Nb_2O_5 (99.9%) and $SrCO_3$ (98%) powders, where the values of $SrCO_3$ were ranged from 1 to 9 mol% with stepwise of 2 mol%. These powders were ball-milled for 24 h in polyethylene container with zirconia

* Corresponding author. Tel.: +66 5394 3376; fax: +66 5335 7512.
E-mail address: rujijanagul@yahoo.com (G. Rujijanagul).

1567-1739/$ - see front matter © 2007 Elsevier B.V. All rights reserved.
doi:10.1016/j.cap.2007.10.026

balls. After drying at 120 °C, the mixed powders were then calcined at 900 °C for 2 h with heating and cooling rate of 10 °C/min. Subsequently, the calcined samples were pressed into disc shape and sintered at 1250 °C for 2 h with constant heating and cooling rates of 10 °C/min. The phase formation of the samples was studied by an X-ray diffractometer. Micro-structure of the ceramics was examined by the scanning electron microscopy (SEM). For electrical properties characterization, the sintered samples were ground to obtain parallel faces, and the faces were then coated with silver as electrodes by evaporation method. The dielectric constants of the sintered ceramics were measured as a function of temperature with an automated dielectric measurement system. The system consists of a LCR-meter and environment chamber, both temperature and dielectric properties were controlled and recorded by a computer.

3. Results and discussion

Fig. 1 shows the XRD patterns of Sr-doped 0.8PZT–0.2PNN ceramics prepared by the conventional solid-state method. Within the detection limit of the equipment, each XRD pattern exhibits a phase-pure perovskite. On the other hand, no evidence of the pyrochlore or other second phases was observed for all samples. The XRD data is consistent with rhombohedral symmetry, which is indicative of a ferroelectric phase. An increase in the mole fraction of Sr^{2+} did not show any evidence of a change in symmetry. Lattice constant as a function of Sr concentration is shown in Fig. 2. It can be seen that the lattice constant decreased as the amount of Sr^{2+} increased due to the smaller ionic radii of Sr^{2+}.

The grain size as a function of Sr concentration is plotted in Fig. 3. A SEM photograph of 0.1 mol% Sr-doped sample is shown in the inset in the same figure. The result revealed that higher Sr concentration produced a decrease in grain size. It is expected that Sr ions are dissolved in the samples, but beyond the solubility limit it may be accumulated at the grain boundary which would result in the inhibition of grain growth. The result is consistent with the study of Hou et al. [7].

The relative permittivity at different frequency versus temperature of Sr-doped 0.8PZT–0.2PNN is shown in Fig. 4. All composition showed a dispersive dielectric behavior with respect to frequency. However, the frequency dispersion in the 0.8PZT–0.2PNN system is not as strong as other relaxor ceramics such as $Pb(Zn_{1/3}Nb_{2/3})O_3$(PZN) [8]. Fig. 5 shows the maximum relative permittiv-

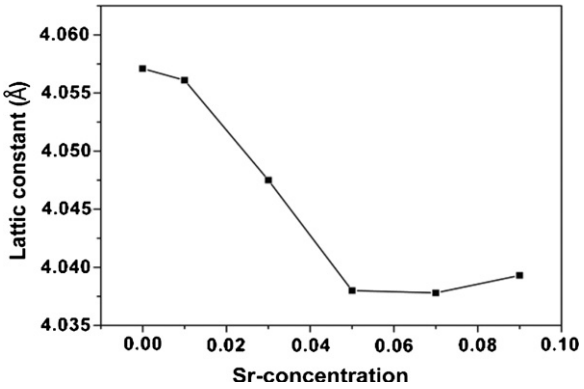

Fig. 2. Lattice parameter (Å) as a function of Sr concentration.

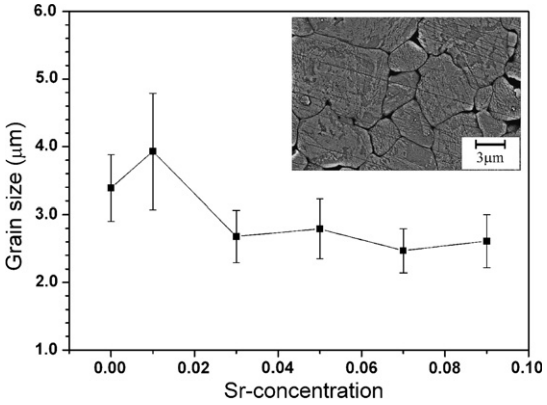

Fig. 3. Grain size as a function of Sr concentration.

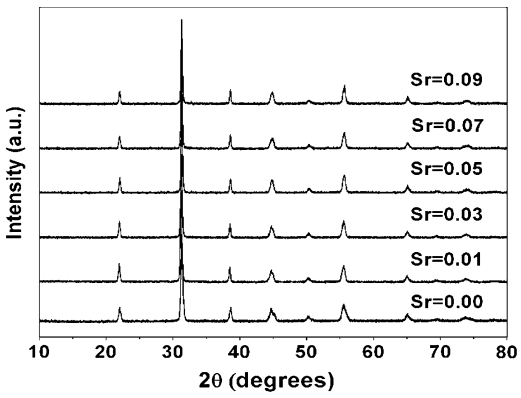

Fig. 1. XRD patterns of 0.8PZT–0.2PNN binary system as a function of Sr concentration.

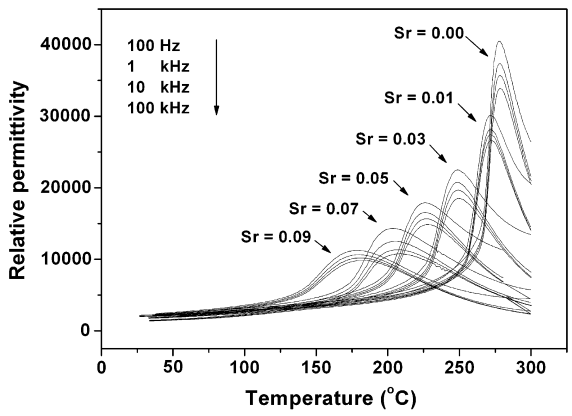

Fig. 4. Relative permittivity as function of temperature for various Sr concentration

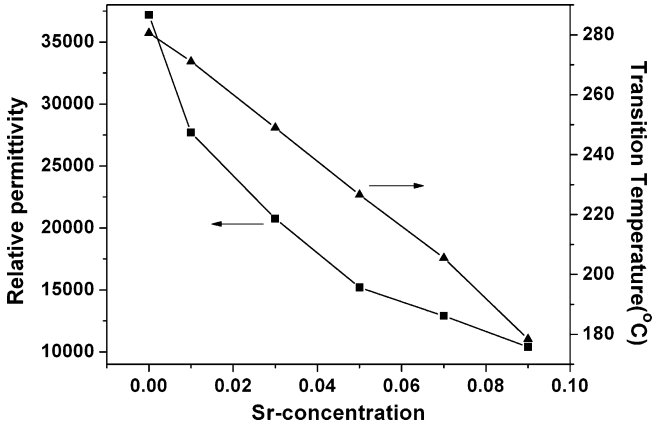

Fig. 5. Transition temperature (T_m) and relative permittivity at T_m as a function of Sr concentration.

ity (ε_m) as a function of Sr concentration. Very high relative permittivity of 30,143 (at 1 kHz) was found for undoped sample at the transition temperature of 278 °C. The maximum relative permittivity at the transition temperature decreased from 30,143 for undoped sample to 12,000 for 9 mol% Sr^{2+}-doped sample. The resulting in reduction of the relative permittivity may be due to the lower polarizability of Sr^{2+} which may weaken the ferroelectricity of a unit cell [9,10].

The transition temperature (T_m) as a function of Sr concentration is shown in Fig. 5. The transition temperature was observed to decrease from 270 °C for undoped sample to 175 °C for 9 mol% doped sample. The relation between T_m and Sr^{2+} concentration can be express by $T_m = 282.1 - 11.26x$ °C, where x is Sr^{2+} concentration. From the XRD result, the lattice parameter was observed to decrease with increasing Sr concentration. Therefore, reduction in the transition temperatures may be due to the distortion of crystal lattice. Similar result was reported in the other system [3,10,11].

In order to investigate the transition behavior of the samples, the diffusiveness parameter (δ) and degree of dielectric relaxation (γ) was calculated from the following expression [12,13]:

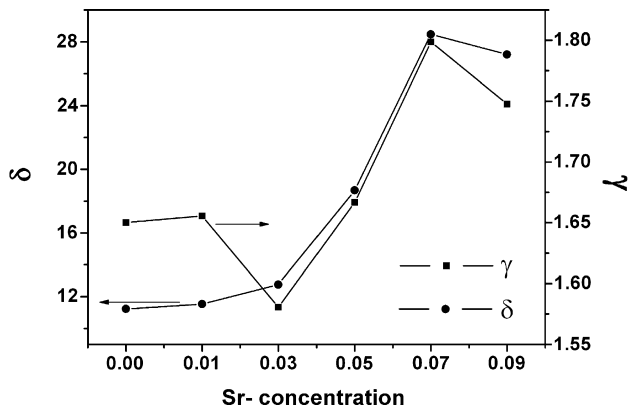

Fig. 6. Parameter γ and degree of diffuseness δ (°C) as a function of Sr concentration.

$$\frac{\varepsilon_m}{\varepsilon} = 1 + \left(\frac{(T - T_m)^{\gamma}}{2\delta^2}\right), \quad (1)$$

where ε_m is maximum value of the relative permittivity at $T = T_m$, γ is the expression of the degree of dielectric relaxation in the relaxor ferroelectric material and ε is the relative permittivity of the sample. In case $\gamma = 1$, Eq. (1) express Curie–Weiss behavior, while for $\gamma = 2$ this equation is identified to the quadratic relationship. Many relaxor ferroelectric materials can be fit to Eq. (1) with $\gamma = 2$ at temperature above T_m. The δ and γ can be determined from the plot of $\log((\varepsilon_m/\varepsilon) - 1)$ versus $\log(T - T_m)$. The parameter δ can be used to measure the degree of diffuseness of the phase transition in the mixed relaxor–normal ferroelectric materials. The value γ and δ are both material constants depending on the composition and structure of the material.

Fig. 6 shows the values of δ and γ as a function of Sr concentration. The values of δ and γ were found to increase with an increase Sr concentration. There have been many attempts to investigate the effect of doping element on the phase transition in lead-base ceramics. Zheng et al. reported that Sr substitution for Pb in PZT shifted compositions away from the MPB toward the tetragonal phase and broadened the phase transition [3]. The different type of domain structure was also observed in the Sr-doped PZT samples. These domain structures are consistent with the broadening of the phase transition with increasing Sr content. In complex lead-base perovskite such as PMN and PMN–PT ($Pb(Mg_{1/3}Nb_{2/3})O_3$–$PbTiO_3$), many authors proposed that that 1:1 ordered nanoregion as observed by transmission electron microscope (TEM) is closely related to the degree of diffuse phase transition [14–16]. However, some authors proposed that the observation of diffuse phase transition can be related to the micro-composition fluctuation [17]. In the present work, it is believed that an increasing in degree of diffuseness of the phase transition may be attributed to the changes of nano- or micro-structure of the samples after doping. However, future work is required to clarify the reasons for the phase transition behavior.

4. Conclusions

In present work, we have demonstrated the effects of Sr-doping on phase transition behavior and dielectric properties of 0.8PZT–0.2PNN ceramics for the first time. The transition temperature was found to have a linear reduction with the Sr concentration. The Sr-doping also made the ferroelectric phase transition to become boarder, resulting an enhancement of degree of diffuse phase transition.

Acknowledgements

This work was supported by The Thailand Research Fund (TRF), Faculty of Science Chiang Mai University, and Commission on Higher Education (CHE) Thailand.

The authors would like to thank Prof. Dr. Tawee Tunkasiri for his help in many facilities.

References

[1] J. Moulson, J.M. Herbert, Electroceramics: Materials, Properties, Applications, Chapman and Hall, New York, 1990.
[2] B. Jaffe, W.R. Cook, H. Jaffe, Piezoelectric Ceramic, R.A.N. Publishers, 1971.
[3] H. Zheng, I.M. Reaney, W.E. Lee, N. Jones, H. Thomas, J. Eur. Ceram. Soc. 21 (2001) 1371.
[4] G.A. Smolenskii, A.L. Agranovskaya, Sov. Phys. Tech. Phys. 13 (1958) 80.
[5] E.A. Buyanova, P.L. Strelets, I.A. Serova, V.A. Isupov, Bull. Acad. Sci. USSR Phys. Ser. 29 (1965) 1877.
[6] N. Vittayakorn, G. Rujijanagul, X. Tan, M.A. Marquardt, D.P. Cann, J. Appl. Phys. 96 (2004) 5103.
[7] Y. Hou, M. Zhu, F. Gao, H. Wang, B. Wang, H. Yan, C. Tian, J. Am. Ceram. Soc. 87 (5) (2004) 847.
[8] J. Kuwata, K. Uchino, S. Nomura, Ferroelectrics 37 (1981) 579.
[9] W. Kinase, K. Harada, Ferroelectrics 283 (2003) 39.
[10] K.H. Yoon, H. Ryul Lee, J. Am. Ceram. Soc. 83 (11) (2000) 2693.
[11] Y. Yang, Y. Yu, in: Proceeding of the 13th IEEE International Symposium on Applications of Ferroelectronic, 2002, p. 57.
[12] H.T. Martirena, J.C. Burfoot, Ferroelectrics 7 (1974) 151.
[13] K. Uchino, S. Nomura, Ferroelectr. Lett. Sect. 44 (1982) 55.
[14] Y. Yang, C. Feng, W. Yao, Y. Yu, Jpn. J. Appl. Phys. 40 (2001) 6884.
[15] H.B. Krause, J.M. Cowlsey, J. Wheatley, Acta Cryst. A 35 (1979) 1015.
[16] J. Chen, H.M. Chan, M.P. Harmer, J. Am. Ceram. Soc. 72 (1989) 593.
[17] K.M. Lee, H.M. Jang, J. Mater. Res. 12 (1997) 1614.

Available online at www.sciencedirect.com
ScienceDirect
Current Applied Physics 8 (2008) 241–245
Current Applied Physics
An official journal of the KPS
www.elsevier.com/locate/cap
www.kps.or.kr

Phase formation and electrical properties of lead-free bismuth sodium titanate–potassium niobate ceramics

K. Pengpat, P. Jarupoom, P. Kantha, S. Eitssayeam, U. Intatha, G. Rujijanagul, T. Tunkasiri *

Department of Physics, Faculty of Science, Chiang Mai University, Chiang Mai 50200, Thailand

Available online 4 November 2007

Abstract

Lead-free piezoelectric ceramics in the $(1-x)(Bi_{0.5}Na_{0.5})TiO_3$–$xKNbO_3$:$(1-x)$BNT–$x$KN system, were prepared by a two-step mixed oxide method and investigated over the entire compositional range where $x = 0.0$ to 1.0. Difficulty in preparing dense ceramics was encountered where the content of KN is greater than 50 mol%. XRD results showed that most of the BNT–KN ceramics contain ferroelectric perovskite phase with a mixture of rhombohedral and orthorhombic symmetries. The dielectric constant at room temperature (ε_r) was found to increase with increasing KN. The maximum piezoelectric coefficient (d_{33}) of about 170 pC/N was obtained in the 0.9BNT–0.1KN sample. The broadness of the dielectric constant peak increased with increasing KN content, especially that of the 0.7BNT–0.3KN ceramic which exhibited a very broad curve over a wide temperature range. This may be useful in the development of lead-free capacitors.

PACS: 61.05.cp; 77.22.Ch; 77.65.Bn; 77.84.Dy

Keywords: BNT; KN; Lead-free piezoelectric ceramic; Two-step mixed oxide method

1. Introduction

It is well-known that $Pb(Zr,Ti)O_3$ (PZT) ceramics are the most important piezoelectric materials that are being widely used in various fields. However, the lead oxide (PbO) present in the PZT causes environmental pollution during processing. For this reason, it is desirable to find lead-free piezoelectric ceramics to replace PZT ceramics in the near future. The lead-free piezoelectric materials of interest are bismuth sodium titanate $(Bi_{0.5}Na_{0.5})TiO_3$ (BNT) and potassium niobate $KNbO_3$ (KN) with perovskite structures.

BNT, discovered by Smolensky et al. [1], is one of the promising lead-free piezoelectrics. Its crystal structure is rhombohedral at room temperature and changes to tetragonal at 200 °C (the ferroelectric to antiferroelectric phase transition (T_p) where the rhombohedral ferroelectric form transforms to the antiferroelectric tetragonal form) [2–4]. The distinct Curie temperature, (T_c) of this material is 320 °C, hence, at this temperature the antiferroelectric tetragonal form changes to paraelectric cubic form. At room temperature, BNT is strongly ferroelectric with a remanent polarization (P_r) and coercive field (E_c) of about 38 μC/cm^2 and 73 kV/cm [5]. However, there are some difficulties in poling BNT ceramics because of their high leakage current. Thus, some modifications have been made to the BNT composition to improve the poling process and electrical properties. Most of the successful works have involved the substitution of the A- or B-site cations of BNT. These have involved La-doping of BNT by Herabut and Safari [6], BNT–$KNbO_3$ (KN) solid-solution ceramics [5], and BNT–BT compositions [3]. Of these the modified BNT ceramics of the BNT–KN system are of the most interest because their high potential for improvement of the piezoelectric and dielectric properties.

* Corresponding author.
E-mail address: tawee@chiangmai.ac.th (T. Tunkasiri).

1567-1739/$ - see front matter © 2007 Elsevier B.V. All rights reserved.
doi:10.1016/j.cap.2007.10.077

Potassium niobate, $KNbO_3$ (KN), is ferroelectric at room temperature and has orthorhombic symmetry. It changes to the paraelectric state at T_c of about 435 °C [7]. This material has a high electromechanical coupling factor over a wide compositional range. Moreover, KN single crystals are known to have high piezoelectric activity. A study of bismuth sodium titanate, (BNT)-based solid solution with KN prepared by hot pressing was reported by Ishii et al. [5]

Interestingly, the two-step mixed oxide preparation method, allowed the physical and electrical properties of BNT based ceramics, with the addition of barium zirconate titanate $Ba(Ti_{1-x})Zr_xO_3$ to be improved, as reported by Peng and his co-workers [8]. They found that these ceramics were well synthesized by this method while the conventional mixed oxide method gave rather poor ceramics. However, the microstructure and piezoelectric coefficient (d_{33}) of these BNT–KN ceramics has not yet been reported in the studies mentioned above, which concentrated mostly on other electrical properties. In this work, therefore, the two-step mixed oxide method was employed in order to obtain better properties of the BNT–KN ceramics. X-ray diffraction (XRD) was used for phase identification and scanning electron microscopy (SEM) was employed in a microstructural study of the ceramics. The dielectric constant (ε_r) and piezoelectric coefficient (d_{33}) were also investigated.

2. Experimental procedure

The BNT–KN ceramics were prepared by the two-step mixed oxide method in which stoichiometric mixtures of reagent-grade metal oxide or carbonate powders of 99% + purity (Bi_2O_3, Na_2CO_3, TiO_2, K_2CO_3 and Nb_2O_5) were used as the starting raw materials. The batch compositions of BNT and KN were prepared and milled separately for 24 h in acetone using zirconia balls. Both the mixtures of BNT and KN were calcined separately at 800 °C for 2 h, then blended according to the $(1-x)$BNT–xKN composition, where $x = 0.0$–1.0. These mixed powders were milled again for 24 h in ethyl alcohol, dried, and sieved in order to obtain fine homogeneous powders which were pressed into pellets 15 mm in diameter and 1.7 mm in thickness. The green pellets were sintered between 1025 and 1100 °C for 2 h in air. The phases in all sintered ceramics were identified using X-ray diffraction (XRD, D500 Siemens). The bulk density of sintered ceramic sample was determined by the ASTM-C373 method and scanning electron microscopy (SEM, JSM-6335fE, JEOL) was used to observe the microstructure of the sintered samples. The grain size of each sample was determined by the mean linear intercept.

For measurement of the electrical properties, silver paste was painted on to both faces of the disks and fired at 750 °C to function as electrodes. The dielectric constant and loss tangent ($\tan\delta$) were measured at room temperature using an LCZ meter (Model 4276A, Hewlett Packard) at 100–10 kHz. The sample for measurement of piezoelectric properties was poled in silicone oil at 80 °C at 3 kV/mm for 5 min. The piezoelectric properties were measured using a piezo d_{33} tester (Model 8000, Pennebaker).

3. Results and discussion

The phase evolution in the BNT–KN ceramics prepared by the two-step mixed oxide method was determined from the X-ray diffraction patterns of $(1-x)$BNT–xKN where x varied from 0.0 to 1.0 (Fig. 1). Peak shifts were observed in XRD patterns where $x > 0.0$, indicating changes in the lattice parameters of these samples compared with the pure BNT phase. Moreover, with increasing KN (x) concentration, the amount of orthorhombic phase was found to increase, especially where $x > 0.7$, when the rhombohedral peak of the plane (1 1 1) disappeared, leaving only the orthorhombic structure.

In order to obtain highly dense ceramics, the optimum sintering temperatures should be chosen carefully. Table 1 shows the optimum sintering temperatures for producing the densest ceramic of each composition, which tend to decrease with increasing content of KN. The sintering tem-

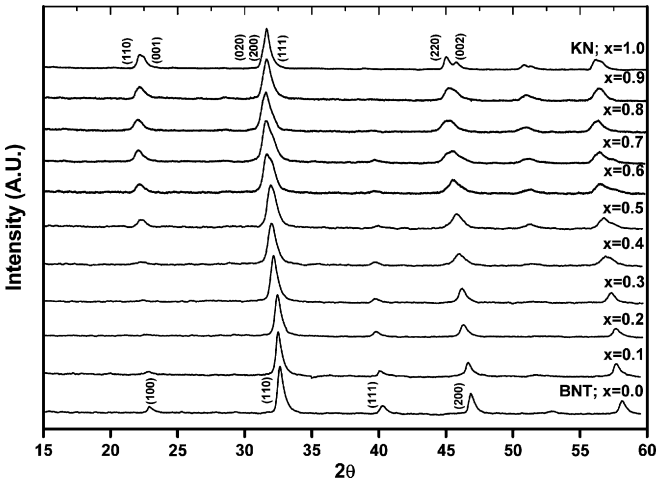

Fig. 1. X-ray diffraction patterns of $(1-x)$BNT–xKN ceramics where $x = 0.0 - 1.0$.

Table 1
Densities and grain sizes of BNT–KN ceramics at their optimum sintering temperatures

Composition	Optimum sintering temperature (°C)	Density (g/cm^3)	Average grain size (μm)
BNT	1100	5.85 ± 0.05	2.35 ± 0.10
0.9BNT–0.1KN	1100	5.72 ± 0.01	1.24 ± 0.07
0.8BNT–0.2KN	1050	5.47 ± 0.02	0.81 ± 0.05
0.7BNT–0.3KN	1050	5.33 ± 0.05	0.66 ± 0.02
0.6BNT–0.4KN	1025	4.91 ± 0.06	0.74 ± 0.03
0.5BNT–0.5KN	1025	5.01 ± 0.01	0.57 ± 0.02
0.4BNT–0.6KN	1005	4.89 ± 0.01	[a]
0.3BNT–0.7KN	1005	4.80 ± 0.01	[a]
0.2BNT–0.8KN	1005	4.68 ± 0.01	[a]
0.1BNT–0.9KN	1005	4.57 ± 0.02	[a]
KN	980	4.31 ± 0.02	0.35 ± 0.01

[a] Poor sample densification made it impossible to observe grain size.

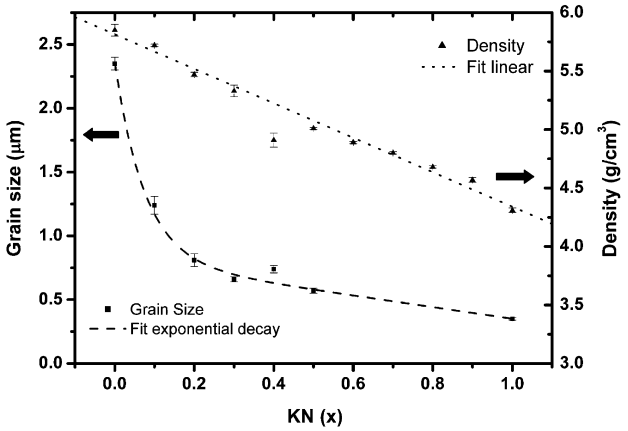

Fig. 2. Trends in grain size and density of $(1-x)$BNT–xKN ceramics with respect to amount of x.

peratures of the $x \geqslant 0.6$ samples, however, could not exceed 1005 °C otherwise the samples will suffer a severe loss of potassium oxide (K_2O), which is a volatile component over 800 °C and the humidity in the sintering environment causes an increase of K_2O evaporation [9–11]. It should be also noted that ceramic samples with a sufficient degree of densification were difficult to prepare when the content of KN was between $x = 0.6$ and 1.0 as the solid-state sintering process was not completed, resulting in samples with extremely high porosity and poor mechanical strength. This may be due to the easily volatile K_2O at elevated firing temperature [10,11]. In order to determine the trends of density and grain size with increasing KN content, the corresponding values of Table 1 were plotted (Fig. 2). It can be clearly seen that the density decreases linearly with increasing KN while the grain size changes

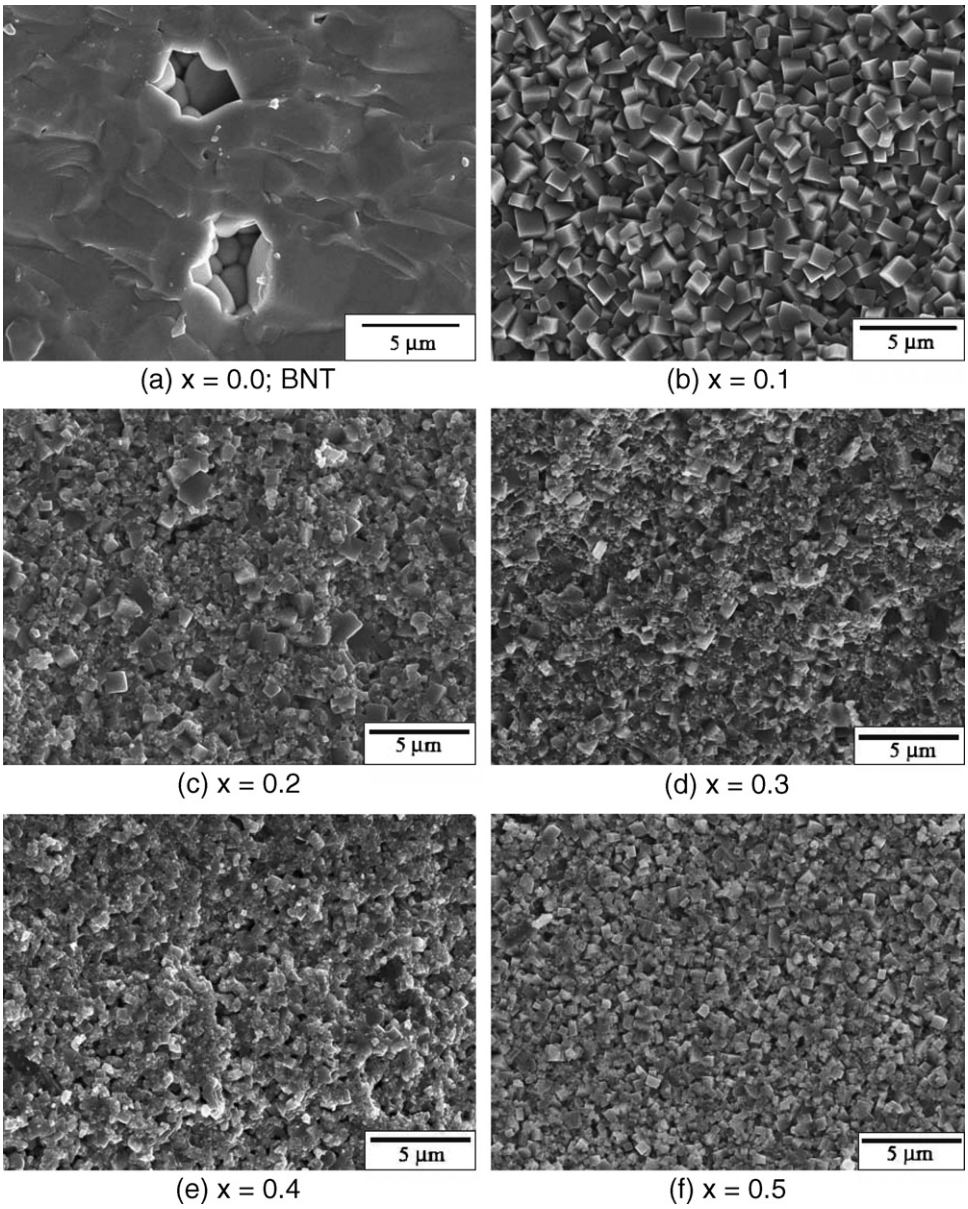

Fig. 3. SEM micrographs of (a) BNT and $(1-x)$BNT–xKN ceramics where (b) $x = 0.1$ to (f) $x = 0.5$.

abruptly by adding only a small amount of KN ($x = 0.1$), showing a profile that fits well to an exponential decay function. This may indicate that the KN is effective in inhibiting grain growth of the BNT-KN ceramics, and may be mainly due to the solubility limit of KN in the BNT system, which in this case should be less than 10 mol%. A further factor may be the ionic radius of K^+ ion (1.33 Å) which is larger than that of Na^+ (0.94 Å) by about 29%. The solubility value therefore plays an important role in the grain growth mechanism as it is believed that beyond the solubility limit the remaining KN segregates at the grain boundaries, leading to the inhibition of grain growth [12,13].

The SEM micrographs of the BNT–KN (Fig. 3) show that a small KN content added to the BNT decreases the density and inhibits grain growth of the BNT–KN ceramics, but may also changes the grain morphology from the equiaxed grains of BNT (Fig. 3a) to the orthorhombic grains in the $(1-x)$BNT–xKN ceramics where $x \geqslant 0.1$ (Fig. 3b–e). The small amount of KN crystals with lower melting point than that of BNT crystals may therefore melt and recrystallize into KN crystals of orthorhombic structure. Thus, during sintering at higher temperature these KN crystals may act as secondary nuclei in the matrix of the BNT particles, giving rise to exaggerated grain growth or secondary recrystallization of orthorhombic-like structures in the BNT–KN ceramics [14]. Moreover, higher KN contents produced ceramics of higher porosity. This may be due to the loss of K^+ at elevated sintering temperature. This result agrees well with the density data.

The dielectric properties of the dense ceramics were measured at various frequencies as shown in Fig. 4. The dielectric constant (ε_r) at room temperature is found to increase with increasing KN (x) up to a value of 1715 at 10 kHZ in the 10 mol% KN sample, thereafter gradually decreasing. The relationship between ε_r and temperature of selected samples is illustrated in Fig. 5. Three phase transitions at T_1, T_2 and T_3 are observed in the KN containing ceramics. This $\varepsilon_r - T$ characteristic indicates dielectric behavior of the composite in these BNT–KN ceramics which may be due to heterogeneity of the A- and B-site cations in the crystal lattices. Additionally, at all transition temperatures, broadening of dielectric constant curves is seen. This is expected, as most BNT-based ceramics show this diffuse phase transition. The result is consistent with previous studies of other systems [15–18]. However, it has been reported that higher sintering temperatures and long soaking periods enhanced the homogeneity, resulting in the formation of more solid solution and flatter dielectric curves are even more flattened [19]. In this work, the 0.7BNT–0.3KN ceramic showed the highest degree of broadness of the dielectric constant curve, presenting a very broad curve of significantly high dielectric constant over a wide temperature range. This particular dielectric behavior may be useful in the development of lead-free capacitors.

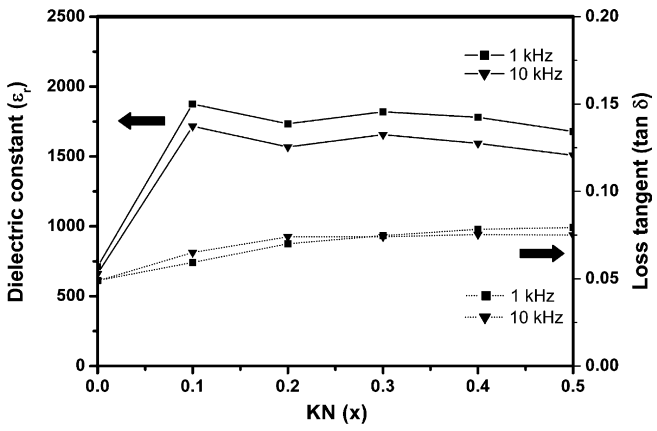

Fig. 4. Dielectric constant (ε_r) and loss tangent ($\tan\delta$) at room temperature versus KN content (x) in the $(1-x)$BNT–xKN system.

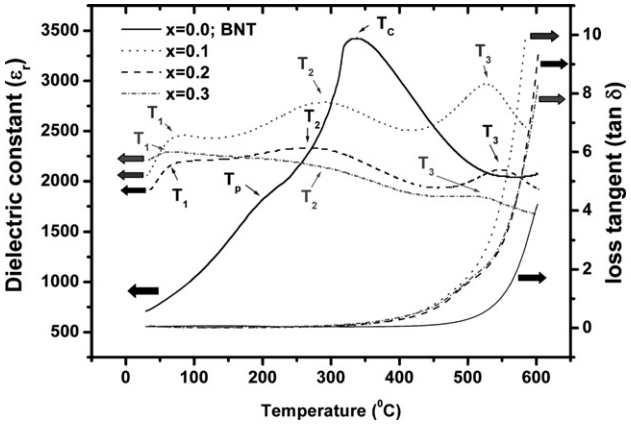

Fig. 5. Variation of dielectric constant (ε_r) and loss tangent ($\tan\delta$) with temperature for $(1-x)$BNT–xKN ceramics at 1 kHz.

The piezoelectric coefficient (d_{33}) values of the ceramic samples were determined only for the samples with KN contents of up to 10 mol%. In modified KN (x) where $x = 0.2 - 1.0$, electrical breakdown occurred during poling which may be caused by the high porosity of these samples where loss tangent ($\tan\delta$) increased monotonically with increasing KN (Fig. 4). However, the piezoelectric property of the ceramic formed in this system increased from 95 pC/N for the pure BNT to 170 pC/N for the 0.9BNT–0.1KN composition. This may be due to the lower porosity and large grain size obtained in this sample. The orthorhombic-like grains are believed to play an important role in enhancing the piezoelectric properties as well as the dielectric properties of the BNT–KN ceramics. This is consistent with the work of Kuharuangrong [20] who found enhancement of the dielectric properties at room temperature in La and K doped BNT–$PbTiO_3$ ceramics containing elongated grains.

4. Conclusions

Ceramics in the BNT–KN system have been prepared by a two-step mixed oxide method. The pure BNT and KN powders were firstly produced by calcining at 800 °C, then mixed in various compositions (with x values between

0.0 and 1.0), pressed into pellets and sintered to form dense ceramics. It was difficult to form ceramics using conventional methods when the content of x (KN) exceeds 0.6. It was found that the addition of KN enhances the piezoelectric and dielectric properties of the $(1-x)$BNT–xKN ceramics, the optimum composition being $x = 0.1$, in which the piezoelectric coefficient (d_{33}) at 3 KV/mm and dielectric constant at room temperature and 1 kHz were about 170 pC/N and 1875, respectively.

Acknowledgements

The authors would like to thank the Thailand Research Fund, graduate school and Faculty of Science, Chiang Mai University for financial support. Sincere thanks also go to the Research Laboratory for Excellent Electronic Materials, department of Physics, Chiang Mai University and P. Jalupoom would like to express his thanks to the Thailand Graduate Institute of Science and Technology for financial support.

References

[1] G.A. Smolenskii, V.A. Isupov, A.I. Agranovskaya, N.N. Kraink, Sov. Phys. Solid State 2 (1961) 2651.
[2] K. Sakata, Y. Masuda, Ferroelectrics 5 (1994) 347.
[3] T. Takenaka, K. Maruyama, K. Sakata, Jpn. J. Appl. Phys. 30 (9B) (1991) 2246.
[4] T. Takenaka, H. Nagata, Applications of Ferroelectrics, 1998. ISAF 98. in: Proceedings of the Eleventh IEEE International Symposium on 24–27 August 1998, p. 559.
[5] H. Ishii, H. Nagata, T. Takenaka, Jpn. J. Appl. Phys. 40 (9B) (2001) 5660.
[6] A. Herabut, A. Safari, J. Am. Ceram. Soc. 80 (11) (1997) 2954.
[7] T. Wada, K. Toyoike, Y. Imanaka, Y. Matsuo, Jpn. J. Appl. Phys. 40 (9B) (2001) 5703.
[8] C. Peng, J.F. Li, W. Gong, Mater. Lett. 59 (2005) 1576.
[9] H. Birol, D. Damjanovic, N. Setter, J. Am. Ceram. Soc. 88 (7) (2005) 1754.
[10] K. Kadokura, J. Shioya, S. Simada, T. Matsushita, J. Mater. Sci. Lett. 1 (1982) 277.
[11] A.N. Eshghi, A.X. Kuang, J.D. Mackenzie, J. Mater. Sci. 25 (1990) 3333.
[12] S. Eitssayeam, U. Intatha, G. Rujijanagul, K. Pengpat, T. Tunkasiri, Appl. Phys. A 83 (2006) 295.
[13] Z. Yang, X. Zong, H. Li, Y. Chang, Mater. Lett. 59 (2005) 3476.
[14] W.D. Kingery, H.K. Bowen, D.R. Uhlmann, Introduction to Ceramic, second ed., John Wiley & Sons, 1976.
[15] S. Kuharuangrong, W. Schulze, J. Am. Ceram. Soc. 79 (1996) 1273.
[16] N.M. Hagh, M. Allahverdi, A. Safari, in: IEEE International Ultrasonics, Ferroelectrics and Frequency Control Joint 50th Anniversary Conference, 2004, p. 246.
[17] T. Takenaka, H. Nagata, J. Eur. Ceram. Soc. 25 (2005) 2693.
[18] K.S. Hong, S.E. Park, J. Appl. Phys. 79 (1996) 388.
[19] M.T. Benlahrache, N. Benhamla, S. Achour, J. Eur. Ceram. Soc. 24 (2004) 1493.
[20] S. Kuharuangrong, J. Mater. Sci. 36 (2001) 1727.

Ferroelectrics
Publication details, including instructions for authors and subscription information:
http://www.informaworld.com/smpp/title~content=t713617887

Effect of Excess Lead Oxide on Phase Transitions and Physical Properties of Provskite Lead Barium Zirconate Ceramics

Theerachai Bongkarn [a]; Gobwute Rujijanagul [b]
[a] Department of Physics, Faculty of Science, Naresuan University, Pitsanuloke, Thailand
[b] Department of Physics, Faculty of Science, Chiang Mai University, Chiang Mai, Thailand

First Published on: 01 November 2007
To cite this Article: Bongkarn, Theerachai and Rujijanagul, Gobwute (2007) 'Effect of Excess Lead Oxide on Phase Transitions and Physical Properties of Provskite Lead Barium Zirconate Ceramics', Ferroelectrics, 358:1, 67 - 73
To link to this article: DOI: 10.1080/00150190701534072
URL: http://dx.doi.org/10.1080/00150190701534072

Ferroelectrics, 358:67–73, 2007

ISSN: 0015-0193 print / 1563-5112 online
DOI: 10.1080/00150190701534072

Taylor & Francis
Taylor & Francis Group

Effect of Excess Lead Oxide on Phase Transitions and Physical Properties of Provskite Lead Barium Zirconate Ceramics

THEERACHAI BONGKARN[1]
AND GOBWUTE RUJIJANAGUL[2,*]

[1]Department of Physics, Faculty of Science, Naresuan University, Pitsanuloke, 65000, Thailand
[2]Department of Physics, Faculty of Science, Chiang Mai University, Chiang Mai 50200, Thailand

Effect of excess PbO on phase transitions and physical properties of perovskite $(Pb_{0.90}Ba_{0.10})ZrO_3$ ceramics have been investigated. The $(Pb_{0.90}Ba_{0.10})ZrO_3$ ceramics were prepared via the conventional mixed oxide method. Excess PbO (1, 3, 5, and 10wt%) was introduced prior to powder calcination. The phase formation and phase transition of $(Pb_{0.90}Ba_{0.10})ZrO_3$ ceramics were characterized by X-ray diffraction and thermal analysis. The result indicated that excess PbO showed an effect on antiferroelectric to ferroelectric phase transition. However, it was not found significant effect of excess PbO on ferroelectric to paraelectric transition temperature.

Keywords Lead barium zirconate; phase transition; antiferroelectric; ferroelectric

Introduction

$(Pb_{1-x}Ba_x)ZrO_3$ (PBZ) was discovered by Roberts in 1950 [1]. Later on, many authors have investigated the properties of PBZ, especially its phase transitions [1–7]. Shirane [3] was one of who first demonstrated the antiferroelectric to ferroelectric (AFE→FE) phase transition in PBZ solid solution compositions with $x \geq 0.05$. In PBZ, the AFE and FE phases were characterized as orthorhombic and rhombohedral structure, respectively. It is reported that the AFE→FE phase transition produces a large increase in volume [5]. Furthermore, the electric-field required to induce AFE→FE switching is much lower than for $PbZrO_3$ (PZ) which has created interest in PBZ for potential use in large displacement actuator devices requiring low switching voltages [8].

Different research groups reported the different results of AFE→FE phase transition [1, 4–8]. Several authors [4, 6] have found no evidence of any AFE→FE transitions, whilst there have been a few reports showing an AFE→FE transition without corresponding FE→AFE transition on cooling [2]. It is suggested that the processing method used to prepare the PBZ powders may be important in influencing phase formation and phase transitions [7].

Received September 3, 2006; accepted September 30, 2006.
*Corresponding author. E-mail: rujijanagul@yahoo.com

An important factor to consider is the possible effect of PbO loss due to evaporation during high temperature processing [7]. Hence, the present work studied the effect of PbO content on the phase transition and properties of $(Pb_{0.90}Ba_{0.10})ZrO_3$ (PBZ10).

Experimental

The raw materials of PbO, ZrO_2, and $BaCO_3$ were weighed and mixed. Each mixture of the starting powders was milled using zirconia grinding media. After drying and sieving, the mixture was calcined at 850°C for 6 h. An excess of PbO, equivalent to 0, 1, 3, 5, and 10wt%, was applied prior to ball milling before calcination. The calcined powders were reground by wet ball-milling with 1wt% binder for 24 h. The calcined powders with binder were dried, crushed and sieved again. The powder mixtures were isostatically pressed into pellets then the pellets were sintered at 1325°C for 4 h in an alumina crucible. In order to minimize the loss of lead due to vaporization, PZ was used as the spacer powder. Thermogravimetry (TG) and differential thermal analysis (DTA) techniques were used to monitor the reactions between the oxide precursors. The thermal expansion of the ceramics samples was measured using a dilatometer. The phase transition temperatures were determined by a differential scanning calorimeter (DSC). All techniques in thermal analysis were performed at a heating of 10°C/min.

Results and Discussion

The TG and DTA curves recorded for an equimolar mixture of lead oxide, barium carbonate and zirconium oxide (PbO: $BaCO_3$: ZrO_2 = 1:1:1), are given in Fig. 1. The TG curve shows three interesting weight losses below 800°C. The first weight loss occurs below 150°C,

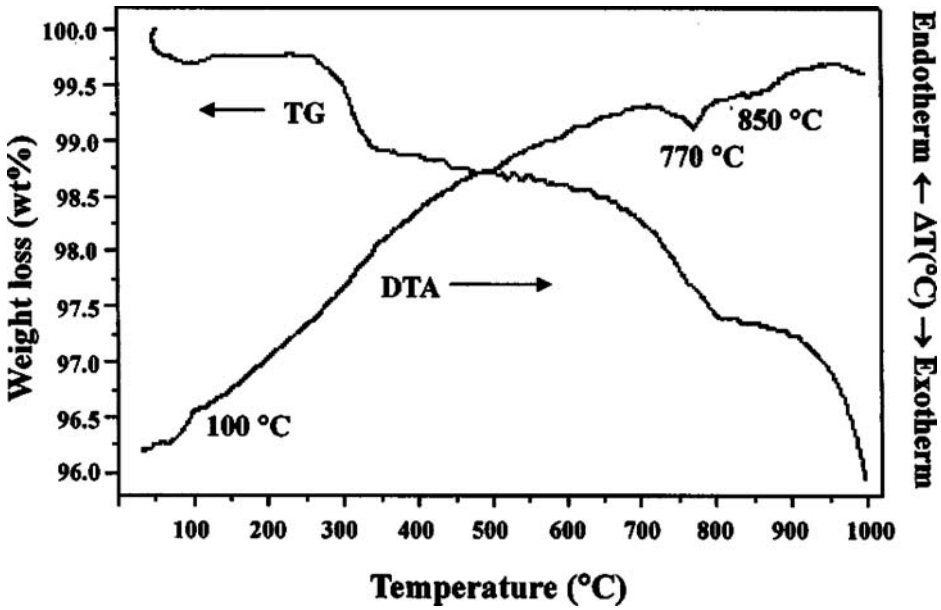

Figure 1. TG and DTA curves for the mixture of PbO, $BaCO_3$ and ZrO_2 powders.

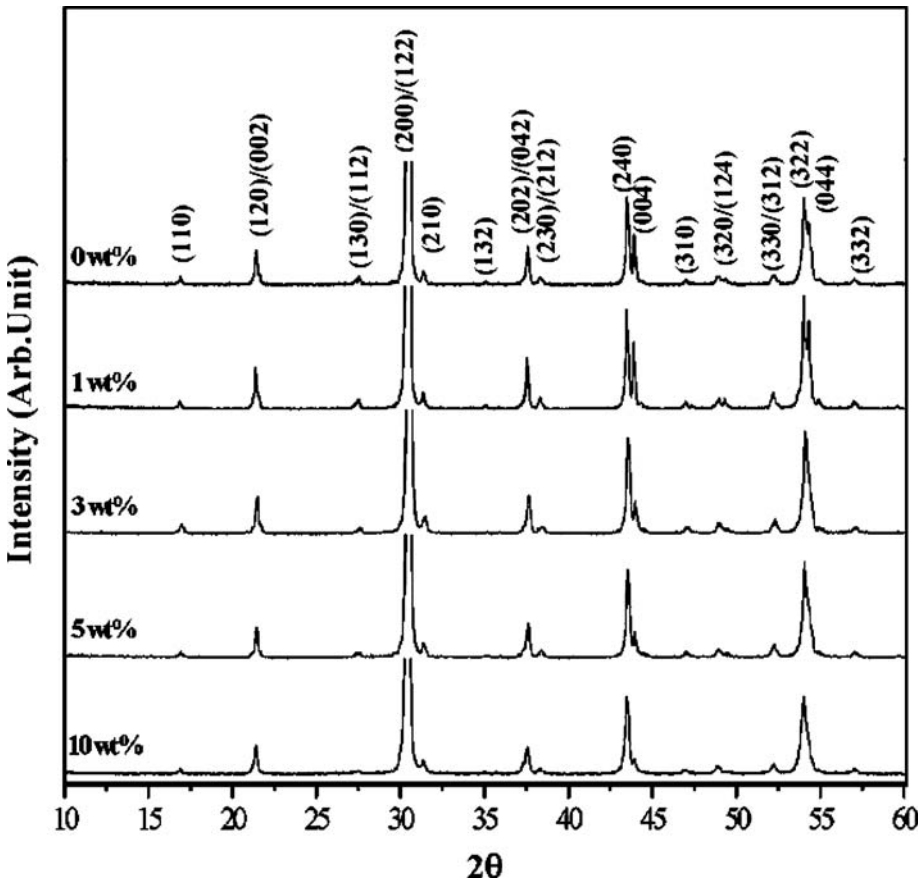

Figure 2. XRD patterns of PBZ10 ceramics made from starting powders with different amounts of starting excess PbO.

attribute to the vaporization of water. The second one between 270 to 350°C, relate to the elimination of organic residual from the milling process. The last one above 700°C, relate to the solid-state reaction between the starting materials. From these data, the temperature of 850°C was selected for calcination to ensure the complete solid-state reaction.

Figure 2 shows XRD patterns of sintered samples. Pure perovskite of PBZ phase was observed for the whole range of the compositions. The intensity ratio of 004/240 peaks ($I_{004/240}$) may be taken as a qualitative indicator of the relative proportion of the orthorhombic (AFE) and rhombohedral (FE) phases. This ratio decreases with increasing amounts of coexisting rhombohedral phase [8]. In the present work, $I_{004/240}$ increases with increasing excess PbO content up to 1 wt%. For the higher PbO content, the intensity ratio continually decreases as shown in Table 1. The result indicates more orthorhombic phase occurred in the 1 wt% excess PbO sample. The lattice parameter and unit cell volume of PBZ10 obtained by least square refinement method is shown in Table 1. The unit cell volume slightly increases with increasing excess PbO content up to 1 wt%. For the higher PbO content, the unit cell volume slightly decreases.

The measurements of the length of a specimen at various temperatures of solid materials are usually applied for the determination of the kinetics of phase transformation of PZ

Table 1
Intensity ratio of 004/240 peak, lattice parameter, unit cell volume, density and transition temperature of PBZ10 ceramics with different amounts of excess PbO

Amount of excess PbO (wt%)	$I_{004/240}$	Lattice parameter (Å)			Unit cell volume ($Å^3$)	Transition Temperature (°C)			
						Dilatometer		DSC	
		a	b	c		AFE→FE	FE→PE	AFE→FE	FE→PE
0	0.57	5.8924	11.6848	8.2158	565.6703	—	197.2	72.81	195.28
1	0.67	5.8966	11.6906	8.2159	566.3614	—	196.7	76.36	196.78
3	0.32	5.8936	11.6942	8.2153	566.2062	—	196.0	73.16	196.63
5	0.29	5.8884	11.6737	8.2119	564.4812	—	193.9	72.33	194.31
10	0.20	5.8881	11.6707	8.2068	563.9569	—	194.4	72.50	195.54

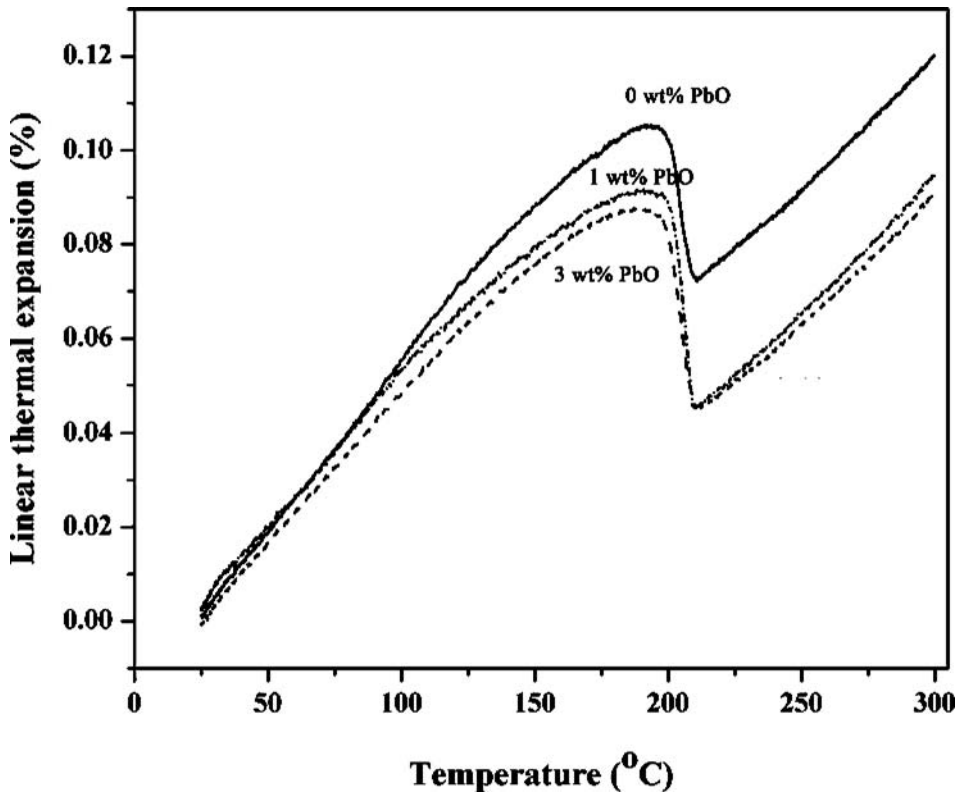

Figure 3. Linear thermal expansion versus temperature of PBZ10 ceramics made from starting powders with different amounts of starting excess PbO.

[12, 13]. The dilatometric thermal expansion of PBZ10 with excess PbO on heating cycle is plotted in Fig. 3. The discontinuously curves can be attributed to the FE to PE phase transition with rising temperature [3, 12]. However, the anomaly of AFE→FE phase transition could not be observed due to sensitivity limit of the dilatometer.

DSC results of PBZ10 with excess PbO on heating cycle are given in Fig. 4. The two distinct endothermic peaks were found. The lower temperature peak is obviously smaller than the higher temperature one. These peaks can be associated with the AFE →FE and FE →PE phase transition, respectively. The list of AFE → FE and FE → PE phase transition temperatures are presented in Table 1.

There is no direction trend for FE → PE transition temperature. However, the FE → PE transition temperature was found between 194–197°C. The AFE → FE transition temperature increases with increasing amount of PbO up to 1wt% then it decreases with further amount of PbO. This result corresponds to the XRD result, indicating that the AFE → FE transition is sensitive to the Pb ions in the compositions. Scott and Burns reported that the temperature interval of the ferroelectric phase (ΔFE) in $PbZrO_3$ depends on stoichiometry [14]. They found that the minimum of ΔFE occurs for samples containing stoichiometric composition. In this study, the resulting change in defect chemistry may be the reason to the change in the transition temperature.

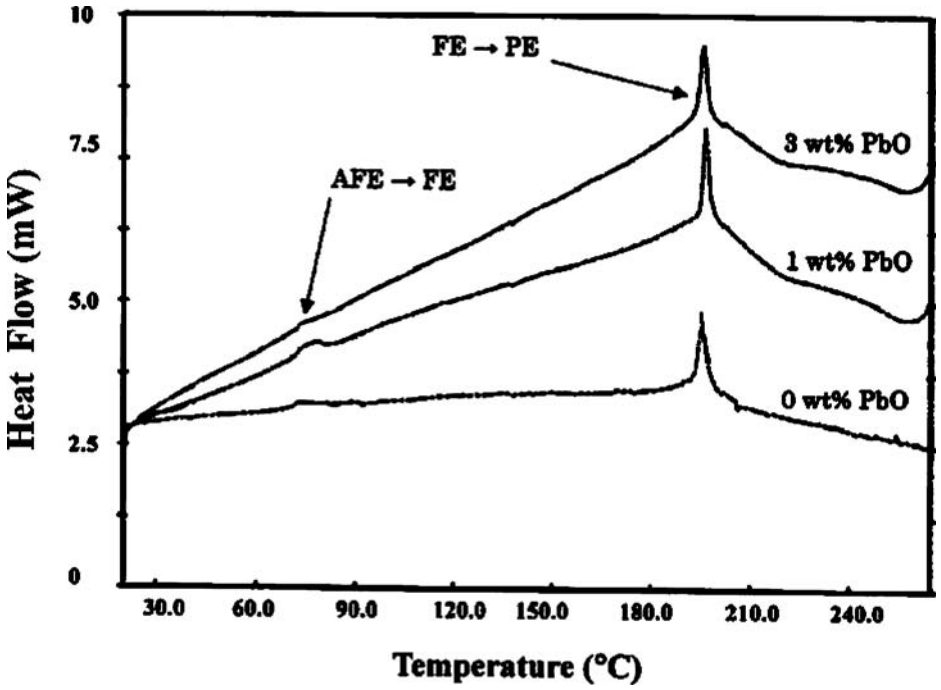

Figure 4. DSC thermographs of PBZ10 ceramics made from starting powders with different amounts of starting excess PbO.

Conclusions

The PBZ10 ceramics with different amount of excess PbO levels were prepared by conventional mixed oxide method. The sample contained 1 wt% excess PbO exhibited the maximum AFE→FE transition temperature. However, there is no significant effect of excess PbO content on FE→PE transition temperature. The results indicate that the AFE→FE transition is sensitive to the Pb ions in the compositions.

Acknowledgments

The authors are grateful to the Thailand Research Fund (TRF), Faculty of Science, Chiang Mai University, Institute of Research and Development Administration Naresuan University, and Commission on Higher Education (Thailand) for financial support. Thanks are also due to Prof. Dr. Tawee Tunkasiri for his help with many facilities.

References

1. S. Roberts, *J. Am. Ceram. Soc.* **63**, 33 (1950).
2. B. P. Pokharel, M. K. Datta, and D. Pandey, *J. Mater. Sci.* **34**, 691 (1999).
3. G. Shirane, *Phys. Rev.* **86**, 219 (1952).
4. K. H. Yoon, S. C. Hwang, and D. H. Kang, *J. Mater. Sci.* **32**, 17 (1997).
5. B. P. Pokharel and D. Pandey, *J. Appl. Phys.* **90**, 2985 (2001).
6. Z. Ujma, J. Handerek, M. Pawelczyk, and D. Dmytrow, *Ferroelectrics* **129**, 127 (1992).
7. B. P. Pokharel and D. Pandey, *J. Appl. Phys.* **88**, 5364 (2000).

8. B. P. Pokharel and D. Pandey, *J. Appl. Phys.* **86**, 3327 (1999).
9. Powder Diffraction File no. 81-2042, International Centre for Diffraction Data, Newton Square, PA (2000).
10. Powder Diffraction File no. 76-1796, International Centre for Diffraction Data, Newton Square, PA (2000).
11. Powder Diffraction File no. 85-1287, International Centre for Diffraction Data, Newton Square, PA (2000).
12. V. J. Tennery, *J. Am. Ceram. Soc.* **49**, 483. (1966).
13. L. Goulpeau, *Sov. Phys. Solid St.* **8**, 1970 (1967).
14. B. A. Scott and G. Burns, *J. Am. Ceram. Soc.* **55**, 331 (1972).

Available online at www.sciencedirect.com
ScienceDirect
Current Applied Physics 8 (2008) 253–257
Current Applied Physics
An official journal of the KPS
www.elsevier.com/locate/cap
www.kps.or.kr

Development of electrical properties in lead-free bismuth sodium lanthanum titanate–barium titanate ceramic near the morphotropic phase boundary

P. Jarupoom, K. Pengpat *, N. Pisitpipathsin, S. Eitssayeam, U. Intatha, G. Rujijanagul, T. Tunkasiri

Department of Physics, Faculty of Science, Chiang Mai University, Chiang Mai 50200, Thailand

Available online 25 October 2007

Abstract

The near morphotropic phase boundary (MPB) of lead-free piezoelectric ceramics based on bismuth sodium lanthanum titanate ($Bi_{0.487}Na_{0.487}La_{0.017}TiO_3$:BNLT) and barium titanate ($BaTiO_3$:BT) was carefully investigated by a modified two step mixed-oxide method. In this case the BNLT and BT powders were produced separately using calcination temperatures of 900 °C and 1200 °C, respectively. After that they were mixed with the desired compositions of $(1-x)$BNLT–xBT, where $x = 0.00$, 0.02, 0.04, 0.06, 0.08, and 0.10. Then the powders were pressed and subsequently sintered at various temperatures to obtain the maximum density under each condition. It was found that the BT addition has a significant effect on grain growth inhibition of the BNLT–BT ceramics and this in turn gave rise to an enhancement in dielectric constant (ε_r) of the corresponding ceramics. The piezoelectric coefficient (d_{33}) was also improved greatly to about 130 pC/N in the 0.96BNLT–0.04BT ceramic sample sintered at 1125 °C. This offered an opportunity to obtain a good candidate for replacing the lead-based piezoelectrics.

PACS: 77.65.Bn; 71.45.Gm; 61.05.cp; 68.37.Hk

Keywords: BNLT; BT; Lead-free piezoelectric ceramic; Two step mixed-oxide method

1. Introduction

In the past few decades, extensive studies have been carried out in order to find replacements for lead-based piezoelectric materials, such as (Pb, Zr)TiO_3 (PZT), $PbTiO_3$ (PT) and $Pb(Mg_{1/3}Nb_{2/3})O_3$ (PMN), because of environmental concern. One of the most studied compounds is ferroelectric bismuth sodium titanate ($Bi_{0.5}Na_{0.5})TiO_3$ (BNT), discovered by Smolenskii et al. [1]. It has interesting electrical properties (good dielectric constant (ε_r) and acceptable piezoelectric coefficient (d_{33})). Its crystal structure is rhombohedral with strongly ferroelectric behavior. The Curie temperature T_c is about 320 °C, remanent polarization $P_r = 38\ \mu C/cm^2$ and coercive field $E_c = 73$ kV/cm. Another phase transition occurs at about 200 °C (T_p) which is believed to be the transition from ferroelectric rhombohedral to antiferroelectric tetragonal, which is further changed to the paraelectric cubic phase at T_c [2,3]. It is normally found that the ε_r–T curve at the T_c of this material has a high degree of broadness, indicating relaxor-type ferroelectric behavior.

However, the Bi ion is highly volatile at high temperature above 1130 °C during sintering, making this material difficult to pole due to its high conductivity [4]. The solution to this problem has been found by many researchers who were able to modify the BNT crystal by the substitution of other A- and B-site cations, such as in $(Bi_{0.5}Na_{0.5})_{(1-1.5x)}La_xTiO_3$: BNLT [5], BNT–$BaTiO_3$ [6], BNT–$KNbO_3$ (KN) [7], and BNT–Ba(Ti, Zr)O_3 [8]

* Corresponding author.
E-mail address: kpengpat@gmail.com (K. Pengpat).

1567-1739/$ - see front matter © 2007 Elsevier B.V. All rights reserved.
doi:10.1016/j.cap.2007.10.010

solid-solution ceramic systems. The piezoelectric properties of these ceramics were significantly improved. Recently, another interesting system was reported by Pengpat et al. [9] who combined two ideas, (1) the rare earth additive of La^{3+} suggested by Herabut and Safari [5], and (2) a solid solution of BNT–BT suggested by Takenaka et al. [6], in order to produce a new system of $(1-y)(Bi_{0.5}Na_{0.5})_{(1-1.5x)}La_xTiO_3$ (BNLT)–$yBaTiO_3$ (BT), where $x = 0.017$ and $y = 0$, 0.06, 0.1, 0.15, 0.2. They found that a maximum d_{33} of about 112 pC/N could be achieved with the composition of $y = 0.15$ which is not the morphotropic phase boundary (MPB) composition ($y = 0.1$) reported in this work. Moreover, this MPB composition is different from that of the $(1-x)$BNT–xBT system of Takenaka et al. whose MPB was observed at about $x = 0.06$. This may be due to different homogeneity of the samples prepared using different preparation methods. Moreover, the series of compositions of varying BT content (y) from $(1-y)$BNLT–yBT is not complete enough to determine the exact MPB of this system, making it difficult to compare the results to those of the previous works.

In this work, the $(1-x)$BNLT–xBT system has been further investigated by conventional methods, where the range of x values was chosen near the MPB of BNT–BT system (about 6 mol% BT) and 1.7 mol% La^{3+} doped BNT which is the optimum composition of the BNLT system. The physical, dielectric and piezoelectric properties of the BNLT–BT ceramics were investigated. The microstructures of the ceramics in this system were also examined. The results were compared to those of the previous works.

2. Experimental procedure

High purity (purity > 99.0%) powders of bismuth oxide (Bi_2O_3), sodium carbonate (Na_2CO_3), lanthanum oxide (La_2O_3), titanium oxide (TiO_2) and barium carbonate ($BaCO_3$) were used as starting materials for producing $(1-x)(Bi_{0.487}Na_{0.487}La_{0.017}TiO_3)$–$x(BaTiO_3)$, where $x =$ 0.0, 0.02, 0.04, 0.06, 0.08 and 1.0. The batch compositions of BNLT and BT were weighed and mixed by ball-milling for 24 h. Then both mixtures of BNLT and BT compositions were dried and calcined at 900 °C and 1200 °C, respectively, which are the optimum calcination temperatures for producing highly pure powders of both phases. Both powders were then mixed corresponding to the above formula by ball-milling for 24 h with acetone as the dispersion media. After drying and sieving the mixtures, the obtained powder was made into pellets of 15 mm in diameter by uniaxial pressing in a stainless steel die. The pellets were sintered between 1050 °C and 1150 °C in an electric furnace in an air atmosphere under controlled heating and cooling rates of 5 °C/min with 2 h dwell time. The phase identification and density of the sintered ceramic samples was investigated using X-ray diffraction (XRD: Siemen D-500) and Archimedes' method, respectively. Scanning electron microscopy (SEM: JSM-6335F) was used to observe the microstructures of the ceramics. The grain sizes of each sample were measured by the mean linear intercept. The two parallel surfaces of the sintered ceramics were polished and coated with silver paste as electrodes for electrical contact. To measure the relevant electrical properties, the prepared ceramic samples were poled in a silicone oil bath at 50 °C at 3.0 KV/mm for 15 min. The samples were then left at room temperature for 24 h after poling, and the piezoelectric measurements were measured using a piezoelectric-d_{33}-meter (Model 8000, Pennebaker). The dielectric constant (ε_r) of all ceramic samples was measured at various frequencies from 1 kHz, 10 kHz and 100 kHz and their temperature vs ε_r curves were also measured using an LCZ-meter (Model 4276A, Hewlett Packard).

3. Results and discussion

The XRD patterns of the dense ceramics from BNLT–BT system are shown in Fig. 1. It can be seen that all the peaks in the XRD pattern of the BNLBT0 ceramic correspond to the BNT phase of the JCPDS file No. 34-0360 with rhombohedral structure. The addition of BT phase of $x \geqslant 0.04$ resulted in a splitting of the 200 peak into two peaks of (002) and (200) reflections. This splitting is obvious at $x = 0.06$ and can be clearly seen in the extended XRD patterns of the corresponding ceramics at 2θ between 44° and 48° (Fig. 2). This indicates the change in crystal structure from rhombohedral to tetragonal symmetry of these ceramics and the MPB of this system is found to lie between $x = 0.04$ and $x = 0.06$, where the rhombohedral and tetragonal symmetries coexist, with more BT added, more of the tetragonal phase could be detected in the XRD patterns of the BNLBT ceramics. From the previous work, it was reported that the MPB of the $(1-x)$BNT–xBT system was at $x = 0.06$ [6]. In this work, La^{3+} doping of the BNT–BT has, however, shown no significant effect on the MPB as we found our MPB in the similar region of x between 0.4 and 0.6. This may be attributed to the difference between the ionic radius of La^{3+} ion (130 pm) and

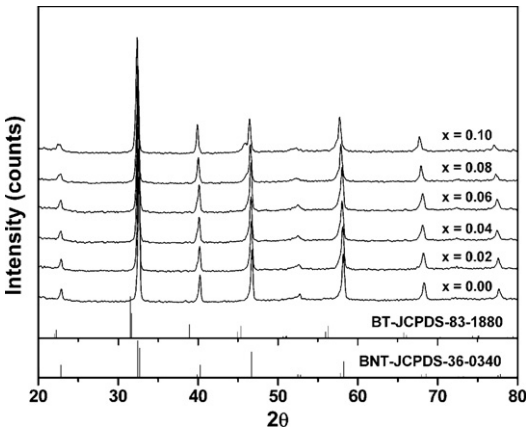

Fig. 1. X-ray diffraction patterns of $(1-x)$BNLT–xBT ceramics, where $x = 0.0$–0.10.

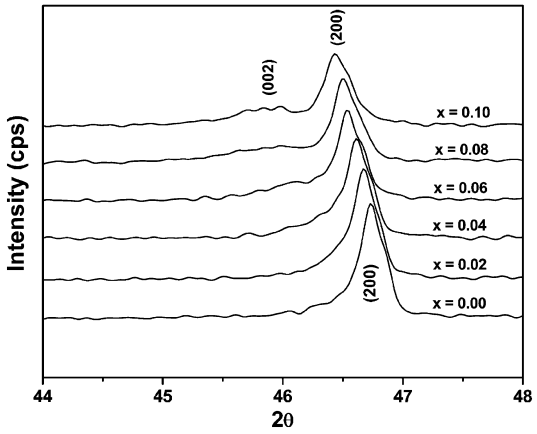

Fig. 2. X-ray diffraction patterns of $(1-x)$BNLT–xBT ceramics at 2θ between 44° and 48°.

Bi^{3+} ion (131 pm) being so small (about 0.8%) and both ions also having the same valency.

The microstructural analysis of all ceramics has been carried out and the SEM micrographs of the as-formed surfaces are illustrated in Fig. 3. All have a dense structure with low porosity. The small addition of BT, however, inhibited grain growth dramatically, as can be seen from the average grain size (Table 1) which was reduced from 4.10 ± 0.46 μm for pure BNLT (Fig. 3(a)) to about 1.86 ± 0.19 μm for the 2 mol% BT added sample (Fig. 3b). This may be attributed to the large difference between ionic radius of Ba^{2+} (156 pm) and Bi^{3+} (131 pm) and the possibility that Ba^{2+} aggregates and forms secondary phases on a very small scale at the grain boundaries. This may prevent grain boundary movement during the sintering process [10]. However, increasing the amount of BT from 0.04 to 0.10 had no significant effect on the grain size and shape of the ceramics as can be seen in Fig. 3c–f.

The experimental on dielectric measurements at room temperature for various BT contents are graphically presented in Fig. 4. It can be clearly seen that ε_r increases with

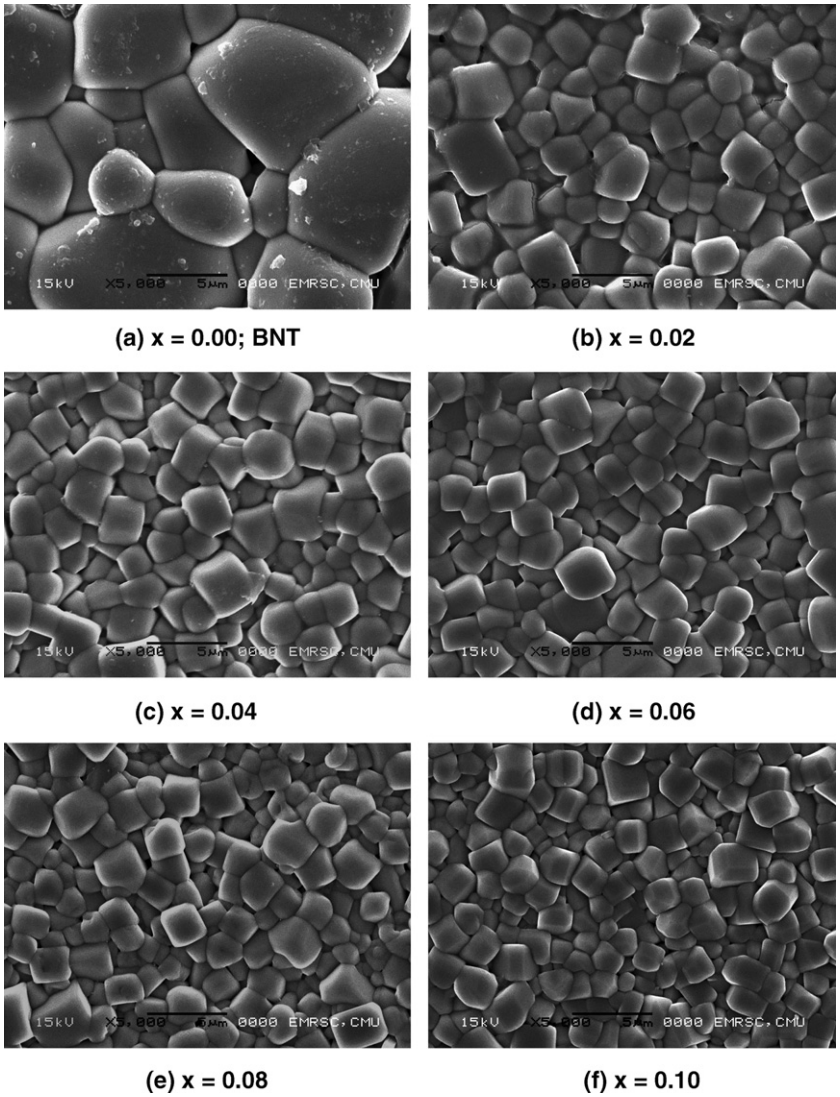

Fig. 3. SEM micrographs of (a) BNT and $(1-x)$BNLT–xBT ceramics, where (b) $x = 0.02$ to (f) $x = 0.10$.

Table 1
The values of density, grain size, dielectric constant (ε_r) and piezoelectric coefficient (d_{33}) at room temperature of $(1-x)$BNLT–xBT samples

Samples	Density (g/cm^3)	Grain size (μm)	ε_r ($T_{room/1\,kHz}$)	d_{33} (pC/N)
BNLT	5.85 ± 0.02	4.10 ± 0.46	780	72
0.98BNLT–0.02BT	5.86 ± 0.03	1.86 ± 0.19	863	118
0.96BNLT–0.04BT	5.86 ± 0.01	1.69 ± 0.16	1060	125
0.94BNLT–0.06BT	5.85 ± 0.01	1.57 ± 0.19	1547	52
0.92BNLT–0.08BT	5.84 ± 0.01	1.55 ± 0.23	1598	24
0.90BNLT–0.10BT	5.84 ± 0.01	1.47 ± 0.15	1615	25

increasing BT (x) and reaches a maximum at $x = 0.06$. Further addition of BT gradually increases ε_r up to $x = 0.10$. Initially, the considerable increase in ε_r values from $x = 0.02$ (rhombohedral structure) to $x = 0.06$ (rhombohedral + tetragonal structures) may be mainly due to the presence of tetragonal phase coexisting in the MPB compositions, but above this point the grain size and density may play a more important role in controlling the ε_r values of these ceramics, since the density values and grain size of the BNLT–BT samples changes slightly with increasing BT as shown in Table 1. This trend was observed at all frequencies. The dielectric loss ($\tan\delta$) was found to increase slightly up to $x = 0.04$, above which it increases monotonically with increasing BT content. This can be related to the density, which was found to decrease, indicating greater porosity, when the BT content is greater than $x = 0.04$.

The temperature dependence of the dielectric constant for all the BNLT–BT ceramics is shown in Fig. 5. A reduction of T_c was observed for the BT-containing samples, which is expected because the BT ceramic has a lower value of T_c (~130 °C compared with that of BNLT, ~340 °C). This result is consistent with the previous work [6]. The $\tan\delta$ value of all BT-containing samples is found to be lower than that of the pure BNLT sample, leading to the lower conductivity of these BNLT–BT ceramics at higher temperature (>90 °C). The important mechanism of ionic

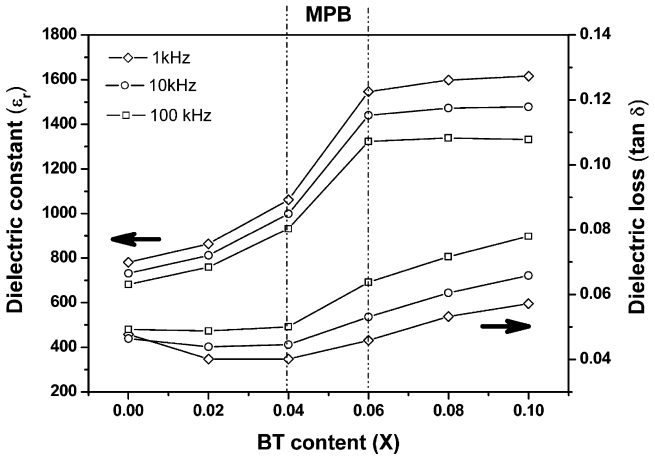

Fig. 4. The dielectric constant (ε_r) and loss tangent ($\tan\delta$) at room temperature vs BT content (x) in the $(1-x)$BNLT–xBT system.

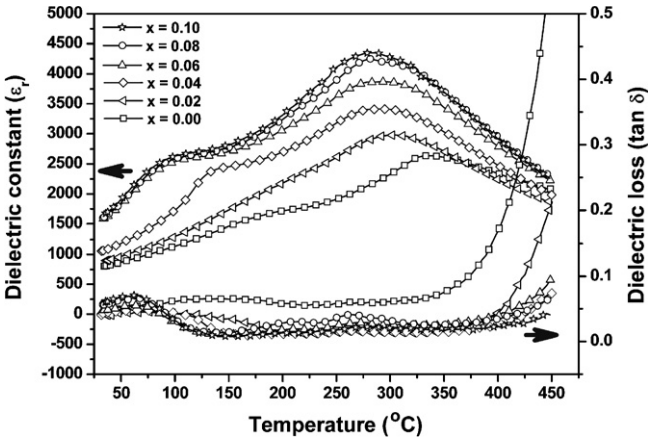

Fig. 5. Variation of dielectric constant (ε_r) and loss tangent ($\tan\delta$) with temperature for $(1-x)$BNLT–xBT ceramics at 1 kHz.

conductivity in these ceramics is the movement of ions which are the current carriers. It has been long known that the alkali ion is a good current carrier in ceramics; therefore, this ion plays an important role in the conductivity of the BNLT ceramics, since the Na^+ ions in BNLT move easily upon heating, resulting in the increase in conductivity with increasing temperature. In BT doping ceramics, the large Ba^{2+} (156 pm) ions are substituted into the A-sites of the BNLT, which possibly blocks the passage of the Na^+ current carriers, causing a reduction of conductivity in the BNLT–BT ceramics which gradually increases upon heating. When the temperature is further increased above T_c, the conductivity or ($\tan\delta$) is found to increase dramatically, as a result of the structural change from tetragonal to cubic at the Curie temperature.

The piezoelectric coefficient (d_{33}) values were measured by a d_{33} meter. Table 2 shows that BT content reaches a limit in enhancing the d_{33} value at $x = 0.04$ at which the maximum d_{33} value is about 130 pC/N. After that, the increase in tetragonal phase lowers the d_{33} value of the ceramics, reducing it to as low as 32 pC/N in the $x = 0.10$ sample. This may be attributed to the decrease in density of the high BT content samples.

Table 2 shows the important properties of the BNLT, and BNLT–BT samples prepared in this work, compared to previous results. It is clearly seen that the BT phase has a significant effect in enhancing the d_{33} of BNLT ceramics. In this work, the maximum d_{33} value was about

Table 2
The values of dielectric constant (ε_r), loss tangent ($\tan\delta$) and piezoelectric coefficient (d_{33}) at room temperature of selected samples compared to the literature values

Samples	ε_r (T_{room})	$\tan\delta$ (T_{room})	d_{33} (pC/N)
BNLT (this work)	730 (1 kHz)	0.05 (1 kHz)	72
0.96BNLT–0.04BT (this work)	1000 (10 kHz)	0.04 (10 kHz)	130
BNLT [5]	550 (1 kHz)	0.04 (1 kHz)	91
0.94BNT–0.06BT [3]	950 (10 kHz)	0.01 (10 kHz)	125

130 pC/N at the MPB composition of $x = 0.04$ (0.96BNLT–0.04BT), which is slightly higher than for the BNT–BT system (about 125 pC/N) [3].

4. Conclusions

The dielectric and piezoelectric properties of $(1 - x)$BNLT–xBT ceramics were determined. The piezoelectric coefficient (d_{33}) can be improved to a value of about 130 pC/N in the 0.96BNLT–0.04BT ceramic sample. The dielectric constant (ε_r) of the BNLT–BT ceramics was enhanced by the addition of BT content, while at the same time, their T_c was lowered. Moreover, BT doping helped to reduce the dielectric loss ($\tan\delta$) of the ceramics at high temperature.

Acknowledgements

The authors would like to thank the Thailand Research Fund and Faculty of Science, Chiang Mai University for financial support. The sincere thanks also go to the Research Laboratory for Excellent Electronic Materials, Department of Physics, and Graduate School, Chiang Mai University.

References

[1] G.A. Smolenskii, V.A. Isupov, A.I. Agranovskaya, N.N. Kraink, Sov. Phys. Solid State 2 (1961) 2651.
[2] K. Sakata, Y. Masuda, Ferroelectrics 5 (1994) 347.
[3] T. Takenaka, K. Maruyama, K. Sakata, Jpn. J. Appl. Phys. 30 (9B) (1991) 2246.
[4] T. Takenaka, H. Nagata, J. Eur. Ceram. Soc. 25 (2005) 2693.
[5] A. Herabut, A. Safari, J. Am. Ceram. Soc. 80 (11) (1997) 2954.
[6] T. Takenaka, K. Sakata, K. Toda, Jpn. J. Appl. Phys. 28 (1989) 59.
[7] H. Ishii, H. Nagata, T. Takenaka, Jpn. J. Appl. Phys. 40 (9B) (2001) 5660.
[8] C. Peng, J.F. Li, W. Gong, Mater. Lett. 59 (2005) 1576.
[9] K. Pengpat, S. Hanphimol, S. Eitssayeam, U. Intatha, G. Rujijanagul, T. Tunkasiri, J. Electroceram. 16 (2006) 301.
[10] S.H. Lee, C.B. Yoon, S.B. Seo, H.E. Kim, J. Mater. Res. 18 (2003) 1765.

Observation of high dielectric constants in $x(Pb(Zn_{1/3}Nb_{2/3})O_3-(0.2-x)Pb(Ni_{1/3}Nb_{2/3})O_3-0.8Pb(Zr_{1/2}Ti_{1/2})O_3$ ternary solid solutions

Sucheewan Nabunmee and Gobwute Rujijanagul[a)]
Department of Physics, Faculty of Science, Chiang Mai University, Chiang Mai 50200, Thailand

Naratip Vittayakorn
Material Science Research Unit, Department of Chemistry, Faculty of Science, King Mongkut's Institute of Technology Ladkrabang, Bangkok 10520, Thailand

David P. Cann
Faculty of Materials Science, Department of Mechanical Engineering, Oregon State University, Corvallis, Oregon 97331, USA

(Received 12 June 2007; accepted 3 October 2007; published online 14 November 2007)

In the present work, we demonstrate the results of combining two excellent ferroelectric materials at their morphotropic phase boundary compositions, i.e., $0.2(Pb(Zn_{1/3}Nb_{2/3})O_3-0.8Pb(Zr_{1/2}Ti_{1/2})O_3$ (0.2PZN-0.8PZT) and $0.2Pb(Ni_{1/3}Nb_{2/3})O_3-0.8Pb(Zr_{1/2}Ti_{1/2})O_3$ (0.2PNN-0.8PZT) to form a ternary solid solution of $x(Pb(Zn_{1/3}Nb_{2/3})O_3-(0.2-x)Pb(Ni_{1/3}Nb_{2/3})O_3-0.8Pb(Zr_{1/2}Ti_{1/2})O_3$ (xPZN-(0.2−x)PNN-0.8PZT) which exhibits superior dielectric properties. Examination of the dielectric spectra indicated that the ternary system exhibits a very high relative permittivity of 49 800 (at 10 kHz) for the composition at $x=0.10$. In addition, an increased amount of PZN was observed to enhance the ferroelectric properties of the system. © *2007 American Institute of Physics*. [DOI: 10.1063/1.2809276]

I. INTRODUCTION

Lead-based perovskites, with the formula of $Pb(B'_xB''_{(1-x)})O_3$, are widely studied and developed because of their superior dielectric, ferroelectric, and piezoelectric properties. Lead zirconate titanate $Pb(Zr_{1-x}Ti_x)O_3$ (PZT) is a lead-based perovskite and it is also a normal ferroelectric material which is host to exceptionally high dielectric and piezoelectric properties. The optimum electrical properties of PZT were reported for compositions close to morphotropic phase boundary (MPB), i.e., $x\sim0.48$. Locating the MPB for the ferroelectric materials is very important for making the phase diagram and for obtaining excellent electrical properties. Therefore, most commercial ferroelectric ceramics are thus designed in the vicinity of the MPB with various doping schemes in order to achieve excellent properties.[1–4]

Up to now, many authors have focused on ferroelectric materials which have relaxor ferroelectric behavior such as $Pb(Zn_{1/3}Nb_{2/3})O_3$(PZN) and $Pb(Ni_{1/3}Nb_{2/3})O_3$(PNN). Submicron-scale heterogeneous distribution of the B cations is believed to be the origin of their relaxor nature, typically having a diffuse and frequency-dependent maximum in the variation of the relative permittivity with temperature.[5–7]

Recently, binary or ternary systems containing a combination of relaxor ferroelectrics with rhombohedral symmetry and normal ferroelectric tetragonal symmetry near the MPB have attracted particular attention owing to their high dielectric and piezoelectric properties.[8–11] The excellent electrical properties can be applied to many areas such as multilayer ceramic capacitors, electrostrictive transducers, sensors, and actuators.[12,13] Our recent works found that binary system of xPZN-(1−x)PZT exhibited two MPBs at $x=0.5$ and $x\sim0.2-0.3$.[14–16] The maximum value of d_{33} (>600 pC/N) and the highest k_p (~0.7) were recorded for the composition $x=0.3$.[15] Furthermore, we also observed a large relative permittivity of more than 30 000 in the xPNN-(1−x)PZT system at $x\sim0.2$.[9] Since both the 0.2PZN-0.8PZT and 0.2PNN-0.8PZT compositions are at their MPB and have excellent electrical properties individually; it is of great interest to combine these two systems to form a PZN-PNN-PZT ternary solid solution. In the present work, the ternary solid solution of xPZN-(0.2−x)PNN-0.8PZT, where $x=0-0.2$, was synthesized. To obtain a homogeneous perovskite solid solution and better electrical properties, the samples were prepared by a columbite method. Figure 1 schematically shows the composition range which was studied in this work. The finding of dielectric constants approaching 50 000 with low dielectric loss in the ternary solid solution is presented. In addition, the effect of PZN on the phase transitions and ferroelectric properties of xPZN-(0.2−x)PNN-0.8PZT are also reported.

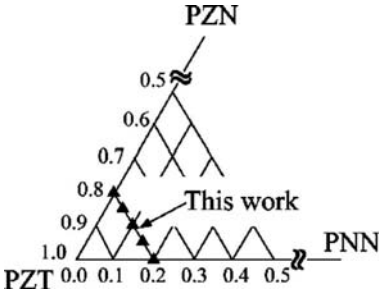

FIG. 1. Compositions studied in the $x(Pb(Zn_{1/3}Nb_{2/3})O_3-(0.2-x)Pb(Ni_{1/3}Nb_{2/3})O_3-0.8Pb(Zr_{1/2}Ti_{1/2})O_3$ ternary solid solutions.

[a)]Author to whom correspondence should be addressed. Tel.: +66 53 943 376. FAX: +66 53 357 512. Electronic mail: rujijanagul@yahoo.com

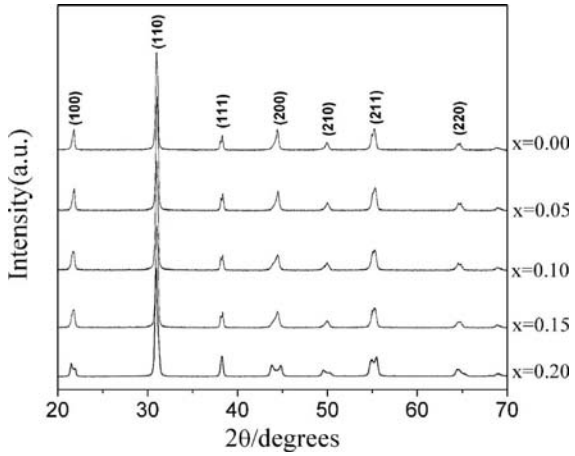

FIG. 2. XRD patterns at room temperature of xPZN-$(0.2-x)$PNN-0.8PZT, $x=0-0.20$ ceramics.

II. EXPERIMENTAL PROCEDURE

The ternary system of xPZN-$(0.2-x)$PNN-0.8PZT, where $x=0.00$, 0.05, 0.10, 0.15, and 0.20, was synthesized by a columbite method. The columbite precursor $ZnNb_2O_6$ was prepared from the reaction between ZnO and Nb_2O_5 at 975 °C for 4 h. The wolframite precursor $ZrTiO_4$ was formed by reaction between ZrO_2 with TiO_2 at 1400 °C for 4 h. The powders of precursors were then mixed with PbO. An excess of PbO equivalent to 2 mol % was also added to the mixed powder. The mixed powders were calcined at temperatures ranging 800, 850, 900, and 950 °C at a dwell time of 2 h in a double crucible configuration with a heating rate of 20 °C/min.[17] The calcined powders were isostatically cold pressed into pellets at a pressure of 100 MPa. Sintering occurred between 1100 and 1200 °C with a dwell time of 4 h. Phase formation in calcined powders and sintered pellets was determined by x-ray diffraction (XRD) using an x-ray diffractometer with Cu $K\alpha$ radiation. The density of the samples was measured by Archimedes' method. The highest density sample in each composition was selected for characterization. The samples for dielectric measurement were polished and electroded with gold sputtering. The dielectric properties were measured with an HP-4284A *LCR* meter utilizing an environmental chamber for the temperature measurements. The ferroelectric polarization versus electric field (P-E) measurements was made using a RT66A ferroelectric measurement.

III. RESULTS AND DISCUSSION

A. Crystal structure and phase transition studies

Figure 2 shows XRD pattern of xPZN-$(0.2-x)$PNN-0.8PZT ceramics, each exhibiting a phase-pure perovskite phase with no secondary phases present within the detection limit of the equipment. Figure 3 shows the evolution of the (200) peak as a function of composition. There was appearance of multiple peaks due to the superposition of the tetragonal and rhombohedral (200) peaks. In general, the single peak of (200) reflection results for the rhombohedral phase, whereas it splits into two peaks for the tetragonal

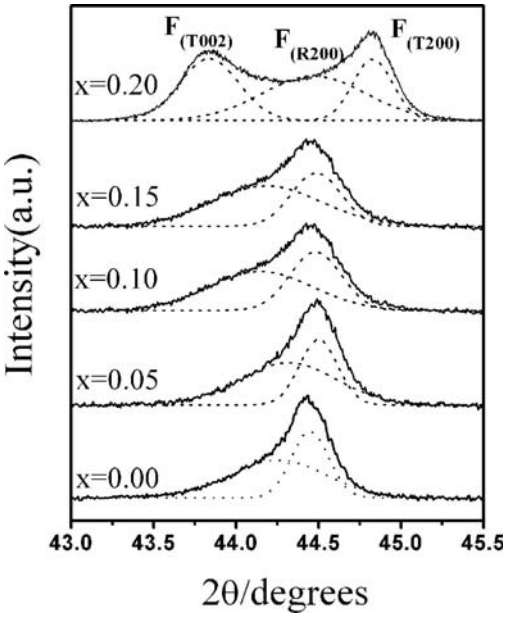

FIG. 3. XRD patterns of the (002) and (200) peaks of xPZN-$(0.2-x)$PNN-0.8PZT ceramics. $F_{T(002)}$, $F_{T(200)}$, and $F_{R(200)}$ indicate (002), (200) tetragonal reflections and (200) rhombohedral reflection, respectively.

phase. In the present work, the XRD pattern for the $x=0.00$ sample shows a weak splitting of the (200) peak. However, a strong splitting of the (200) peak was observed as the PZN content increased. In order to identify the phase compositions between rhombohedral and tetragonal phases, the (200) peaks can be fitted with Gaussian peaks, as seen in Fig. 3. For the $x=0.00-0.15$ samples, it can only be fitted with two Gaussian peaks because of the intensive overlap of the (200) tetragonal and (200) rhombohedral planes. This result implies the dominance of the rhombohedral phase (rhombohedral rich). However, it can be well fitted with three peaks for the $x=0.20$ samples, indicating a stabilization of the tetragonal phase at high PZN concentrations. Similar behavior was reported by other authors in different ferroelectric systems.[18] Thus there is a transformation from the rhombohedral rich phase to the tetragonal rich phase across the compositional range $x=0.05-0.20$. It can be assumed that a MPB separating the tetragonal rich phase from the rhombohedral rich phase exists between $x=0.05$ and 0.15.

B. Dielectric properties

The characteristic temperature and frequency dependence of the relative permittivity for xPZN-$(0.2-x)$PNN-0.8PZT, $x=0-0.20$, are shown in Fig. 4. All compositions showed a dispersive dielectric behavior with respect to frequency. It can be noted that the $x=0.00$ and $x=0.20$ samples displayed a pronounced frequency dependence of the relative permittivity, while the frequency dispersion for $x=0.1$ sample was not as strong. The maximum permittivity ($\varepsilon_{r,\max}$) and $T_{\max}$ as a function of PNN content are shown in Fig. 5. A clear transition in $T_{\max}$ at the tetragonal to cubic phase transition was observed as $T_{\max}$ increased with the amount of PZN. The $T_{\max}$ of the constituent compounds

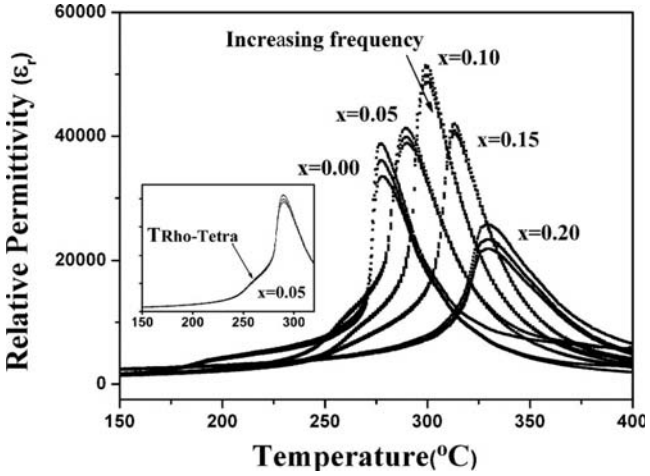

FIG. 4. Temperature dependence of the relative permittivity ε_r for xPZN-(0.2−x)PNN-0.8PZT, x=0–0.20. Measurement frequencies include 1, 10, and 100 kHz.

PNN, PZN, and PZT are −120, 140, and 390 °C, respectively, which can be used to calculate an empirical estimate of $T_{\max}$ by the equation

$$T_{\max} = x(140\ ^\circ\mathrm{C}) + (0.2 - x)(-120\ ^\circ\mathrm{C}) + 0.8(390\ ^\circ\mathrm{C}). \quad (1)$$

The values of the experimentally measured $T_{\max}$, the calculated $T_{\max}$, and the measured $\varepsilon_{r,\max}$ as a function of composition x are also shown in Fig. 5. It is evident that Eq. (1) gives a reasonable indication of the transition temperature $T_{\max}$, suggesting that this system is a well behaved complete solid solution. The deviation between the calculated and measured $T_{\max}$ values may be attributed to Zn volatility. The highest $\varepsilon_{r,\max}$ of 49 800 at 300 °C at 10 kHz was recorded for the x=0.10 sample. In addition, the transformation from the relaxor ferroelectric to the normal ferroelectric state displayed a shoulder at the rhombohedral to tetragonal phase transition temperature ($T_{\text{rho-tetra}}$) for compositions x =0.00–0.10, as shown in the inset of Fig. 4. A similar transition has been reported in other systems.[9,19] In this work, the transition temperatures were approximately 195, 257, and 265 °C for compositions x=0.00, 0.05, and 0.10, respectively. However, it is less obvious in compositions x=0.15 and 0.20.

It is well known that the permittivity of a first-order normal ferroelectric can be described by the Curie-Weiss law according to

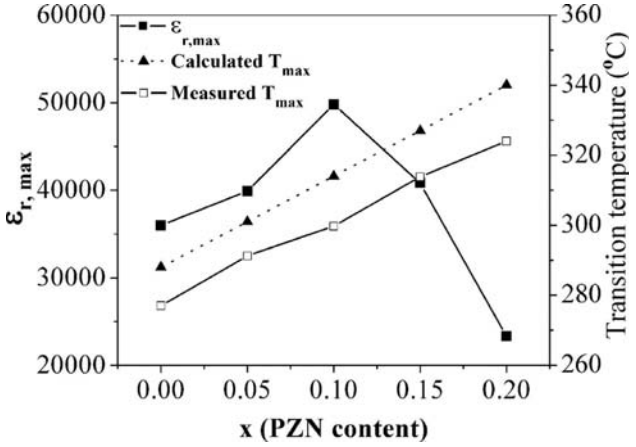

FIG. 5. Measured $T_{\max}$, calculated $T_{\max}$, and $\varepsilon_{r,,\max}$ as a function x for xPZN-(0.2−x)PNN-0.8PZT ceramics.

$$\frac{1}{\varepsilon_r} = \frac{T - \theta}{C}, \quad (2)$$

where θ is the Curie-Weiss temperature and C is the Curie constant. In the case of a normal ferroelectric in solid solution with a relaxor ferroelectric, the ε_r versus T relationship follows a similar function with the additional variables γ and δ_γ,[20,21]

$$\frac{\varepsilon'_m}{\varepsilon'(f,T)} = 1 + \frac{[T - T_m(f)]^\gamma}{2\delta_\gamma^2}, \quad (3)$$

where $1 \leqslant \gamma \leqslant 2$. When γ=1, Eq. (2) simplifies to the Curie-Weiss law; when γ=2 this equation describes the ideal relaxor behavior with a quadratic dependence. The parameter ε'_m is the maximum value of the permittivity at $T=T_m(f)$ and $\varepsilon'(f,T)$ is the relative permittivity of the sample. If $\ln[\varepsilon'_m/\varepsilon'(f,T)-1]$ is plotted versus $[T-T_m(f)]^2$, the values of γ and δ_γ can be determined as seen in Table I. The parameter γ was determined to be in the range of 1.60–1.75 and the diffuseness parameter δ_γ was measured to be 7.56–16.2. At x=0.10, the lowest values of δ_γ and γ were found, indicating a decreased diffuseness in the phase transition.

C. Ferroelectric properties

Figure 6 shows the result of polarization-field (P-E) measurements for xPZN-(0.2−x)PNN-0.8PZT ceramics. All samples showed normal ferroelectric behavior with a rectangular loop. The values of P_r and E_c determined from the hysteresis loops are listed in Table I. The addition of PZN

TABLE I. Dielectric and ferroelectric properties of xPZN-(0.2−x)PNN-0.8PZT ceramics.

PZN content (x)	ε_r at 25 °C	tan δ at 25 °C	$T_{\max}$(°C) at 10 kHz	ε_r at $T_{\max}$	tan δ at $T_{\max}$	δ_γ (°C)	γ	P_r (μC/cm^2)	P_s (μC/cm^2)	E_c (kV/cm)	R_{sq}
0.00	727	0.016	286	36 000	0.045	9.65	1.65	20.4	25.5	8.32	1.27
0.05	765	0.017	291	39 900	0.050	9.53	1.63	21.6	28.7	7.42	1.29
0.10	739	0.023	300	49 800	0.025	7.56	1.60	24.5	31.1	7.56	1.36
0.15	705	0.030	314	40 800	0.020	9.18	1.67	33.4	38.8	7.80	1.61
0.20	1540	0.022	329	23 300	0.070	16.2	1.75	41.1	45.9	9.36	1.86

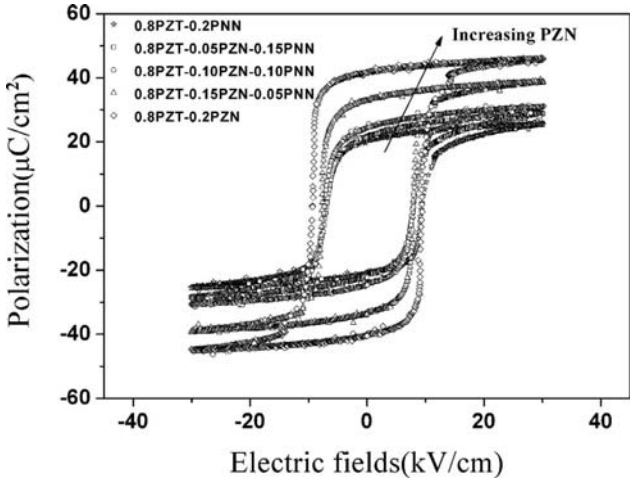

FIG. 6. Room temperature polarization vs electric field hystersis loops for xPZN-(0.2−x)PNN-0.8PZT ceramics.

was observed to produce a dramatic increase in the remanent polarization, which can be fitted to the following exponential relationship:

$$P_r = 3.924 \exp(x/0.1) + 15.78 \ \mu\text{C/cm}^2, \quad (4)$$

as a function of composition (x). The E_c value was found to be in the range of 7.42–9.36 kV/mm. The value of E_c decreased from 8.32 μC/cm^2 for x=0.00 to 7.42 μC/cm^2 for x=0.05 and then increased to 9.36 for x=0.20.

Jin *et al.*[22] derived an empirical relationship between remanent polarization, saturation polarization, and the polarization beyond the coercive field. This permits the quantification of changes in the hysteresis behavior for each sample through the following equation:

$$R_{\text{sq}} = \frac{P_r}{P_s} + \frac{P_{1.1E_c}}{P_r}, \quad (5)$$

where R_{sq} is the squareness of the hysteresis loop, P_r is the remanent polarization, P_s is the saturation polarization, and $P_{1.1E_c}$ is the polarization at an electric field equal to 1.1 times the coercive field. In this equation, an ideal hysteresis loop would have a squareness parameter equal to 2. The squareness values of the hysteresis loops of the samples are listed in Table I. The values of R_{sq} increased from 1.27 for x =0.00 to 1.86 for x=0.2, which indicates that PZN helps to improve the ferroelectric properties with better squareness and remanent polarization.

IV. CONCLUSIONS

In the present work, xPZN-(0.2−x)PNN-0.8PZT ceramics prepared by a columbite method showed a very high relative permittivity at the x=0.1 composition. Improved ferroelectric properties were also observed at higher PZN contents. Our results indicate great potential to find the better electrical properties in other PZN-PNN based systems for future work.

ACKNOWLEDGMENTS

This work was supported by The Thailand Research Fund (TRF), Faculty of Science and Graduate School Chiang Mai University, King Mongkut's Institute of Technology Ladkrabang (KMITL), and Commission on Higher Education (CHE) Thailand. The authors would like to thank Professor Dr. Tawee Tunkasiri for his help in many facilities.

[1] B. Jaffe, W. R. Cook, and H. Jaffe, *Piezoelectric Ceramics* (Academic, New York, 1971).
[2] Y. Xu, *Ferroelectric Materials and Their Applications* (Elsevier Science, Amsterdam, 1991).
[3] G. H. Haertling, J. Am. Ceram. Soc. **82**, 797 (1999).
[4] P. Seung-Eek and T. R. Shrout, Ultrason., Ferroelectr. Freq. Control, IEEE Trans. **44**, 1140 (1997).
[5] C. A. Randall, A. S. Bhalla, T. R. Shrout, and L. E. Cross, J. Mater. Res. **5**, 829 (1990).
[6] C. A. Randall, A. S. Bhalla, T. R. Shrout, and L. E. Cross, Ferroelectrics **11**, 103 (1990).
[7] C. A. Randall and A. S. Bhalla, Jpn. J. Appl. Phys., Part 1 **29**, 327 (1990).
[8] H. Fan, L. Zhang, L. Zhang, and X. Yao, J. Phys.: Condens. Matter **12**, 4381 (2000).
[9] N. Vittayakorn, G. Rujijanagul, X. Tan, M. A. Marquardt, and D. P. Cann, J. Appl. Phys. **96**, 5103 (2004).
[10] S. Wongsaenmai, Y. Laosiritaworn, S. Ananta, and R. Yimnirun, Mater. Sci. Eng., B **128**, 83 (2005).
[11] N. Vittayakorn and S. Wirunchit, Smart Mater. Struct. **16**, 851 (2007).
[12] K. Uchino, *Piezoelectric Actuators and Ultrasonic Motors* (Kluwer Academic, Boston, 1996).
[13] K. Uchino, *Ferroelectric Devices* (Dekker, New York, 2000).
[14] N. Vittayakorn, G. Rujijanagul, T. Tunkasiri, X. Tan, and D. P. Cann, Mater. Sci. Eng., B **108**, 258 (2004).
[15] N. Vittayakorn, C. Puchmark, G. Rujijanagul, X. Tan, and D. P. Cann, Curr. Appl. Phys. **6**, 303 (2006).
[16] N. Vittayakorn, G. Rujijanagul, X. Tan, H. He, M. A. Marquardt, and D. P. Cann, J. Electroceram. **16**, 141 (2006).
[17] N. Vittayakorn, G. Rujijanagul, T. Tunkasiri, X. Tan, and D. P. Cann, J. Mater. Res. **18**, 2882 (2003).
[18] H. Fan and H. E. Kim, J. Am. Ceram. Soc. **84**, 636 (2001).
[19] M.-S. Yoon and H. M. Jang, J. Appl. Phys. **77**, 3991 (1995).
[20] K. Uchino and S. Nomura, Ferroelectr., Lett. Sect. **44**, 55 (1982).
[21] H. T. Martirena and J. C. Burfoot, Ferroelectrics **7**, 151 (1974).
[22] B. M. Jin, J. Kim, and S. C. Kim, Appl. Phys. A: Mater. Sci. Process. **65**, 53 (1997).

Available online at www.sciencedirect.com
ScienceDirect
Current Applied Physics 8 (2008) 88–92
Current Applied Physics
An official journal of the KPS
www.elsevier.com/locate/cap
www.kps.or.kr

Influence of fabrication processing on phase transition and electrical properties of $0.8Pb(Zr_{1/2}Ti_{1/2})O_3$–$0.2Pb(Ni_{1/3}Nb_{2/3})O_3$ ceramics

G. Rujijanagul [a,*], N. Vittayakorn [b]

[a] Department of Physics, Faculty of Science, Chiang Mai University, Chiang Mai 50200, Thailand
[b] Department of Chemistry, Faculty of Science, King Mongkut's Institute of Technology, Ladkrabang, Bangkok 10520, Thailand

Received 9 January 2007; received in revised form 11 May 2007; accepted 21 May 2007
Available online 31 May 2007

Abstract

The binary system of $0.8Pb(Zr_{1/2}Ti_{1/2})O_3$–$0.2Pb(Ni_{1/3}Nb_{2/3})O_3$ ceramics were synthesized by conventional mixed oxide and columbite method. X-ray diffraction analysis demonstrated the coexistence of both the rhombohedral and tetragonal phases for the columbite prepared sample. Rhombohedral to tetragonal phase transition for columbite method was different compared with those of the mixed oxide method. The permittivity shows a shoulder at the rhombohedral to tetragonal phase transition temperature $T_{Rho-Tetra} = 195$ °C, and then a maximum permittivity (36,000 at 10 kHz) at the transition temperature $T_m = 277$ °C on ceramics prepared with the columbite method. However, piezoelectric coefficient (d_{33}) was measured to be 282 pC/N for the conventional method and higher than the columbite method. The results were related to the phase compositions and porosity of the ceramics.

PACS: 77.22.−d; 77.22.Gm; 77.84.Dy

Keywords: Phase transition; Dielectric properties; Ferroelectric properties; Columbite method

1. Introduction

$Pb(Ni_{1/3}Nb_{2/3})O_3$ (PNN) is a relaxor ferroelectric material which has a cubic structure at room temperature. It shows a broad dielectric peak near $T_c \approx -120$ °C with relative permittivity near 4000 at 1 kHz [1]. Nanometer-level chemical heterogeneity in the form of short range ordering of Ni^{2+} and Nb^{5+} on the B′ site was proposed to account for the diffuse phase transition [2]. Pure perovkite phase of PNN can be prepared by the columbite method. This material can be alloyed with normal ferroelectric to optimize the electrical properties [3].

Lead zirconate-titanate, $Pb(Zr_xTi_{1-x})O_3$ (PZT) is a normal ferroelectric material which has been extensively investigated in the past because of their owing to the exceptionally good dielectric and piezoelectric properties as well as high Curie temperature (>350 °C) [4]. The high dielectric and piezoelectric of PZT was found for the composition close to the morphotropic phase boundary (MPB). This MPB is located around $PbZrO_3$:$PbTiO_3 \sim 0.52$:0.48 and separates the Ti-rich tetragonal phase from the Zr-rich rhombohedral phase [4]. PZT-based ceramics were applied in many areas such as spark igniters, micro-actuators, sensors, piezo-transformers, transducers and multilayer ceramic capacitors, electro-optical and micro-electromechanical systems applications [4,5].

Recently, the high electrical properties have been reported in binary and ternary systems containing a combination of normal and relaxor ferroelectric materials such as $PbTiO_3$–$Pb(Mg_{1/3}Nb_{2/3})O_3$ (PT–PMN), $Pb(Zr,Ti)O_3$–$Pb(Zn_{1/3}Nb_{2/3})O_3$ (PZT–PZN), $Pb(Zr,Ti)O_3$–$Pb(Ni_{1/3}Nb_{2/3})O_3$ (PZT–PNN) [3,6–9], $PbZrO_3$–$PbTiO_3$–$Pb(Mg_{1/3}Nb_{2/3})O_3$ (PZ–PT–PMN) [10], $PbZrO_3$–$PbTiO_3$–$Pb(Ni_{1/3}Nb_{2/3})O_3$ (PZ–PT–PNN) [7–9] and $Pb(Zn_{1/3}Nb_{2/3})O_3$–$PbZrO_3$

* Corresponding author. Tel.: +66 53 943 376; fax: +66 53 357 512.
E-mail address: rujijanagul@yahoo.com (G. Rujijanagul).

1567-1739/$ - see front matter © 2007 Elsevier B.V. All rights reserved.
doi:10.1016/j.cap.2007.05.002

(PZN–PZ) [4]. The solid solution of lead nickel niobate $Pb(Ni_{1/3}Nb_{2/3})O_3$ (PNN) with $Pb(Zr_{1-x}Ti_x)O_3$ (PZT) is also a relaxor-type ferroelectrics, which has drawn much interest in recent years for its excellent dielectric, especially electrostrictive properties [7–9]. Our recent work found that the maximum relative permittivity ($\varepsilon_{r(max)}$) of MPB compositions in the PNN–PZT binary systems is higher than 30,000 [3]. However, the properties and phase transition of the lead-based ferroelectric materials are strongly influenced by density, composition, phase, and microstructure which in turn depend on the method of preparation. In the present work, the columbite precursor method and conventional mixed oxide method were used in synthesizing the 0.8PZT–0.2PNN ceramics. The columbite precursor method is used as an initial step of preparing columbite precursor ($NiNb_2O_6$) and wolframite ($ZrTiO_4$) precursor followed by a reaction with PbO to form the binary ceramics system whereas the conventional method utilizes a one-step reaction with all of the starting materials. The phase formation, phase transition and electrical properties of the ceramics prepared by both the methods were compared and discussed.

2. Experiment procedure

Ceramics of the binary system 0.8PZT–0.2PNN were prepared via the columbite method and the conventional method. For the columbite method, the columbite structure ($NiNb_2O_6$) and wolframite structure ($ZrTiO_4$) was synthesized first. $NiNb_2O_6$ was formed by reacting NiO and Nb_2O_5 at 1100 °C for 4 h, while $ZrTiO_4$ was prepared by reaction between ZrO_2 and TiO_2 at 1400 °C for 4 h. The precursors and PbO (with 2 mol% excess PbO) were weighed and mixed by ball-milling in a polyethylene bottle together with partially stabilized zirconia media. The mixture was calcined at 950 °C for 4 h in a double crucible configuration with a heating rate of 20 °C/min. After grinding and sieving, 5 wt.% of polyvinyl alcohol binder was added. The calcined powder was cold isostatically pressed into pellets at a pressure of 150 MPa. The pellets were sintered in a sealed alumina crucible at 1250 °C for 2 h. To compensate PbO volatilization, the PbO atmosphere for the sintering was maintained using $PbZrO_3$ as the spacer powder. For the conventional method, oxides of PbO, NiO, ZrO_2, TiO_2 and Nb_2O_5 were mixed in the required stoichiometric ratios to form the composition 0.8PZT–0.2PNN. The mixture was then followed the same processing condition as the columbite method. The density of the sintered samples was measured by Archimedes' method with distilled water as the fluid medium. Perovskite phase formation of sintered pellets was checked by X-ray diffraction (XRD). The microstructures of the sintered samples were examined using a scanning electron microscopy (SEM). For the electrical measurement, the pellets were polished and then electroded by gold sputtering. The relative permittivity (ε_r) at various temperature was measured using a LCR meter in junction with an environmental chamber with a heating rate of 3 °C/min. The ferroelectric polarization versus electric field (P–E) measurements was made using a Sawyer-Tower circuit at 50 Hz. The ceramics were poled for piezoelectric measurement in silicone oil at 80 °C for 30 min at field strength of 2 kV/mm. The d_{33} piezoelectric coefficient was measured using a d_{33} meter, 24 h after poling.

3. Results and discussion

Fig. 1 shows XRD patterns of the 0.8PZT–0.2PNN ceramics prepared by columbite and conventional methods. Perovskite phase was observed for both the methods. XRD patterns for the ceramics over the range $2\theta = 42–48°$ are shown in Fig. 2. There was appearance of multi peaks due to the superposition of the tetragonal and rhombohedral (200) peaks. In general, the single peak of (200) reflection results for the rhombohedral phase, whereas it

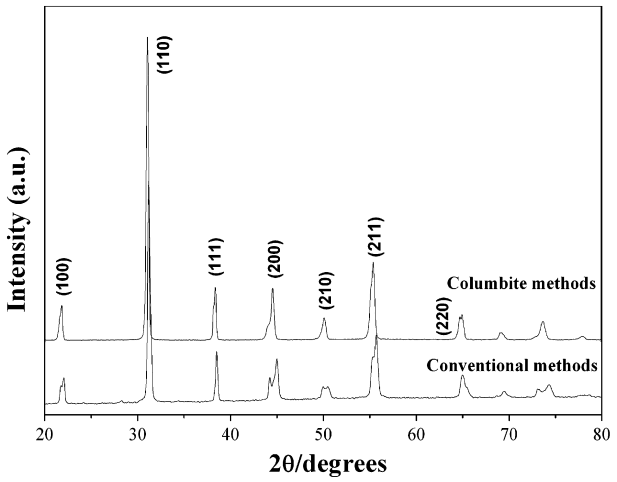

Fig. 1. XRD patterns of 0.8PZT–0.2PNN ceramics prepared by the conventional method and the columbite method.

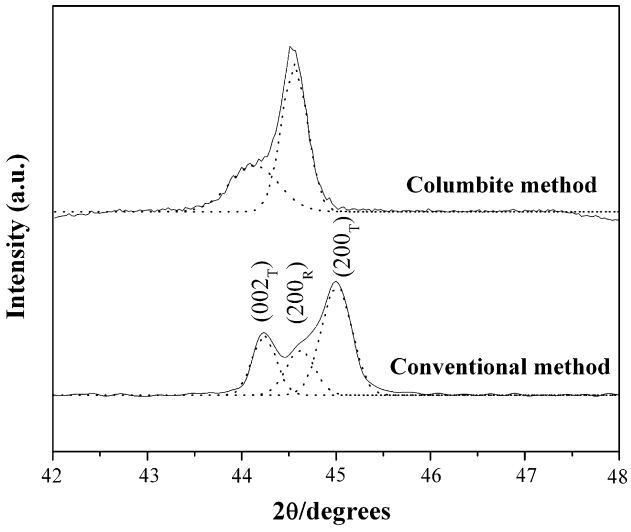

Fig. 2. XRD patterns of the (002) and (200) peaks of 0.8PZT–0.2PNN ceramics prepared by the conventional method and the columbite method.

splits into two peaks for the tetragonal phase. In the present work, the XRD pattern for the columbite prepared sample shows a weak splitting of the (200) peak, while the conventionally prepared sample exhibits a strong splitting of the peak. In order to identify the phase compositions between rhombohedral and tetragonal phase, the (200) peaks can be fitted with Gaussian peaks. For the conventionally prepared sample, it can be well fitted with three Gaussian peaks as seen in Fig. 2. However, it can only be fitted with two peaks for the columbite prepared sample because of the intensive overlap of the (200) tetragonal and (200) rhombohedral plane. The result indicates that the columbite method produced the ceramics with the dominance of the rhombohedral phase (rhombohedral rich) compared with the conventional method. Similar behavior was reported by previous authors in another ferroelectric system [11].

The ceramic density was measured to be 7.49 g/cm^3 and 7.90 g/cm^3 for columbite and conventional methods, respectively. The SEM images of fracture surface for 0.8PZT–0.2PNN ceramics prepared by both the methods are shown in Fig. 3. The porosity levels evident in SEM micrographs of the ceramics were consistent with the density values. In addition, the columbite method produces ceramics with courser grains compared with the conventional method. By using the linear intercept method to the SEM images, the average grain size was determined to be 5.8 and 2.1 μm for the columbite and conventionally prepared samples, respectively. The results suggested that different processing methods develop the ceramics with different density and grain size.

In polar dielectric, in most cases the molecules cannot orient themselves in the low-temperature region. When the temperature rises, the orientation of dipoles facilitates, and this increases the permittivity. Characteristic sets of curves are obtained if the dependence of the permittivity of strong polarized dielectrics is plotted versus two variable factors – temperature and frequency. The variations of the relative permittivity of the material under investigation were measured as a function of temperature between 1 kHz and 100 kHz. From Fig. 4, the temperature dependences of dielectric constant depict a typical relaxor behavior with strong dispersion of the dielectric peak at $T < T_m$ (T_m, the temperature of permittivity maximum) for both methods. The broad dielectric maxima shifting towards higher temperature with increasing frequency signify the

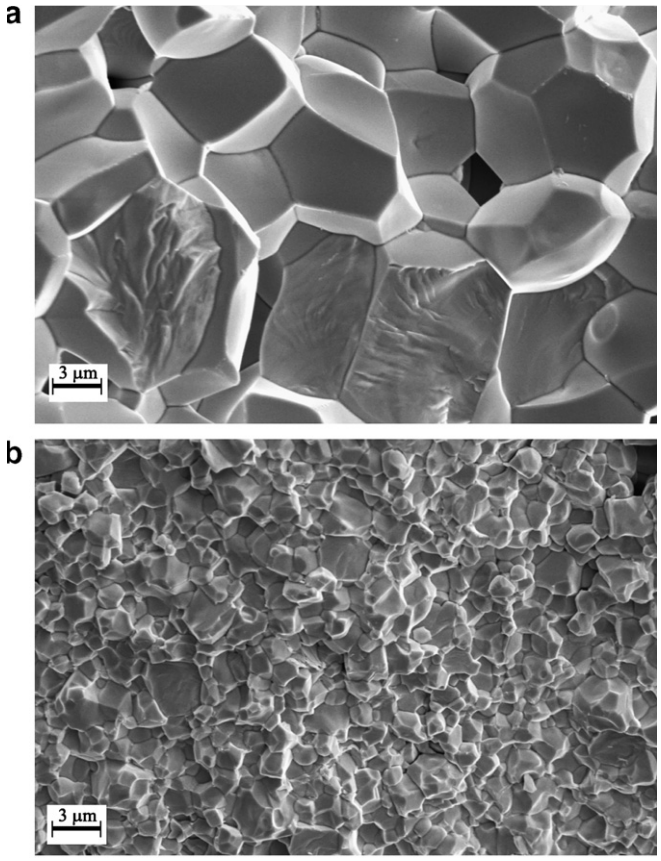

Fig. 3. Fracture surface of 0.8PZT–0.2PNN ceramics prepared by (a) columbite method and (b) conventional method.

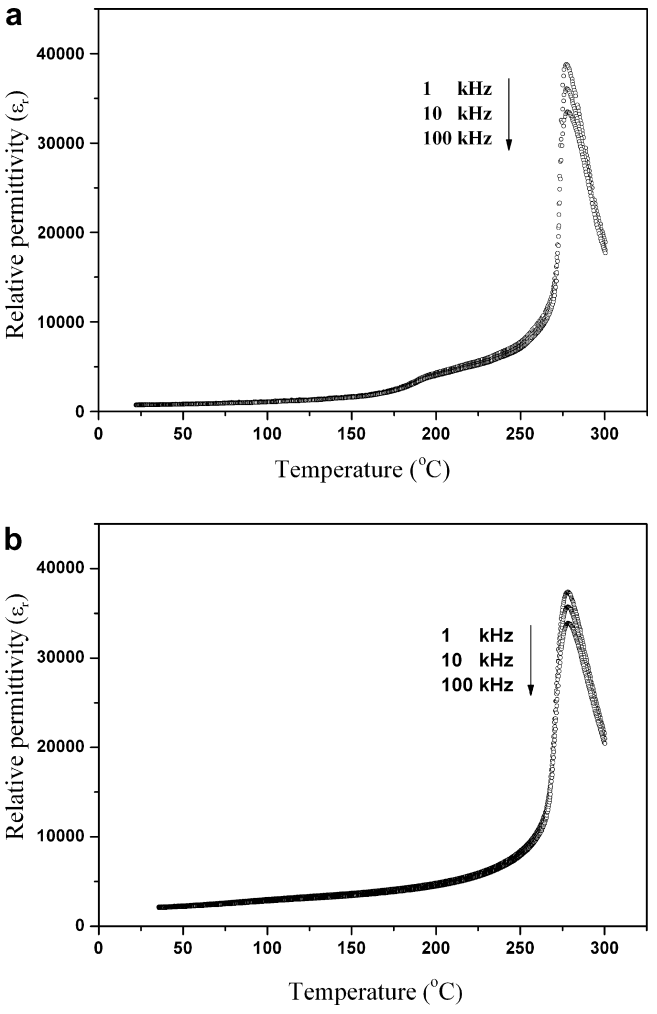

Fig. 4. Temperature dependence on the relative permittivity of 0.8PZT–0.2PNN at frequencies between 1 kHz and 100 kHz: (a) columbite method; (b) conventional method.

relaxor-like type behavior of the ceramics. Furthermore, the columbite prepared sample shows stronger frequency dependence compared with the conventional prepared sample. However, the frequency dispersion in the 0.8PZT–0.2PNN ceramics prepared by both the methods is not as strong as that in the pure relaxor PZN. Fig. 5 shows a comparison dielectric result (measured at 10 kHz) between the conventional and columbite prepared sample. The temperature at which the permittivity is maximum T_m and the relative permittivity (measured at 10 kHz) for both at room temperature and at T_m is listed in Table 1. The columbite prepared sample shows a sharp dielectric maximum at the ferroelectric transition temperature (T_m) of 277 °C with maximum permittivity value of 36,000 and the conventionally prepared sample exhibits a maximum permittivity value of 35,700 at $T_m \sim 278$ °C. Although the columbite method helps to improve the dielectric permittivity, the porosity of the samples was also found to influence on this value. Therefore, the ceramic prepared via columbite method exhibits a slightly higher relative permittivity at T_m than that of ceramics synthesized by the conventional method.

The ε_r versus T curves shown in Fig. 4 are also indicative of thermally induced phase transitions. The permittivity shows a shoulder at the rhombohedral to tetragonal phase transition temperature ($T_{Rho-Tetra}$) ~ 195 °C for the columbite prepared sample as seen in the Fig. 5. However, for the conventional method, there was observed only one peak present at the tetragonal to cubic phase transition $T_m \sim 278$ °C. Similar transition (rhombohedral to tetragonal transition) has been reported by previous authors in other systems [3,12]. The results for the rhombohedral to tetragonal transition can be related to the XRD results, i.e. rhombohedral rich composition was observed in ceramic prepared by columbite method.

In relaxor ferroelectric materials, the value of relative permittivity above T_m does not follow the Curie–Weiss law. A number of materials show behavior intermediate between proper ferroelectric and relaxor. A simple quadratic law can be used to describe a second order relaxor ferroelectric. This arises from the fact that the total number of relaxors contributing to the permittivity response in the vicinity of the permittivity peak is temperature dependent. The diffusiveness parameter (δ_γ) of the transition was determined from the equation [13,14]:

$$\frac{\varepsilon_{r(max)}}{\varepsilon_r} = \exp\left(\frac{(T - T_m)^2}{2\delta_\gamma^2}\right) \quad (1)$$

where $\varepsilon_{r(max)}$ is maximum value of the relative permittivity at $T = T_m$ and ε_r is the dielectric constant of sample. The value of the diffuseness parameter can be calculated from the slope of $\ln(\varepsilon_{r(max)}/\varepsilon_r)$ versus $(T - T_m)^2$ curve. This value is valid for the range of $\varepsilon_{r(max)}/\varepsilon_r < 1.5$, as clarified by Pilgrim et al. [13]. The graphs of $\ln(\varepsilon_{r(max)}/\varepsilon_r)$ versus $(T - T_m)^2$ is shown in Fig. 6. The values of parameter δ_γ are listed in Table 1. The parameter δ_γ is calculated to be 14.6 and 16.1 in ceramics prepared with columbite method and conventional method, respectively. A significant increase in δ_γ for the conventionally prepared sample indicates an increased diffusiveness in the phase transition. This may be due to the homogeneity at the atomic scale of the columbite

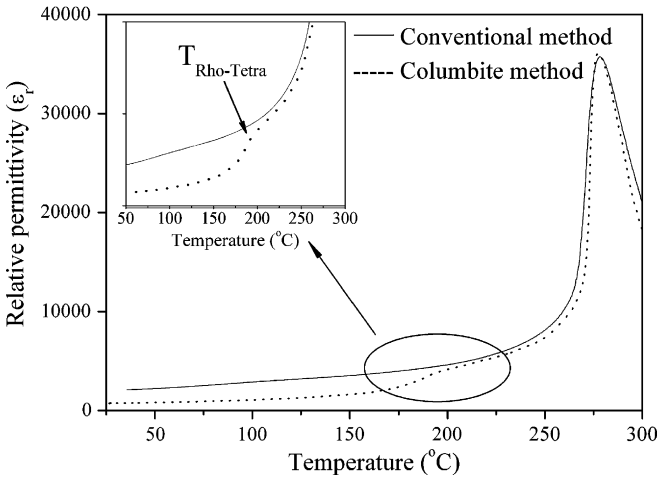

Fig. 5. Temperature dependence on the relative permittivity of 0.8PZT–0.2PNN ceramics prepared by the conventional method and the columbite method measured at 10 kHz.

Table 1
Comparisons of dielectric properties measured at 10 kHz of 0.8PZT–0.2PNN ceramics prepared by the conventional method and the columbite method

Method of preparation	ε_r at 25 °C	$\tan\delta$ at 25 °C	T_m (°C)	$\varepsilon_{r(max)}$	$\tan\delta$ at T_m	δ_γ (°C)
Columbite method	825	0.011	277	36,000	0.047	14.6
Conventional method	2100	0.014	278	35,700	0.030	16.1

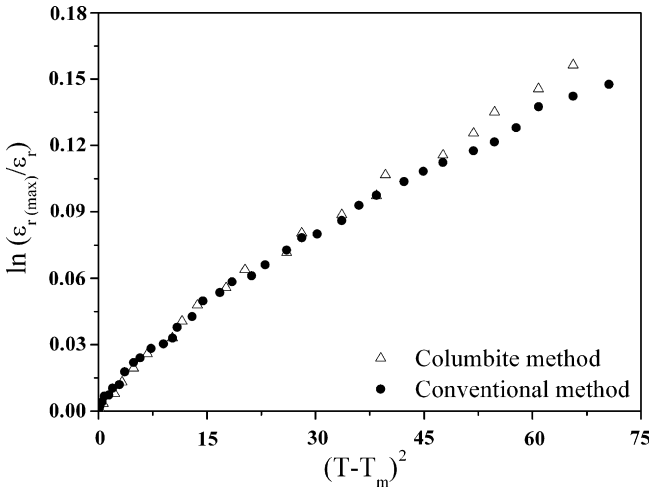

Fig. 6. The $\ln(\varepsilon_{r(max)}/\varepsilon_r)$ versus $(T - T_m)^2$ for 0.8PZT–0.2PNN ceramics prepared by the conventional method and the columbite method.

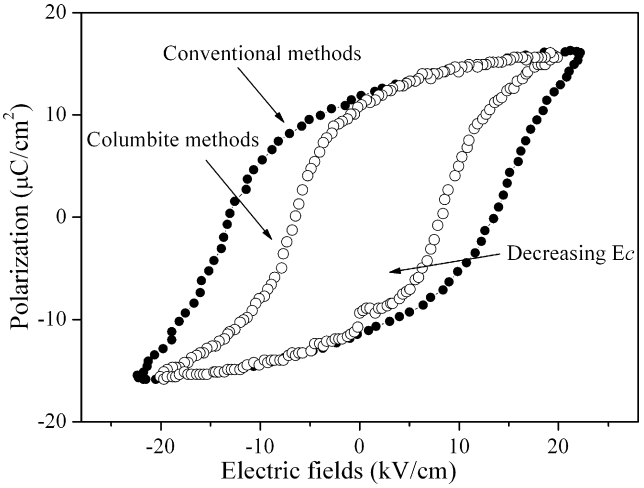

Fig. 7. P–E hysteresis of 0.8PZT–0.2PNN ceramics prepared by the conventional method and the columbite method.

prepared sample which is much higher than that in the ceramics prepared by conventional method.

The result of polarization–field (P–E) measurement (at 50 Hz) for ceramics prepared from both the methods is shown in Fig. 7. The polarization loop of both samples are well developed showing a large remanent polarization at zero field. The hysteresis loops have a typical "square" form stipulated by switching of a domain structure in an electrical field, which is typical of a phase that contains long-range cooperation between dipoles. That is characteristic of a ferroelectric micro-domain state. From the fully saturated loops, the remanent polarization P_r and coercive field E_c were determined. The values of P_r and E_c for conventional method are 10.1 μC/cm^2 and 13.3 kV/cm, respectively, whereas for columbite methods the remanent polarization P_r and coercive field E_c are 10.9 μC/cm^2 and 7.2 kV/cm, respectively. It can be noted that P_r for the columbite method is not too much higher than the conventional method, which may be due to the porosity effect. However, the higher P_r and lower E_c can be related to the more rhombohedral phase in the columbite prepared sample [15]. This trend is agreed with the results from the previous works in PMN–PZ–PT and PZT ceramics [16,17].

In order to study the piezoelectric property of the samples, the d_{33} piezoelectric coefficient was measured at the same condition. The d_{33} values were found to be 282 and 202 pC/N for the ceramics prepared by conventional and columbite method, receptively. The d_{33} value for the conventional method is relatively high compared to those reported in the literature for the same system [18]. However, d_{33} value for the columbite sample was lower than the conventional method. The lower d_{33} value is likely due to the higher porosity of the columbite prepared sample. This effect also made the ceramics difficult to pole.

4. Conclusions

The properties of 0.8PZT–0.2PNN ceramics prepared by the conventional method and the columbite methods were investigated. Phase transition behavior, dielectric, and ferroelectric properties were found to depend on the phase composition of the samples with association with the methods of preparation. Although a slightly higher dielectric constant was observed in the columbite prepared sample, the better piezoelectric property was found for the conventionally prepared sample. These results were attributed to the porosity effect.

Acknowledgements

This work was supported by The Thailand Research Fund (TRF), Faculty of Science Chiang Mai University, King Mongkut's Institute of Technology Ladkrabang (KMITL), and Commission on Higher Education (CHE) Thailand. The authors would like to thank Prof. Dr. Tawee Tunkasiri for his help in many facilities.

References

[1] G.A. Smolenskii, A.L. Agranovskaya, Sov. Phys. Tech. Phys. 2 (1958) 1380.
[2] C.A. Randall, A.S. Bhalla, Jpn. J. Appl. Phys. 29 (1990) 327.
[3] N. Vittayakorn, G. Rujijanagul, X. Tan, M.A. Marquardt, D.P. Cann, J. Appl. Phys. 96 (12) (2004) 5103.
[4] Y. Xu, Ferroelectric Materials and Their Application, Elsevier Science Publishers B.V., 1991.
[5] K. Uchino, Ferroelectrics 151 (1994) 321.
[6] K. Uchino, Solid State Ionics 108 (1998) 43.
[7] N. Vittayakorn, C. Puchmark, G. Rujijanagul, X. Tan, D.P. Cann, Curr. Appl. Phys. 6 (2006) 303.
[8] N. Vittayakorn, G. Rujijanagul, X. Tan, H. He, M.A. Marquardt, D.P. Cann, J. Electroceram 16 (2006) 141–149.
[9] N. Vittayakorn, G. Rujijanagul, T. Tunkasiri, X. Tan, D.P. Cann, Mat. Sci. Eng. B 108 (2004) 258.
[10] R. Yimnirun, S. Ananta, P. Laoratanakul, J. Eur. Ceram. Soc. 25 (2005) 3235.
[11] H. Fan, H.E. Kim, J. Am. Ceram. Soc. 84 (3) (2001) 636.
[12] M.-S. Yoon, H.M. Jang, J. Appl. Phys. 77 (1995) 3991.
[13] S.M. Pilgrim, A.E. Sutherland, S.R. Winzer, J. Am. Ceram. Soc. 73 (10) (1990) 3122.
[14] N. Vittayakorn, S. Uttiya, G. Rujijanagul, D.P. Cann, J. Phys. D: Appl. Phys. 38 (2005) 2942–2946.
[15] K.H. Yoona, H.R. Lee, J. Appl. Phys. 89 (7) (2001) 3915.
[16] W.Z. Zhu, A. Kholkin, P.Q. Mantas, J.L. Baptista, J. Mater. Sci. 36 (2001) 3447.
[17] T. Yamamoto, H. Moriwake, J. Korean Phys. Soc. 32 (1998) S1301.
[18] X. Zhu, Z. Meng, J. Mater. Sci. 31 (1996) 2171.

Antiferroelectric-ferroelectric phase transitions in $Pb_{1-x}Ba_xZrO_3$ ceramics: Effect of PbO content

T. Bongkarn,[1] G. Rujijanagul,[2] and S. J. Milne[3,a)]
[1]*Department of Physics, Naresuan University, Pitsanulok 65000, Thailand*
[2]*Department of Physics, Chiang Mai University, Chiang Mai 50200, Thailand*
[3]*Institute for Materials Research, University of Leeds, Leeds LS2 9JT, United Kingdom*

(Received 17 December 2007; accepted 10 February 2008; published online 6 March 2008)

The irreversibility of the antiferroelectric (AFE) to FE phase transition in $Pb_{1-x}Ba_xZrO_3$, $x=0.75-0.1$, compositions is shown to be a consequence of lattice vacancies arising from PbO evaporation during ceramic processing. Previously, the absence of a FE→AFE cooling transition was thought to be due to the transformational strain and the fragmentation of ferroelectric domains. Appropriate compensating levels of excess PbO added to starting powders generate the FE →AFE transition. For lower levels of Ba^{2+} substitution, $x=0.05$, the transition is reversible in noncompensated samples, but PbO compensation raises the FE→AFE transition temperature by ~25 °C. © *2008 American Institute of Physics*. [DOI: 10.1063/1.2890060]

Lead zirconate, $PbZrO_3$, transforms on heating from an orthorhombic antiferroelectric (AFE) to a rhombohedral FE phase just below the Curie temperature of 233 °C.[1–5] The antiferroelectric-ferroelectric phase transition can be induced by the application of an electric field or by hydrostatic pressure.[6,7] Substitution of Ba^{2+} for Pb^{2+} ions lowers transition temperatures, reduces the switching field, and increases the volume change associated with the field-induced transition.[8] Consequently, the $Pb_{1-x}Ba_xZrO_3$ system (PBZ) is of interest for energy storage and actuator applications.[8,9] In addition, for compositions which are ferroelectric at room temperature, favorable fatigue resistance has been demonstrated in thin films, while relaxor behavior has also been investigated.[10,11]

For antiferroelectric $Pb_{0.9}Ba_{0.1}ZrO_3$, no heating transition to the ferroelectric phase is reported to occur in ceramics made by conventional mixed-oxide processing involving powder calcination at ~1000 °C.[8,9,12,13] However, for ceramics made from chemically coprecipitated $Pb_{0.9}Ba_{0.1}CO_3$ powders, in which $Pb_{0.9}Ba_{0.1}ZrO_3$ calcination temperatures could be reduced to ~850 °C, an AFE→FE heating transition was realized, but the transition was irreversible on the cooling cycle.[8,9] The latter samples were assumed not to exhibit any PbO loss due to volatilization during ceramic processing and to be chemically homogeneous.[9] The realization of heating AFE→FE transition at ~114 °C was thought to be due to a more homogeneous Pb^{2+}/Ba^{2+} ion distribution compared to mixed-oxide samples. The absence of the cooling FE→AFE transition was proposed to be a result of a large transformational strain associated with an ~0.8% increase in unit-cell volume at the AFE→FE heating transition. This was considered to cause fine-scale fragmentation of ferroelectric domains which altered the free-energy balance in favor of retention of the FE phase.[8,9] No AFE→FE transition was recorded on cooling to −50 °C. Partial recovery of the AFE phase was evident after prolonged aging at room temperature for 10 months.[8] This was thought to be due to the "healing" of fragmented domains and eradication of broken and dangling bonds over time.[8] Here, it is demonstrated that for mixed-oxide samples, the AFE→FE transition in $Pb_{0.9}Ba_{0.1}ZrO_3$ and, more notably, the reverse FE →AFE cooling transition can be realized during normal heating-cooling cycles through additions of excess PbO to offset volatilization losses. Lattice vacancies are known to affect ferroelectric transitions in other perovskites,[14] and for $PbZrO_3$, it has been shown that lead and oxygen vacancies induced by annealing under reduced pressure extend the temperature range over which the FE phase exists.[15,16]

Excess PbO (1, 3, 5, and 10 wt %) were introduced into the precursor mixture of PbO, $BaCO_3$ and ZrO_2, followed by conventional ball milling and calcination at 1000 °C for 1 h in covered alumina crucibles. Pellets were pressed at 100 MPa and sintered at 1200 °C for 3 h, while being embedded in a $PbZrO_3$ powder in a closed crucible. Phase transitions were investigated for $Pb_{1-x}Ba_xZrO_3$, $x=0.05$, 0.075, and 0.1, ceramics using differential scanning calorimetry (PerkinElmer DSC7, heating/cooling rate of 10 °C/min). Onset differential scanning calorimetry (DSC) transition temperatures, $T_{AFE\text{-}FE}$ and $T_{FE\text{-}AFE}$, are quoted, unless otherwise stated; transition enthalpy was calculated using instrument software. Relative permittivity ε_r measurements were carried out from room temperature to 250 °C using an impedance analyser (HIOKI 3532-50, heating/cooling rate of 1 °C/min).

Plots of ε_r versus temperature for an $x=0.1$ mixed-oxide ceramic, made without excess PbO in the starting mixture, were in agreement with literature reports where no AFE →FE heating transition was detected. However, using DSC, a faint peak, centered at ~70 °C, appeared on the heating cycle, suggesting that a limited volume of the sample, possibly close to the surface, had transformed to the higher volume FE phase.

The DSC technique was used as the primary tool to investigate the effects of excess PbO on phase transitions. Transition temperatures, including paralectric (PE) transitions, are summarized in Table I. There were no significant changes in $T_{AFE\text{-}FE}$ or $T_{FE\text{-}PE}$ with added PbO. Introducing 5 or 10 wt % PbO to the $x=0.1$ precursor powder increased the size of the AFE→FE heating peak at ~70 °C and generated a cooling DSC anomaly at 4 °C for 5 wt %, and at −3 °C

a)Electronic mail: s.j.milne@leeds.ac.uk.

TABLE I. Summary of DSC onset and peak (numbers in italics enclosed in parentheses) transition temperatures..

Composition x	PbO content (wt %)	Transition temperatures (°C)			
		AFE-FE	FE-PE	PE-FE	FE-AFE
0.050	0	152(*157*)	210(*213*)	211(*209*)	73(*67*)
0.050	3	153(*156*)	212(*215*)	214(*211*)	76(*71*)
0.050	5	155(*161*)	210(*214*)	212(*209*)	101(*94*)
0.075	0	117(*122*)	204(*206*)	205(*202*)	···
0.075	3	113(*119*)	200(*205*)	205(*201*)	32(*27*)
0.075	5	118(*124*)	200(*203*)	202(*200*)	56(*53*)
0.100	0	71 (*83*)	193(*197*)	196(*193*)	···
0.100	5	73 (*86*)	191(*195*)	196(*192*)	4(–1)
0.100	10	73 (*81*)	191(*195*)	195(*191*)	–3(–8)
Second heating/cooling		70 (*79*)	191(*195*)	194(*191*)	–3(–9)

for 10 wt % PbO (Fig. 1). A second DSC run, a few minutes after the first cycle, displayed an AFE→FE heating peak at a similar temperature and with a similar transition enthalpy to the first run, confirming that the cooling peak represented a FE→AFE transition. Thus, a reversible AFE↔FE transition was realized in $Pb_{0.9}Ba_{0.1}ZrO_3$.

The AFE→FE transition temperature of $Pb_{0.9}Ba_{0.1}ZrO_3$ ceramics made from chemically precipitated powders quoted in the literature, ~114 °C, is considerably higher than the ones found here (onset and peak values of 71 and 83 °C, respectively, Table I).[8,9] One possible explanation may lie in a slightly lower Ba content in the former samples, which could arise from differences in the solubility of Pb and Ba carbonate species involved in the precipitation reaction. This could also have an effect on the realization of an AFE→FE heating transition using chemically prepared samples. For example, a $x=0.075$ noncompensated mixed-oxide sample shows an AFE→FE but no reverse FE→AFE transition (Table I).

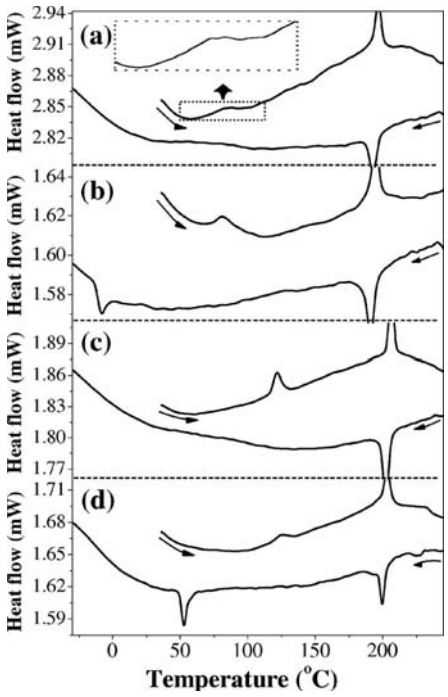

FIG. 1. DSC plots showing heating and cooling cycles for $Pb_{1-x}Ba_xZrO_3$: (a) $x=0.1$, (b) $x=0.1+10$ wt % PbO, (c) $x=0.075$, and (d) $x=0.075+5$ wt % PbO.

A 3 wt % starting excess of PbO was sufficient to generate a FE→AFE cooling transition in $x=0.075$, with $T_{FE\text{-}AFE}=32$ °C. The value of $T_{FE\text{-}AFE}$ increased to 56 °C for 5 wt % PbO (Fig. 1) but with little further change at 10 wt %. In the case of the already reversible $x=0.05$ transition, there was an increase in $T_{FE\text{-}AFE}$ from 76 °C (for 3% PbO) to 101 °C at a PbO content of 5 wt % PbO. Transition enthalpy in $x=0.05$ increased from 0.84 to 1.49 J/g when the PbO starting excess was raised to 5 wt %. A faint DSC anomaly at ~233 °C (peak temperature, heating cycle) occurred in a few samples, irrespective of PbO content. This is attributed to a minor amount of secondary phase $PbZrO_3$ which has been reported previously for $Pb_{1-x}Ba_xZrO_3$ ceramics and may be due to incomplete reaction.[12]

The effects of excess PbO on ε_r-T plots of a $x=0.075$ sample are shown in Fig. 2. A dielectric anomaly, consistent with a FE→AFE cooling transition, occurred in 3 and 5 wt % excess PbO samples at temperatures comparable to those determined using DSC. The lower peak ε_r value of the 5 wt % PbO example may in part be due to a decrease in density at moderate to high levels of starting excess PbO.[17]

Chemical analysis by electron probe microanalysis (EPMA) was conducted on a $Pb_{0.95}Ba_{0.05}ZrO_3$ (nominal) sample. The average Ba and Zr contents were 0.049 and 1.00 [standard deviation (S.D.)$\leqslant$0.002] confirming the accuracy of the mixed-oxide route in controlling bulk composition. Without excess starting PbO, the Pb ratio was analyzed to be 0.942 (S.D.=0.004), rising to 0.953 (S.D.=0.005) for samples with 10 wt % excess PbO. The EPMA data for Pb, in combination with the foregoing results on changes to phase transition temperatures, are consistent with a slight PbO loss occurring in "standard" ceramics and infer that this can be prevented by appropriate excess PbO additions to starting powders. Little or no excess PbO remains after ceramic processing.

Grain sizes in $x=0.1$ ceramics were $\leqslant 2$ μm for both unmodified and 10% excess PbO samples, with an average of ~1 μm (estimated using the linear intercept method). Hence, AFE↔FE switching was not facilitated by grain growth due to the excess PbO added to starting powders. Instead, it seems probable that the additive acts by compensating for process-induced lead and oxygen vacancies which stabilize the rhombohedral ferroelectric phase. For

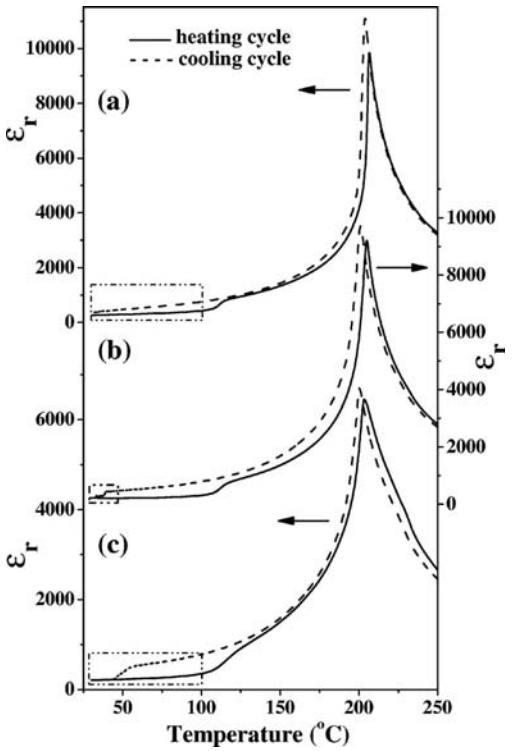

FIG. 2. Plot relative permittivity ε_r vs temperature for $Pb_{1-x}Ba_xZrO_3$, $x=0.075$: (a) no excess starting PbO, (b) 3 wt % excess PbO, and (c) 5 wt % excess PbO.

$Pb_{1-x}Ba_xZrO_3$ compositions, $x=0.075$ and 0.1, no FE $\rightarrow$AFE cooling transition occurs without compensation. In $x=0.05$, the transition from rhombohedral to orthorhombic is present, but $T_{FE\text{-}AFE}$ is lowered by $\sim$25 °C through PbO volatilization losses. Transformational strain was thought previously to account for the irreversibility of the AFE $\rightarrow$FE transition during heating-cooling cycles.[8,9] It is plausible that some PbO loss may also have occurred in $x=0.1$ samples made from chemically precipitated powders, despite the lower calcination temperature of 850 °C.[8,9] Changes in vacancy distribution over time may have contributed to the reported recovery of the AFE phase after long term aging. Strain may contribute to the large AFE$\leftrightarrow$FE temperature hysteresis of the present PbO-compensated samples; however, it is not the principal reason for the retention of the FE phase.

The work was supported by Thailand Research Fund (TRF), Commission on Higher Education (CHE), Institute of Research and Development Administration (IRDA), Faculty of Science, Naresuan University, Facuty of Science, Chiang Mai University, and Institute of Materials Research, Leeds. EPMA analysis was kindly performed by E. Condliffe.

[1]V. J. Tennery, J. Am. Ceram. Soc. **49**, 483 (1966).
[2]B. A. Scott and G. Burns, J. Am. Ceram. Soc. **55**, 331 (1972).
[3]R. W. Whatmore and A. M. Glaezer, J. Phys. C **12**, 1505 (1979).
[4]Z. Xu, X. Dai, D. Viehland, D. Payne, Z. Li, Y. Jiang, J. Am. Ceram. Soc. **78**, 2220 (1995).
[5]X. Dai, Z. Xu, and D. Viehland, J. Appl. Phys. **77**, 5086 (1995).
[6]X. Dai, J. F. Li, and D. Veihland, Phys. Rev. B **51**, 2651 (1995).
[7]H. Futaru, S. Endo, L. C. Ming, and H. Fujishita, J. Phys. Chem. Solids **60**, 65 (1999).
[8]B. P. Pokharel and D. Pandey, J. Appl. Phys. **86**, 3327 (1999).
[9]B. P. Pokharel and D. Pandey, J. Appl. Phys. **88**, 5364 (2000).
[10]B. P. Pokharel, R. Ranjan, D. Pandey, V. Siruguri, and S. K. Paranjpe, Appl. Phys. Lett. **74**, 756 (1999).
[11]J. H. Tseng and T. B. Wu, Appl. Phys. Lett. **78**, 1721 (2001).
[12]Z. Ujma, J. Handerek, M. Pawelczyk, and D. Dmytrow, Ferroelectrics **129**, 127 (1992).
[13]K. H. Yoon, S. C. Hwang, and D. H. Kang, J. Mater. Sci. **32**, 17 (1997).
[14]S. Lee, Z.-K. Liu, M.-H. Kim, and C. A. Randall, J. Appl. Phys. **101**, 054119 (2007).
[15]Z. Ujma and J. Handerek, Phase Transitions **4**, 157 (1984).
[16]Z. Ujma and J. Handerek, Phase Transitions **3**, 121 (1983).
[17]T. Bongkarn, G. Rujijanagul, and S. J. Milne, Mater. Lett. **59**, 1200 (2005).

Available online at www.sciencedirect.com
ScienceDirect
Current Applied Physics 8 (2008) 359–362
Current Applied Physics
An official journal of the KPS
www.elsevier.com/locate/cap
www.kps.or.kr

Influence of graphite particle size on electrical properties of modified PZT–polymer composites

Gobwute Rujijanagul *, Saowakhon Jompruan, Arnon Chaipanich

Department of Physics, Faculty of Science, Chiang Mai University, Chiang Mai 50200, Thailand

Available online 25 October 2007

Abstract

Piezoceramics–polymer composites using modified lead zirconate titanate ($Pb_{0.88}Sr_{0.12}Zr_{0.54}Ti_{0.44}Sb_{0.02}O_3$) and polyethylene (PE) were prepared by a calendaring method. The modified ceramic powder was prepared by a conventional solid-state method. Graphite powder of various particle sizes was also added into the composites. Properties of the composites as a function of particle sizes of the ceramics and graphite were studied. The relative permittivity and piezoelectric coefficient (d_{33}) of the composites were found to increase with increasing the particle size of the modified ceramics. Composites contained finer graphite particle also found to give higher d_{33} values.

PACS: 81.05.Qk; 81.05.Zx; 77.84.–s

Keywords: Composites; Dielectric properties; Piezoelectric properties

1. Introduction

The works on piezoceramic–polymer composites have been carried out for over a decade due to their potential for use in many applications such as hydrophones or ultrasonic transducer [1–3]. The simplest type of piezoceramics–polymer composite is a 0–3 connectivity, which consists of a polymer matrix filled with piezoceramic powder. Lead zirconate titanate (PZT) is a well known material used as a piezoceramic due to its large piezoelectric and large coupling coefficients and many investigations have been carried out on the properties of the piezoceramic–polymer composites made using PZT. A number of authors reported that the properties of the piezoceramics–polymer composites depends on many factors such as method of preparation, designation (connectivity), properties of dispersed phase powder, etc. [1–5]. It is also reported that the particle size of the dispersed phase has an effect on the piezoceramic–polymer composites [6,7]. Lee et al. prepared the 0–3 composite of $PbTiO_3$ (PT) and a dielectric gel polymer [6]. They found that the particle size of PT had an effect on the piezoelectric coefficient (d_{33}) of the composites. A similar result was reported by other investigators [7]. In order to induce the piezoelectric properties in the piezoceramics, a high electric field must be applied to the ceramics, a process known as poling [1–3]. However, it is difficult to pole piezoceramics–polymer composites. This is because the electric field will pass through the lower dielectric constant phase (polymers matrix phase). Therefore, many researchers have been investigating on the mechanism of poling and have been trying to develop a suitable method for poling these composites [6,8]. In order to resolve this difficulty with poling, a third conducting phase, such as carbon, germanium, or silicon can be introduced between the piezoelectric particles [9]. This can make poling easier. It is also reported that particle size of graphite has an effect on the conductivity of wax–graphite composite [10]. Finer graphite particle was found to give higher conductivity in the reported composite. Since the particle size of the ceramics and the conducting phase such as graphite have effects on the properties of these composites.

* Corresponding author. Tel.: +66 5394 3376; fax: +66 5335 7512.
E-mail address: rujijanagul@yahoo.com (G. Rujijanagul).

1567-1739/$ - see front matter © 2007 Elsevier B.V. All rights reserved.
doi:10.1016/j.cap.2007.10.031

Thus, it is interesting to study the effect of particle size of graphite on the electrical properties of the composites. Recently, modified PZT by substitution of Sr and Sb in PZT was reported to possess better piezoelectric properties [11]. In this work, piezoelectric composites consist of polyethylene (PE) matrix and the modified PZT ceramics powders were prepared but with an addition of graphite powder of different particle size. Effect of graphite and its particle size on electrical properties of the composites were then investigated for the first time.

2. Experimental procedure

In order to prepare ceramic phase powder in the composites, modified PZT ceramics with the formula of $Pb_{0.88}Sr_{0.12}Zr_{0.54}Ti_{0.44}Sb_{0.02}O_3$ (PZT_{SrSb}) were prepared by a conventional mixed oxide route. The starting powder of PbO, ZrO_2, $SrCO_3$, Sb_2O_3 and TiO_2 were mixed and calcined at 925 °C for 4 h. The ceramic disc of about 10 mm in diameter and 2 mm in thickness were obtained by pressing and sintering at 1250 °C for 2 h. To minimize the loss of lead due to vaporization, the PbO atmosphere for the sintering was maintained using $Pb(Zr_{0.52}Ti_{0.48})O_3$ (PZT) as the spacer powder. X-ray diffraction (XRD) was employed to identify phase of the PZT_{SrSb} ceramics. The PZT_{SrSb} powder was obtained by grinding the ceramics. Powders of various sizes of PZT_{SrSb} and graphite were obtained by sieving [7]. The ranges of particles of PZT_{SrSb} and graphite used in the investigation are shown in Table 1. Mid points of each particle size range are also represented in the Table. Difference sizes of the PZT_{SrSb} and graphite powders were mixed with PE using a volume ratio of 60:1.5:38.5 (PZT_{SrSb}:graphite:PE). In order to obtain uniformity, the mixtures were put into xylene solution and intermittently stirred for 30 min. The samples were then left to dry and a composite sheet of about 2–3 mm in thickness was formed by the calendaring method. Microstructure of the composites was examined by scanning electron microscopy (SEM). Composite discs of 10 mm in diameter were punched out from the composite sheet. The pellets were polished, and then electrodes were formed by gold sputtering. The relative permittivity was measured using an impedance meter (Hewlett Packard 4194A). The composites were poled for piezoelectric measurement in silicone oil at 80 °C for 30 min at field strength of 3 kV/mm. The piezoelectric coefficient d_{33} was measured using a d_{33} meter (piezometer System Model PM25) 24 h after poling.

Table 1
Range of particle size and its mid point of disperse phase

Disperse phase	Range of particle size (μm)	Mid point of the particle range (μm)
PZT_{srSb}	750–1000	875
PZT_{SrSb}	530–749	640
PZT_{srSb}	300–529	415
Graphite	70–100	85
Graphite	38–69	54
Graphite	0–38	19

3. Results and discussion

XRD trace result of PZT_{SrSb} ceramic was found to show diffraction pattern as attributed to the PZT with the provskite structure, as seen in Fig. 1. The inset of Fig. 1 shows microstructure of PZT_{SrSb} ceramic. The average grain size of the PZT_{SrSb} ceramic is ~1.4 μm as determined by intercept method. The relative permittivity of the composites with various particle sizes of ceramics and graphite is shown in Fig. 2. The samples exhibited an increase in the relative permittivity with increase particle size of the ceramic powders.

The changes of relative permittivity in relation to different particle size of graphite used can also be seen in Fig. 2. Although there is no direct trend between particle size of graphite and relative permittivity, the highest relative permittivity of 104 was found for the composites contained 750–1000 μm (mid point = 875 μm) PZT_{SrSb} particle and 38–69 μm (mid point = 54 μm) graphite particles. The higher relative permittivity for coarser PZT_{SrSb} powder may be related to less interface area between ceramic

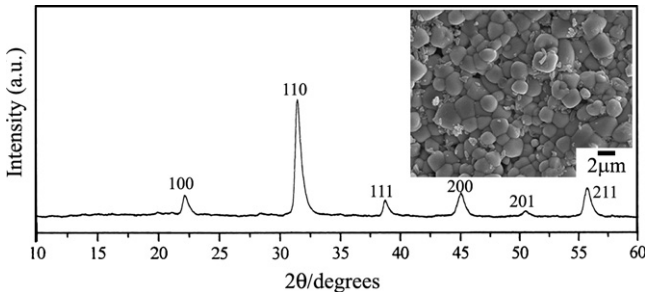

Fig. 1. XRD pattern of PZT_{SrSb} ceramics (microstructure of the ceramics is shown in the inset).

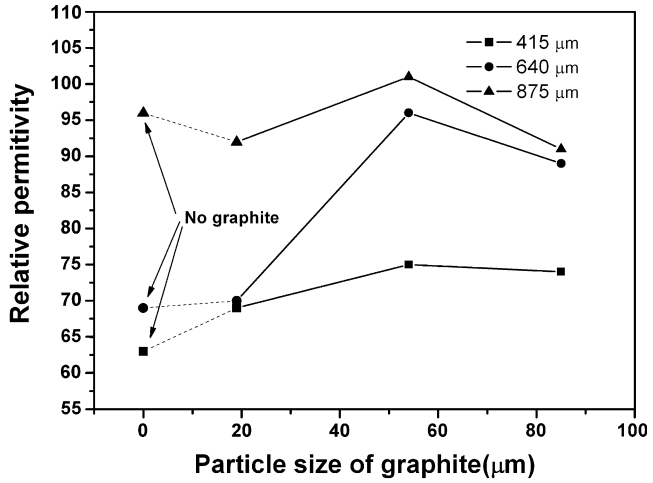

Fig. 2. Relative permittivity of the composites as a function of particle size of graphite: ■, ♦, and ▲ indicate the particle size of PZT_{SrSb}.

particle and polymer, and less imperfection in the joining [12]. Furthermore, composites with coarser ceramic phase powder exhibit higher connectivity thus may also contributed to better results. The maximum relative permittivity value in this work was found to be higher compared with the composites between PZT, PT and polymers reported by previous authors [2,7,13]. This is may be due to the better properties of PZT_{SrSb} ceramics powder and the higher connectivity in the composites [14]. However, the relative permittivity of the composites is limited by the dielectric properties of the polymer matrix, amount and type of the third phase.

The influence of the particle size of the modified PZT_{SrSb} powder on the piezoelectric coefficient d_{33} of the composites is shown in Fig. 3. Composites with larger PZT_{SrSb} particle size were found to give higher d_{33} values. Again, this is believed to be due to less interface area and the higher connectivity in composites containing coarser ceramic particles thus would result in better poling efficiency of the composites than those containing finer ceramic particles. The piezoelectric coefficient d_{33} as a function of particle size of graphite is also shown in Fig. 3. The results show that the d_{33} value increased with decreasing particle size of the graphite filler. Thus agreeing with the work by Rajagopal and Satyam [10] whom reported that conductivity of wax–graphite composites increased with decreasing the particle size of the graphite and that finer graphite particles would lead to greater electrical path in the composites. The higher value of d_{33} in the composites containing finer graphite particles in this work is believed to be due to such a conduction path existing in these composites. Better conduction path would therefore enable easier poling in such composites.

The microstructure of graphite particles and of the composite with graphite and PZT_{SrSb} particles were examined by SEM. Fig. 4a shows morphology of the graphite particles in the range of 0–38 μm. The graphite particles can be seen to be platelet in shape. For the composites, platelet

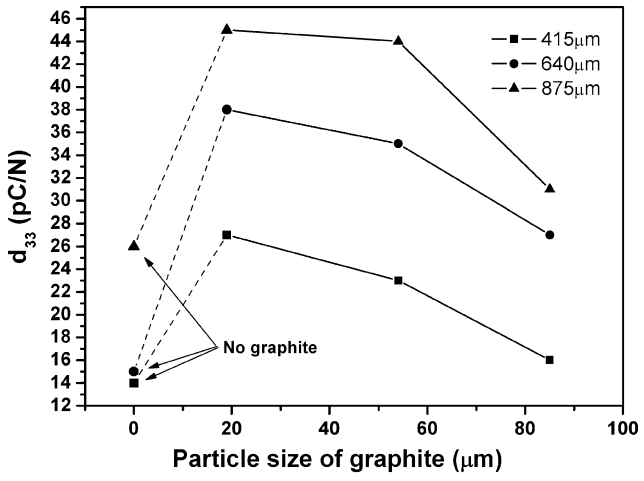

Fig. 3. The piezoelectric coefficient d_{33} of the composites as a function of particle size of graphite: ▲, ●, and ■ indicate the particle size of PZT_{SrSb}.

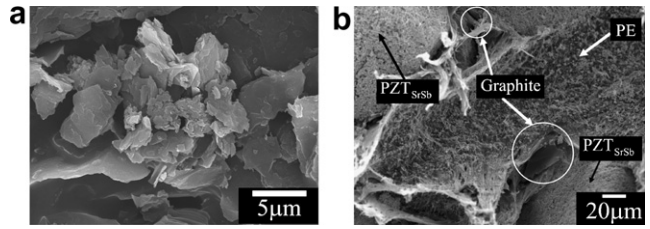

Fig. 4. SEM micrographs for (a) graphite particle (particle size range of 0–38 μm) and (b) fracture surface of the composites contained PZT_{SrSb} particle in rage of 300–500 μm and graphite particle in range of 0–38 μm.

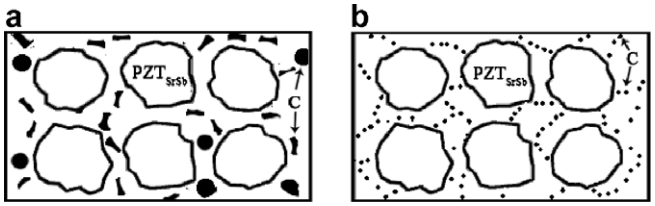

Fig. 5. Models for the composites containing (a) coarse and (b) fine particle of graphite (graphite particles indicated by C).

graphite particles can be seen placed close to PZT_{SrSb} particles which indicated that the conduction path was established between the ceramic particles as shown in Fig. 4b. The composite models contained fine and coarse particles of graphite with the same size of PZT_{SrSb} particles are shown in Fig. 5. It can be noted that the composites containing finer graphite particle has better network path of graphite which result in better piezoelectric property after poling.

4. Conclusions

Composites of PE, $PZT_{SrSb,}$ and graphite powder were prepared with various particle sizes of PZT_{SrSb} and graphite. Particle sizes of the PZT_{SrSb}, and graphite were controlled by sieving. The d_{33} values were found to be higher in the composites containing coarser particles of the PZT_{SrSb} and finer graphite particles. Increase possibility of better conduction path in the composites when containing finer graphite particle is believed to be the reason in giving higher d_{33} value in these composites. Although no direct trend was found in the effect of particle size of the graphite and the relative permittivity, optimum relative permittivity was obtained when the particle size ranges of graphite and ceramics were 38–69 and 750–1000 μm, respectively.

Acknowledgments

This work was supported by The Thailand Research Fund (TRF), Graduate School, Chiang Mai University and Commission on Higher Education (CHE) Thailand. The authors would like to thank Prof. Dr. Tawee Tunkasiri for his help in many facilities.

References

[1] R.E. Newnham, Ann. Rev. Mater. Sci. 16 (1986) 47.
[2] A.J. Moulson, J.M. Herbert, Electroceramics: Materials, Properties and Application, second ed., John Wiley & Sons, West Sussex, 2003.
[3] A. Safari, J. Phys. III France 4 (1994) 1129.
[4] R. Fries, A.J. Moulson, J. Mater. Sci. 5 (1994) 238.
[5] K. Han, A. Safari, R.E. Riman, J. Am. Ceram. Soc. 74 (1991) 1699.
[6] M.H. Lee, A. Halliyal, R.E. Newnham, J. Am. Ceram. Soc. 72 (1989) 986.
[7] G. Rujijanagul, S. Boonyakul, T. Tukasiri, J. Mater. Sci. Lett. 20 (2001) 1943.
[8] D. Waller, T. Iqbal, A. Safari, J. Am. Ceram. Soc. 72 (1989) 322.
[9] G.S. Gong, A. Safari, S.J. Jang, R.E. Newnham, Ferroelectrics Lett. 5 (1986) 131.
[10] C. Rajagopal, M. Satyam, J. Appl. Phys. 49 (1978) 5536.
[11] H. Zheng, I.M. Reaney, W.L. Lee, J. Am. Ceram. Soc. 85 (2002) 207.
[12] H.G. Lee, H.G. Kim, J. Am. Ceram. Soc. 72 (1989) 938.
[13] W. Nhuapeng, T. Tunkasiri, J. Am. Ceram. Soc. 85 (2002) 700.
[14] D.M. Reed, T.T. Srinivasan, Q.C. Xu, R.E. Newnham, in: Proceedings of the seventh International Symposium on the Applications of Ferroelectrics (ISAF'90), 1990, p. 324.